

AD-A118 763

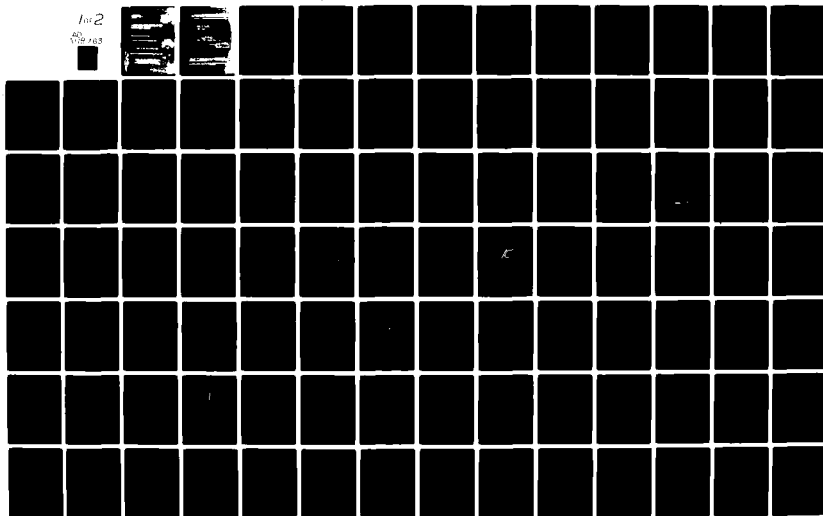
GEORGIA INST OF TECH ATLANTA ENGINEERING EXPERIMENT --ETC F/6 17/9
A FIBER OPTIC BEAM CONTROLLER FOR PHASED ARRAY RADARS.(U)

JUN 82 R B EFURD, E O RAUSCH, M A CORBIN F19628-81-C-0026
GIT/EES-A-2832 RADC-TR-82-173 NL

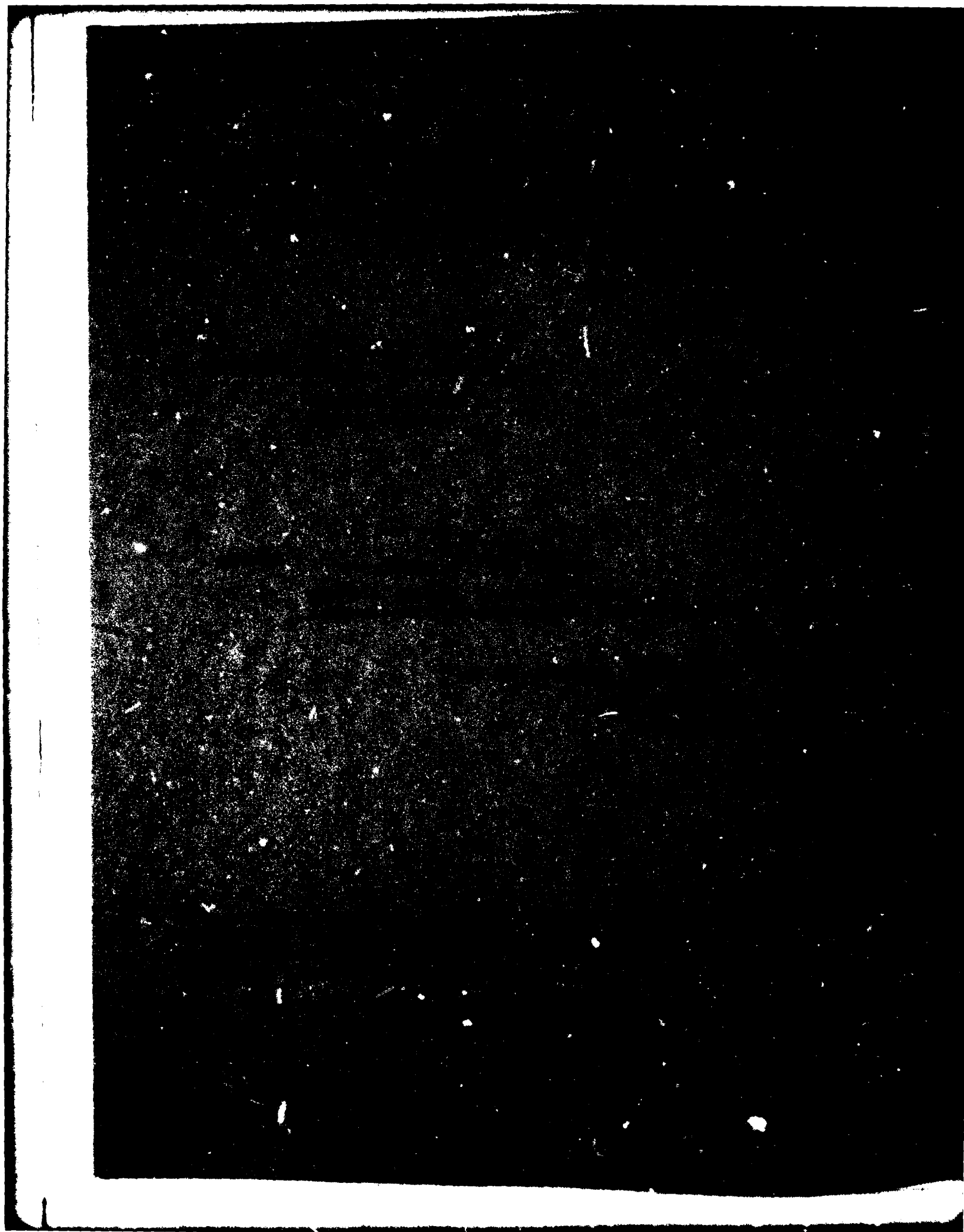
UNCLASSIFIED

1 of 2

400
17/6 103



AD A118763



UNCLASSIFIED

SECURITY CLASSIFICATION OF THIS PAGE (When Data Entered)

REPORT DOCUMENTATION PAGE		READ INSTRUCTIONS BEFORE COMPLETING FORM
1. REPORT NUMBER RADC-TR-82-173	2. GOVT ACCESSION NO. AD-A118763	3. RECIPIENT'S CATALOG NUMBER
4. TITLE (and Subtitle) A FIBER OPTIC BEAM CONTROLLER FOR PHASED ARRAY RADARS		5. TYPE OF REPORT & PERIOD COVERED Final Technical Report 10 Dec 80 - 9 Feb 82
7. AUTHOR(s) R.B. Efurd B.E. Huitt E.O. Rausch M.A. Corbin		6. PERFORMING ORG. REPORT NUMBER GIT/EES Project A-2832 8. CONTRACT OR GRANT NUMBER(s) F1962S-81-C-0026
9. PERFORMING ORGANIZATION NAME AND ADDRESS Georgia Institute of Technology Engineering Experiment Station Atlanta GA 30332		10. PROGRAM ELEMENT, PROJECT, TASK AREA & WORK UNIT NUMBERS PE61101F LDFFP02C1
11. CONTROLLING OFFICE NAME AND ADDRESS Rome Air Development Center (EEA) Hanscom AFB MA 01731		12. REPORT DATE June 1982 13. NUMBER OF PAGES 138
14. MONITORING AGENCY NAME & ADDRESS (if different from Controlling Office) Same		15. SECURITY CLASS. (of this report) UNCLASSIFIED 15a. DECLASSIFICATION/DOWNGRADING SCHEDULE N/A
16. DISTRIBUTION STATEMENT (of this Report) Approved for public release; distribution unlimited		
17. DISTRIBUTION STATEMENT (of the abstract entered in Block 20, if different from Report) Same		
18. SUPPLEMENTARY NOTES RADC Project Engineer: Martin R. Stiglitz (EEA) This effort was funded totally by the Laboratory Directors' Fund		
19. KEY WORDS (Continue on reverse side if necessary and identify by block number) Fiber Optics Time Delay RF Phase Delay RF Amplitude Modulated Light Radar Beam Controller		
20. ABSTRACT (Continue on reverse side if necessary and identify by block number) The general objectives of this project were to: (1) design a laboratory demonstration of a phase shifter using optical fibers as the delay mechanisms, (2) perform analyses of the laboratory demonstration phase shifter; and (3) test the laboratory demonstration phase shifter for losses, dynamic range, phase shifter accuracy, etc.		

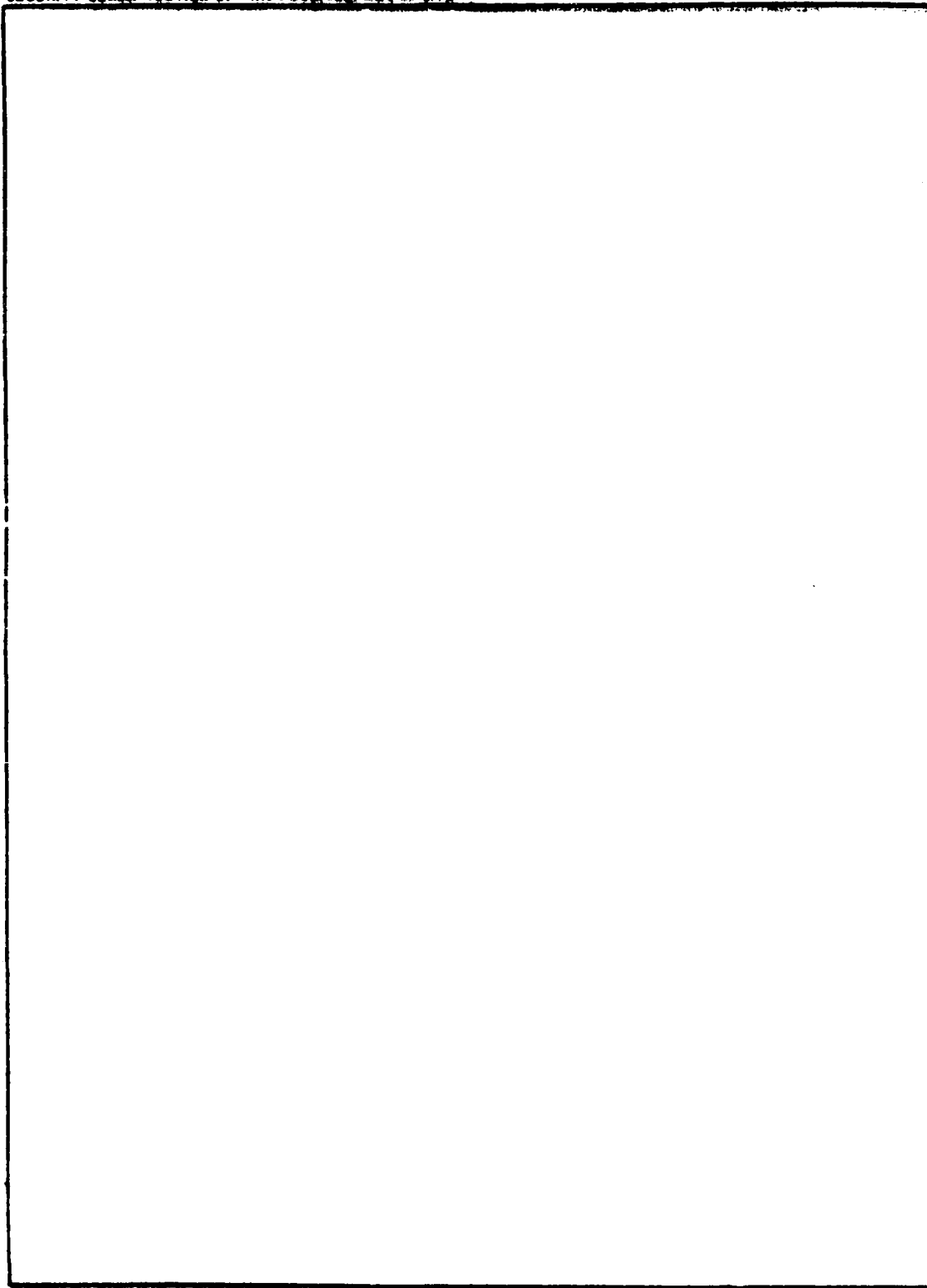
DD FORM 1 JAN 73 1473 EDITION OF 1 NOV 65 IS OBSOLETE

UNCLASSIFIED

SECURITY CLASSIFICATION OF THIS PAGE (When Data Entered)

UNCLASSIFIED

SECURITY CLASSIFICATION OF THIS PAGE(When Data Entered)



UNCLASSIFIED

SECURITY CLASSIFICATION OF THIS PAGE(When Data Entered)

FOREWARD

This research project (GIT/EES A-2832) was conducted by the Radar Applications Division of the Radar and Instrumentation Laboratory, Engineering Experiment Station, Georgia Institute of Technology, Atlanta, Georgia 30332. Mr. R. B. Efurd and Dr. E. O. Rausch served jointly as Project Director for this effort. The project was sponsored by Electromagnetic Sciences Division, Rome Air Development Center, Hanscom AFB, Ma. 01732 with Mr. M. Stiglitz as the technical monitor.

The technical effort described in this report was performed during the period 09 December 1980 to 09 February 1982. The objective of this effort was to build and test a phase delay device using fiber optics.

The technical results were: (1) the phase delay device was built and tested, (2) the device exhibited the predicted time delay performance, (3) the device has an adequate S/N and dynamic range for many applications, and (4) better optical switches are a prerequisite to a practical device.

Respectfully submitted,

R. B. Efurd
E. O. Rausch

R. B. Efurd

E. O. Rausch

Joint Project Directors

Approved:

J. L. Eaves

J. L. Eaves, Acting Division Chief
Radar Applications Division



Accession For	
NTIS GRA&I	<input checked="checked" type="checkbox"/>
DTIC TAB	<input type="checkbox"/>
Unannounced	<input type="checkbox"/>
Justification	
By _____	
Distribution/	
Availability Codes	
Dist	Avail and/or Special
A	

TABLE OF CONTENTS

<u>SECTION</u>	<u>TITLE</u>	<u>PAGE</u>
1	INTRODUCTION AND BACKGROUND.....	1
1.1	Contract Overview	1
1.2	Review of the History of Fiber Optics.....	1
1.3	Fiber Optics as a Method of Phase Shifting	2
2	TECHNOLOGY SURVEY	4
2.1	Optical Fibers	4
2.1.1	Modal Dispersion.....	4
2.1.2	Wavelength Dispersion	7
2.1.3	Optical Fiber Losses.....	8
2.1.4	Optical Fiber Selection	8
2.1.5	Optical Fiber Use	8
2.2	Light Emitters.....	12
2.2.1	Injection Laser Diode (ILD).....	12
2.2.2	Light Emitting Diode (LED).....	14
2.3	Detectors	20
2.3.1	Pin Diode	20
2.3.2	Avalanche Photodiode (APD).....	23
2.3.3	Comparison between APD and Pin Photodiodes	24
2.3.4	Longer Wavelength Performance and Future Developments	24
2.3.5	Application to Current Project	24
2.4	Optical Switches	25
2.4.1	Mechanical and Electromechanical Switches	25
2.4.1.1	Bell Labs Mechanical Fiber Optic Switch	25
2.4.1.2	Nippon Electric Company (NEC) Mechanical Switch.....	25
2.4.1.3	IBM Single-Pole Double-Throw Low Loss Fiber Optic Switch	27
2.4.1.4	IBM Field-Assisted Fiber Optic Switch	27
2.4.1.5	Mechanical One-To-Many Fiber Optic Switch	27
2.4.2	Electro-Optical Switches.....	31

TABLE OF CONTENTS (cont.)

<u>SECTION</u>	<u>TITLE</u>	<u>PAGE</u>
2.4.2.1	Electro-Optic Switches as Coupled Wave Devices	32
2.4.2.2	Integrated Optics Directional Coupler.....	36
2.4.2.3	Stepped-Delta Base Coupler	38
2.4.2.4	Bistable Delta Beta Coupler	39
2.4.3	Electro-Optic Multimode Switches.....	39
2.4.4	Magneto-Optic Switching.....	40
2.4.5	Acousto-Optic Switch.....	43
2.4.6	Optical Switch Summary	43
2.5	Fiber Optic Couplers	46
2.5.1	Coupler Parameters	46
2.5.2	Tee Coupler	47
2.5.3	Star Coupler.....	47
2.6	Fiber Optic Interconnections.....	50
2.6.1	Splicing Techniques.....	50
2.6.2	Fiber Optic Connectors	54
2.7	Laboratory Practices	62
2.7.1	Connector Preparation.....	62
2.7.2	Epoxying.....	66
2.7.3	Metal Retaining Assembly	66
2.7.4	Polishing.....	67
2.7.5	Analysis of Connector Fabrication.....	67
3	LABORATORY SYSTEM DESCRIPTION.....	68
3.1	System Description.....	68
3.1.1	ILD	70
3.1.2	Fiber	70
3.1.3	Avalanche Photodiode (APD).....	73
3.1.4	Coupler.....	73
3.1.5	Optical Switch.....	73
3.1.6	Connectors	73
3.2	System Analysis and Measurements	78

TABLE OF CONTENTS (cont.)

<u>SECTION</u>	<u>TITLE</u>	<u>PAGE</u>
3.2.1	Derivation of Signal Power for a Monomode Fiber Delay Line	78
3.2.2	Derivation of Noise Power.....	82
3.2.3	Numerical Estimations	84
3.2.4	Derivation of SNR for a Multimode Fiber Delay Line with a CW Signal	88
3.2.5	Power Calculations of a Pulsed Signal in a Multimode Fiber Delay Line	91
3.2.6	Temperature Stability	97
3.2.7	Maximum SNR	98
3.2.8	Analysis Summary	98
3.2.8.1	Induced Delay/Induced Pulse Spreading	98
3.2.8.2	S/N Ratio	100
3.2.9	Phase Shift	100
3.2.9.1	Measured Phase Shift	101
3.10	Frequency Response	103
4	CONCLUSIONS	106
4.1	Conclusions Drawn from Experimental Results	106
4.2	Conclusions Drawn from Experimental Results and an Intuitive Model of Near Term Technology Changes	106
4.3	Impact on Radar System Design	107
5	RECOMMENDATIONS	108
5.1	Yes to Question One and No to Question Two	108
5.2	No to Question One and Yes to Question Two	108

TABLE OF CONTENTS

<u>SECTION</u>	<u>TITLE</u>	<u>PAGE</u>
	REFERENCES	111
APPENDIX A	THE SUM OF TWO SINUSOIDS	113
APPENDIX B	DERIVATION OF THE OUTPUT POWER OF A CW SIGNAL PROPAGATING THROUGH A MULTIMODE FIBER	115
APPENDIX C	THE CONVOLUTION OF A GAUSSIAN PULSE WITH A GAUSSIAN RESPONSE FUNCTION	118

LIST OF ILLUSTRATIONS

<u>FIGURE</u>	<u>TITLE</u>	<u>PAGE</u>
2.1	Optical fiber configurations	5
2.2	Typical optical fiber dimensions	6
2.3	Progress in low loss fiber fabrication	9
2.4	Spectral loss curve, low loss, high silica, multimode optical fiber	10
2.5	Basic building blocks of an optical fiber communication system	11
2.6	Homojunction ILD schematic	13
2.7	Heterostructure ILD schematic	15
2.8	Typical ILD characteristics	16
2.9	Burrus-type LED	17
2.10	PIN photodiode schematic	21
2.11	Bell Laboratories one to four switch	26
2.12	NEC prism switch	28
2.13	IBM field assisted switch	29
2.14	One-to-many switch	30
2.15	Four port EDC switch	33
2.16	4 x 4 switching network	34
2.17	Integrated optics version of the optical directional couples	37
2.18	Liquid crystal switch	41
2.19	Acousto-optic switch	44
2.20	Tee coupler	48
2.21	Star coupler	49
2.22	Splice loss due to extrinsic parameters	51
2.23	Splice loss due to intrinsic parameters	52
2.24	Splice loss due to α mismatch	53
2.25	Fusion splicing apparatus	55
2.26	Loose tube splice	56
2.27	AMP, Inc. connector	57
2.28	Splice bushing	59

LIST OF ILLUSTRATIONS (cont.)

<u>FIGURE</u>	<u>TITLE</u>	<u>PAGE</u>
2.29	TRW cinch optalign connector	60
2.30	Fiber alignment by three balls	61
2.31	Diagram of array connector	63
2.32	Location of AMP and NEC connectors	64
2.33	Fabrication of AMP connector	65
3.1	Fiber optic phase delay network	69
3.2	Biconical taper directional coupler	76
3.3	Relative laser noise spectrum for various mean photon levels in the laser mode, \bar{N}_p	80
3.4	Low frequency (< 1 GHz) normalized noise power versus laser output power. Normalized noise power is defined as absolute noise power per 1 Hz bandwidth divided by the average laser power	81
3.5	Noise power versus total attenuation in fiber. Amplifier gain, G_A , is 1. system bandwidth, $\Delta\nu$, is 1 Hz	87
3.6	Signal-to-noise versus total attenuation in multimode fiber	90
3.7	Measured signal-to-noise ratio in a short (1m) optical transmission line versus input voltage	92
3.8	AC output voltage from a short (1m) fiber optic transmission line versus input voltage. The dynamic range is the ratio of the maximum V_o^2 to minimum V_o^2 within the linear region	99
3.9	Measured and calculated phase difference of optical fiber pair in test system	102
3.10	Oscilloscope display at 1, 2, 3, and 4 GHz	104
3.11	Laser-receiver system gain vs. frequency. Both curves found experimentally using laser #2807	105
5.1	Four position optical switch time delay phasing system	109

LIST OF TABLES

<u>TABLE</u>	<u>TITLE</u>	<u>PAGE</u>
1	Comparison of the Present Characteristics of the Major Classes of Light-Emitting Diodes	18
2	Comparison of the Advantages and Disadvantages of the Major Classes of Light-Emitting Diodes	19
3	NEC Switch Characteristics	28
4	Multimode Fiber Optic Switching Techniques	45
5	Injection Laser Diode (ILD) Characteristics	71
6	Galite® Fiber	72
7	Avalanche Photodiode (APD) Characteristics	74
8	Coupler Characteristics	75
9	Optical-Switch	77

SECTION 1 INTRODUCTION AND BACKGROUND

1.1 CONTRACT OVERVIEW

Contract F196228-81-C-0026, a new Beam Controller for Phased Array Radars, was initiated at Georgia Institute of Technology on approximately 10 December 1980. The contractual agreement period was from 10 October 1980 to 10 February 1982. This contract was initiated with Electromagnetic Sciences Division, RADC, Hanscom AFB, MA 01732 through an unsolicited proposal submitted by the Radar and Instrumentation Laboratory of the Engineering Experiment Station of Georgia Institute of Technology.

The general objectives of this project were:

- (1) Design a laboratory demonstration of a phase shifter using optical fibers as the delay mechanisms.
- (2) Perform analyses of the laboratory demonstration phase shifter.
- (3) Test the laboratory demonstration phase shifter for losses, dynamic range, phase shifter accuracy, etc.

These objectives were achieved through the execution of these four tasks:

- (1) Literature Search - Develop the background data for components and techniques.
- (2) Design Phase - Design of a laboratory demonstration model of an active phase shifter consisting of optical switches and fiber optics delay lines.
- (3) Construction Phase - Construct an optical source, the phase shifter device, and the necessary support devices.
- (4) Test and Evaluation Phase - Evaluate the performance of the laboratory demonstration phase shifter.

These four tasks were executed with the changes that normally occur in a research project and the results are reported in this Final Report.

1.2 REVIEW OF THE HISTORY OF FIBER OPTICS

It has been known for approximately two centuries that total internal reflection of light can occur at the interface between "transparent" substances when the light approaches the interface through the substance with the higher index of refraction. The necessary condition is that the angle of incidence be above a certain critical angle which marks the boundary between light transmission and light reflection.

Although this effect was well explored and well explained by science, it had not been exploited on a large scale up to the decade of 1960. In this decade, it was suggested that this effect could be used to construct optical waveguides.

By the late 1960's and early 1970's optical waveguides had evolved as practical structures for special purposes, but their losses were still too large for many applications. In the middle 1970's, the fiber losses dropped to minimums of approximately 2 dB per kilometer. With this event, the restrictions on wide use of fiber optics shifted to detectors, sources, connectors, and skilled manpower. The detector and source restrictions were adequately solved in the late 1970's. The connector restrictions were only partially solved, but the solutions are adequate for many applications.

At the beginning of the 1980 decade, the prime restrictions on the use of fiber optics are the cost of components and the absence of a large pool of skilled manpower. For many applications, the economic advantage of fiber optics will ensure its use. This is especially true in the area of long distance broadband communications. This single industry mass user will invest sufficient research and capital to ensure that the economies of large scale use will apply to the fiber optics technology. On this communications industry technology base, a large number of industrial and military uses will be engineered. One such potential use (Fiber Optics as Phasing Devices) is the subject of this report and it is summarized in the next paragraph.

1.3 FIBER OPTICS AS A METHOD OF PHASE SHIFTING

The time delay in an optical fiber is approximately 0.66 nanosecond per foot of fiber. Thus a delay accuracy of one picosecond requires the fiber to be cut to a length accuracy of 0.00066 feet, or 7 parts in 10,000. This is a precise manufacturing requirement, but it is an achievable requirement. Time delay accuracies of a few picoseconds can be routinely produced, given that the proper production tools and equipment are available. A one gigahertz signal has an in-filter wavelength of approximately 0.66 feet and can, therefore, be delayed with an accuracy of a thousandth of its wavelength.

The optical fibers have a bandwidth-length potential from a few kilohertz-km to, perhaps, 100 gigahertz-kilometer depending on the type of fiber optics employed and the care exercised in production. The common graded index fibers have bandwidth-length products in excess of 500 megahertz-kilometer.

The objective of the research documented in this report was to determine if the accurate time delay and the broad bandwidth of fiber optics could be exploited to construct a time delay phasing device for a microwave antenna. Time delay phasing of microwave antennas is highly desirable because there is no coupling between the signal bandwidth and the antenna beam angle for a time delay antenna. This enables radiation of broad bandwidth signals necessary for close range resolution at precise angles from a phased array microwave antenna.

SECTION 2

TECHNOLOGY SURVEY

In this section the components available for a fiber optics system will be surveyed. These components will be surveyed for their engineering characteristics with limited discussion of the underlying physics. The components which will be surveyed are: (1) Optical Fibers, (2) Light Emitters, (3) Light Detectors, (4) Optical Switches, (5) Optical Couplers, and (6) Optical Connectors. In addition to the component survey, a subsection on laboratory practices with fiber optics components is included. This subsection discusses the experience gained on this project in working fiber optics and its supporting equipments.

2.1 OPTICAL FIBERS

Optical fibers are constructed in three different configurations as shown in Figure 2.1 (Reference 1). These configurations are (1) Single Mode, (2) Graded Index Multimode, and (3) Step Index Multimode. The typical dimensions for these fibers are shown in Figure 2.2 (Reference 1). The primary functional difference between these fibers is in the signal bandwidths that they can transmit. This varies from gigahertz-kilometer for the monomode fiber to 200 megahertz-kilometer for the step index multimode fiber. The mechanisms that limit the bandwidth are (1) modal dispersion, (2) wavelength dispersion, (3) and index profile errors due to preform fabrication. These mechanisms are functions of the fiber length.

2.1.1 MODAL DISPERSION

Modal dispersion arises from the variation in the propagation time of the multiple modes in multimode fibers. The simplest modes are those in a step index fiber. The step index fiber allows energy to propagate at only certain discrete angles relative to the fiber longitudinal axis. These angles or modes occur because they satisfy the boundary conditions for reflection at the core to cladding interface and interfere constructively in the body of the core. For angles at which energy does not propagate, the signals interfere destructively in the core or do not reflect at the core to cladding boundary. If θ is the acute angle between the longitudinal axis of the fiber and the ray path at a constructive interference angle (i.e., guided mode), then the path length for this mode is:

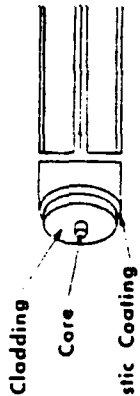
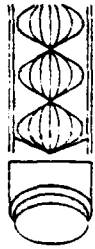

SINGLE MODE FIBER		GRADED INDEX MULTIMODE FIBER	STEP INDEX MULTIMODE FIBER
			
SOURCE	REQUIRES LASER	LASER or LED	LASER or LED
BANDWIDTH	VERY VERY LARGE > 3 GHz/Km	VERY LARGE 200 MHz - 3 GHz/Km	LARGE < 200 MHz/Km
SPLICING	VERY VERY DIFFICULT DUE TO SMALL CORE	DIFFICULT BUT DOABLE	DIFFICULT BUT DOABLE
EXAMPLE OF APPLICATION	SUBMARINE CABLE SYSTEM	TELEPHONE TRUNK BETWEEN CENTRAL OFFICES	DATA LINKS
COST	LESS EXPENSIVE	MOST EXPENSIVE	LEAST EXPENSIVE

Figure 2.1. Optical fiber configurations.

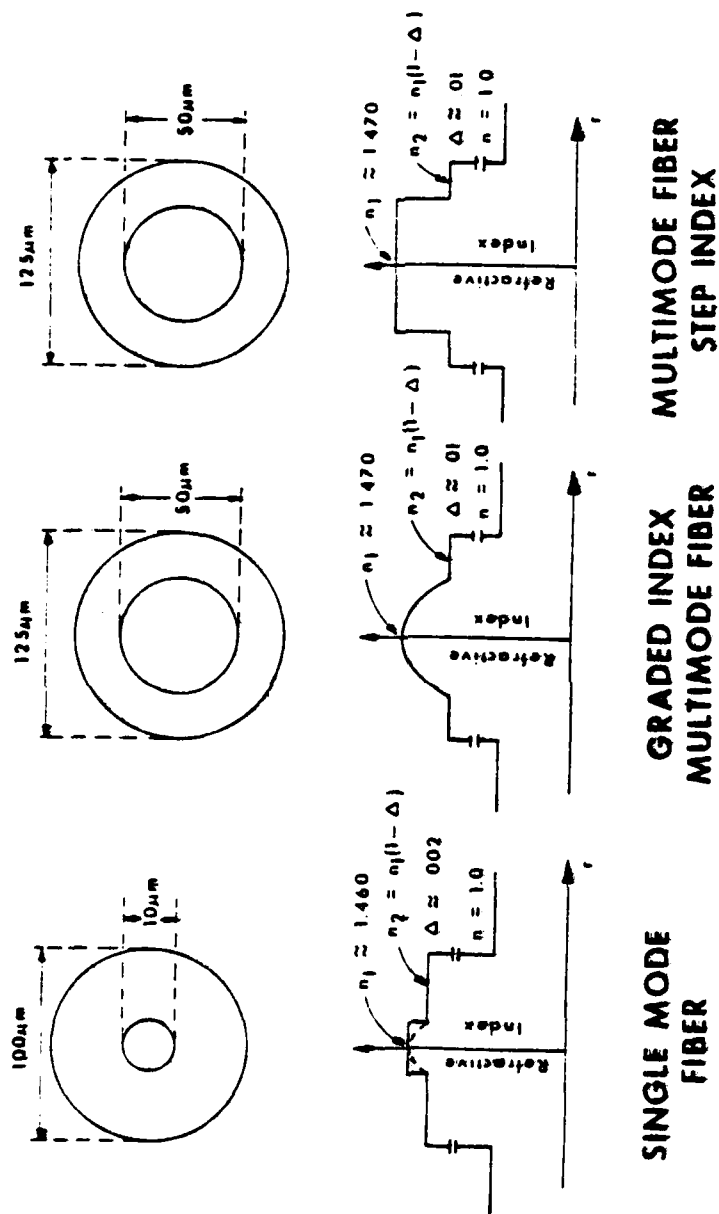


Figure 2.2. Typical optical fiber dimensions.

$$\text{Path length} = \text{axial length} / \cos \theta$$

$$PL = AL / \cos \theta \quad (1)$$

The time delay (TD) over the path length is given by:

$$TD = PL / CN$$

$$TD = AL / (\cos \theta) \cdot CN$$

C = Speed of light in vacuum

N = index of refraction

Therefore, the modal delay through the fiber is a function of the ray path angle (mode) within the fiber.

The discussion above is adequate for the modal delay in the step index fiber, but a more complicated analysis is required for the graded index fiber. This analysis is carried through in Yariv (Reference 2) for a parabolic index of refraction. The essence of the argument is: Those rays/modes that spend a large amount of time away from the longitudinal axis have the longest paths and they also spend more time where the index of refraction is low. These two effects oppose each other and approximately cancel each other. This extends the bandwidth of the graded index fiber beyond several gigahertz-kilometer versus the 200 megahertz-kilometer limit for the step index optical fiber.

2.1.2 WAVELENGTH DISPERSION

Wavelength or material dispersion is a second source of dispersion in an optical fiber. It is caused by the change of the index of refraction with the optical wavelength. If a wavepacket of wave interval $(\lambda - \Delta\lambda)$ to $(\lambda + \Delta\lambda)$ is injected into the fiber, the extreme wavelengths will travel at different velocities and there will be a near linear variation in velocity across the wavelengths of the wavepacket. The net effect is to disperse the injected wavepacket.

The wavelength dispersion for the components of this experiment was approximately ten picoseconds. This number is based on: (1) a fiber dispersion coefficient of 100 picosecond per kilometer per nanometer of source width (ps/km/nm), (2) an Injection Laser Diode (ILD) spectral width of 1 nm, and (3) an optical fiber length of 100 meters (i.e., $100 \text{ ps/km/nm} \times 1 \text{ nm} \times \frac{1}{20} \text{ km} = 10 \text{ ps}$). The wavelength dispersion is dominant. Therefore, the combined wavelength dispersion and the modal dispersion were approximately 10 picoseconds for the equipment of this project.

2.1.3 OPTICAL FIBER LOSSES

The achieved losses in optical fibers for the decades of 1960 and 1970 are shown in Figure 2.3 (Reference 1). The rapid progress from 1000 dB/km in the mid 1960s to the 1980 value of 1 dB/km was achieved by the telecommunications industry's research efforts at both the fundamental level and the manufacturing level. The primary requirement is to maintain the contaminants in the feed chemicals at levels of a few parts per million. One of the key contaminants is water, because the OH^- radical is a strong absorber in the infrared region of the spectrum.

The loss curve for a low loss silica graded index multimode fiber is shown in Figure 2.4 (Reference 1). Because the sources and detectors were first available at 0.8 to 0.9 micrometers, the first generation fiber optic systems were developed at these wavelengths. The 2 to 3 dB loss per kilometer in the 0.8 to 0.9 wavelength interval decreases to near 1 dB per kilometer near 1.2, 1.3, and 1.5 μm micrometers. The 1.3 and 1.5 wavelengths are also near a dispersion minimum. The telecommunications industry is actively researching these wavelength regions for use in long-haul communication channels. The use of longer wavelengths to exploit the advantages of low fiber loss and dispersion will require a change in optical detector-technology. Many of the detectors currently available are based upon Silicon. However, Silicon's band gap energy is not appropriate for wavelengths larger than approximately 1.1 micrometer and, therefore, a technology conversion to gallium arsenide appears to be necessary. Gallium arsenide detectors which operate at these higher wavelengths are becoming commercially available.

2.1.4 OPTICAL FIBER SELECTION

Based on early analysis, the optical fiber selected was a multimode graded index fiber by Calite[®]. This optical fiber has a bandwidth of 8 GHz for the 100 meter lengths required by this project. This exceeds the bandwidth of the ILD signal source and the Avalanche Photodiode (APD) detector.

2.1.5 OPTICAL FIBER USE

Figure 2.5 illustrates the use of optical fibers in a digital or analog communications system. The optical signal modulated by the baseband signal is

[®]Registered Trademark of E. I. DuPont

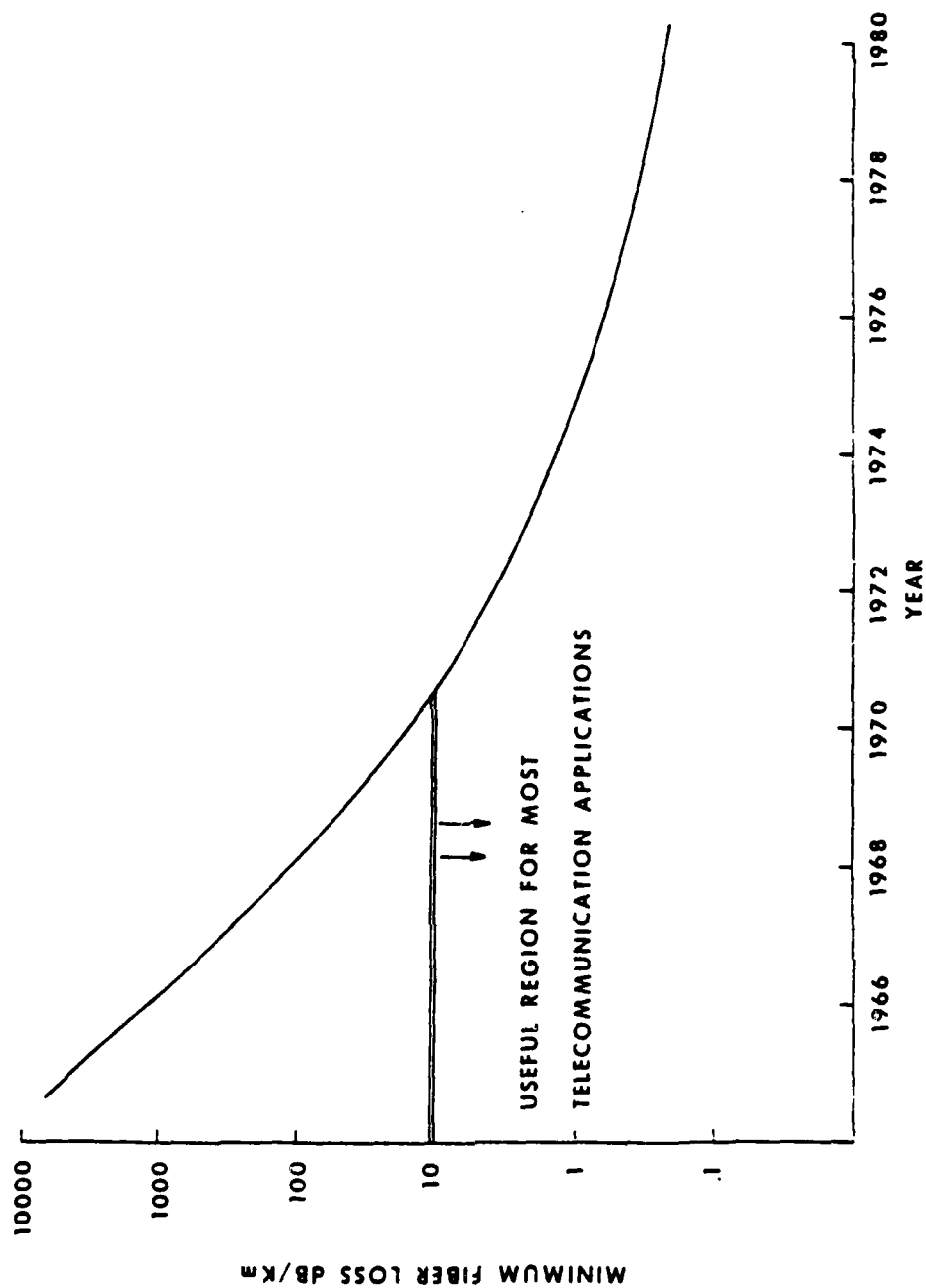


Figure 2.3. Progress in low loss fiber fabrication.

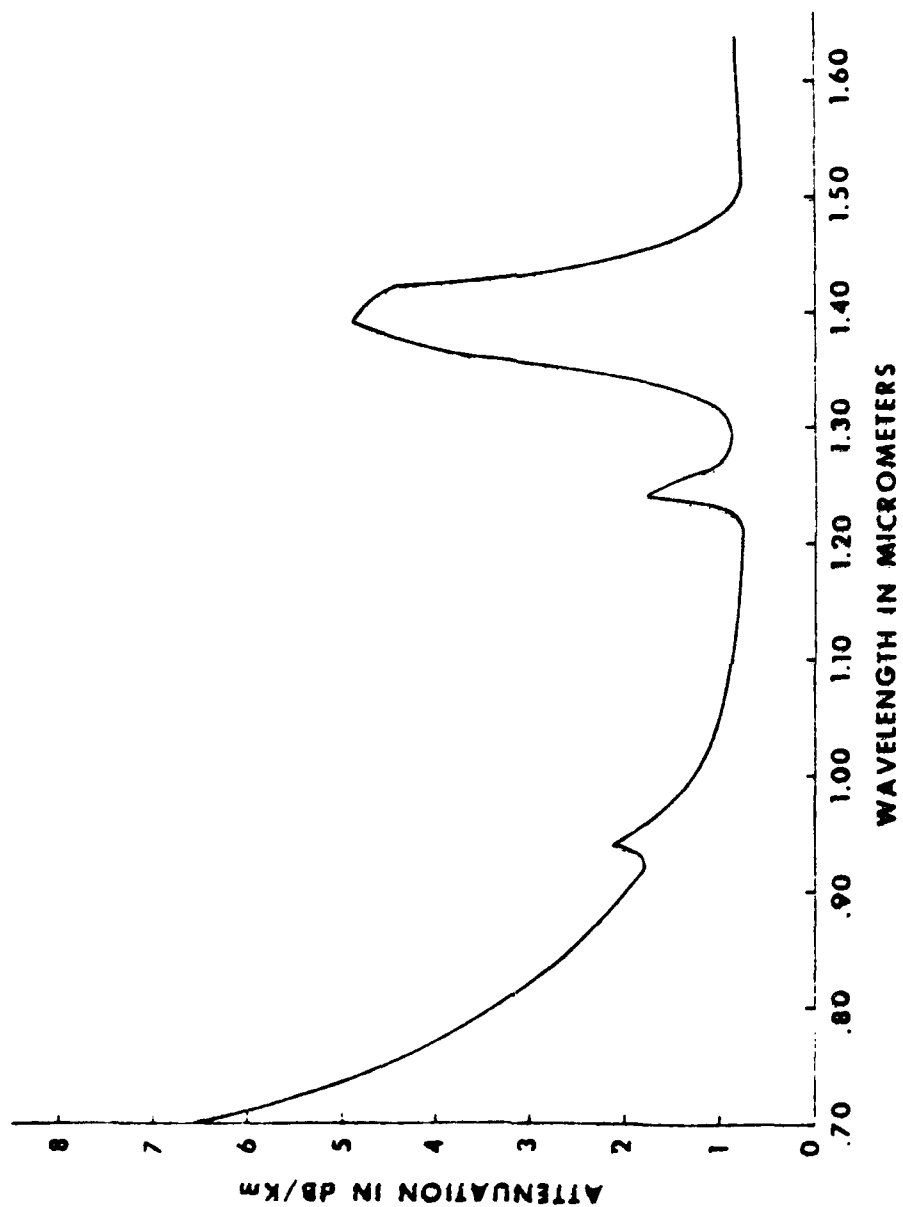


Figure 2.4. Spectral loss curve, low loss, high silica, multimode optical fiber.

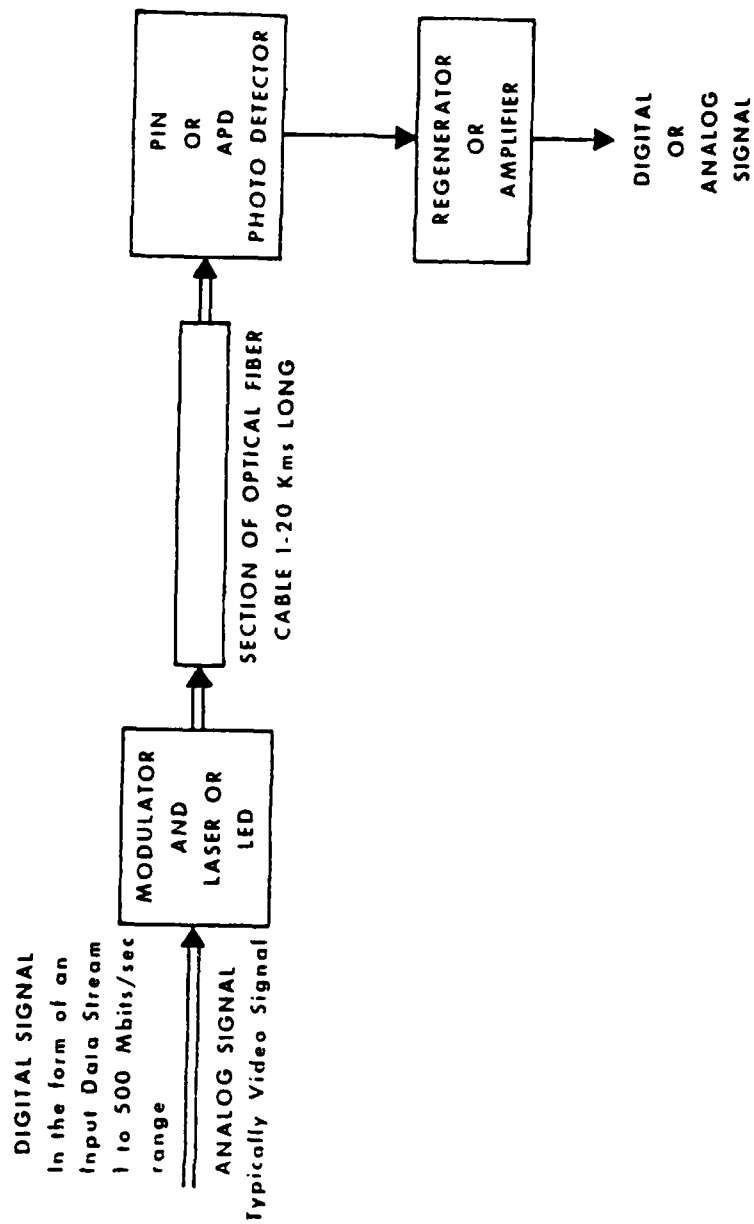


Figure 2.5. Basic building blocks of an optical fiber communication system.

transmitted through the optical fiber; at the far end of the fiber it is detected by an APD, and the recovered baseband signal is amplified or regenerated for application to downstream equipment. This same signal path architecture was used for this project and the details are described in Section 3.

2.2 LIGHT EMITTERS

There are many possible sources of light, but only two are small in size with the ability to be directly modulated. These two sources are the light emitting diode (LED) and the injection laser diode (ILD). These devices are: (1) both results of solid state technology, (2) both based on gallium arsenide (GaAs) technology, (3) both diode structures, and (4) both dependent on electron injection for light generation. Their characteristic light outputs are, however, very different.

The bandwidth of LED light is spread, relative to the bandwidth of the ILD light. This is an important difference for wide bandwidth optical fiber systems because the dispersion in optical fibers is wavelength/frequency dependent.

The ILD can be modulated at higher rates than the LED because the time required for an electromagnetic field stimulated emission of a photon is less than the time required for a spontaneous emission of a photon.

2.2.1 INJECTION LASER DIODE (ILD)

The edge emitting semiconductor injection laser diode (ILD) is the preferred optical power source for optical communication systems having bandwidths in excess of 100 MHz. The principle advantages of the ILD are the smaller emission area, higher radiance, narrower spectral width, and higher frequency response.

The earliest ILDs were Fabry-Perot cavities consisting of rectangular GaAs chips that contained a P-N junction oriented perpendicular to the chips cleaved ends. These cleaved ends acted as partial mirrors (Figure 2.6). Light is generated in this device by the injection of electrons into the P-region with subsequent radiative recombinations in the active region. This device is not a practical laser because of the high current densities required ($>10^4$ A/cm²).

The homojunction laser was successively replaced by single heterojunction, double heterojunction, and the double heterojunction stripe lasers (Reference 3). The objectives

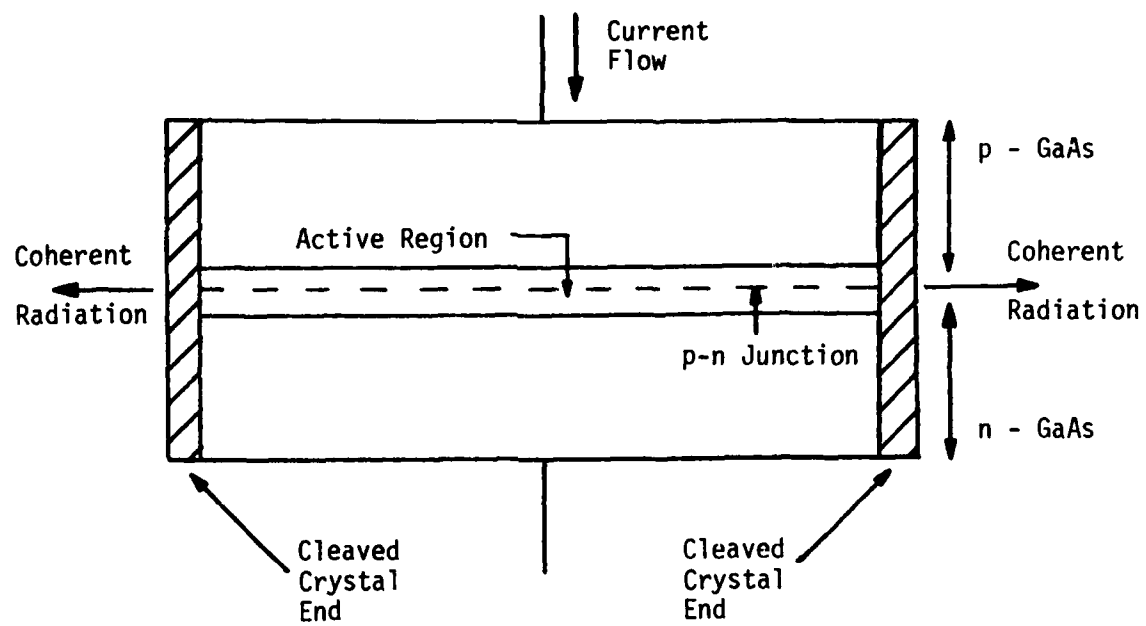


Figure 2.6 Homojunction ILD schematic.

of these designs were to: (1) reduce the required injection current, and (2) confine the light generation to a well defined region of the laser. Concurrent with these structural designs, the ILD manufacturing processes were improved to increase the yield and the operational life of these devices. The resultant two-dimensional stripe laser exhibits a laser threshold current of 100 mA or less. These devices exhibited a non-linear response to drive current. The solution to the non-linearity problem of the stripe, or lateral light confinement by current confining techniques, is to use a physical waveguide structure along the plane of the P-N junction. The replacement of the gain induced lateral waveguide by the physical lateral waveguide leads to a different type of ILD called the buried-heterostructure laser (Figure 2.7).

The buried-heterostructure ILD is the laser type selected for this project. The device has proven satisfactory and, therefore, other lasers were not reviewed in any detail. The current-voltage characteristics and the light output versus current characteristics of a typical ILD are shown in Figure 2.8. The prime characteristic required by this project is the linearity of the light curve relative to a bias point of approximately 100 milliamperes. This linear characteristic and the bandwidth of the device allows phase information to be maintained for RF modulations of several gigahertz.

2.2.2 LIGHT EMITTING DIODE (LED)

The light emitting diode is an inexpensive and reliable source of noncoherent optical power. LED's are classed as planar, dome, edge, and Burrus. The characteristics of these classes are compared in Tables 1 and 2 from Reference 3.

The Burrus diode is the most suitable for fiber optic communications because it allows close direct coupling between the light emitting volume of the diode and an optical fiber. A LED of the Burrus type is illustrated in Figure 2.9.

Useful commercial LED's are exemplified mainly by GaAs and GaAlAs semiconductor devices. These materials meet the three prerequisites of: (1) photon-emitting transition, (2) P-N junction formation and (3) appropriate bandgap energy. The photon-emitting transition is, obviously, fundamental. The P-N junction formation is required before an excited electron can be created by current injection and swept into the P region for recombination. The bandgap energy must be correct for the generation of wavelengths in the low loss regions of optical fibers. These low loss regions exist at several "windows" in the 800 to 1600 nanometer wavelength interval.

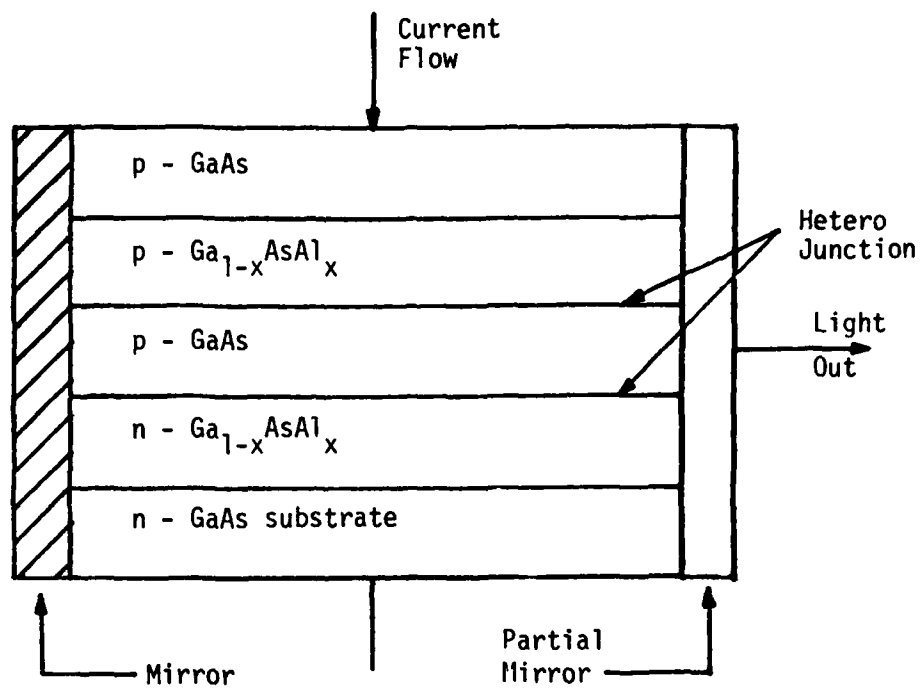
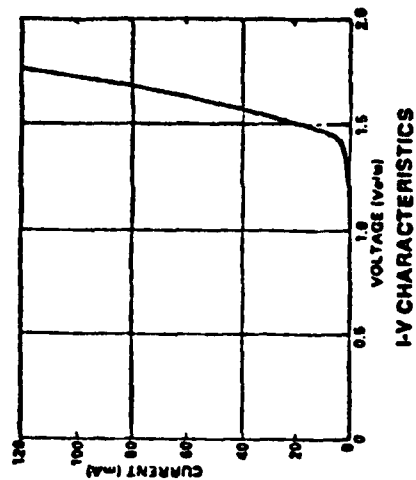
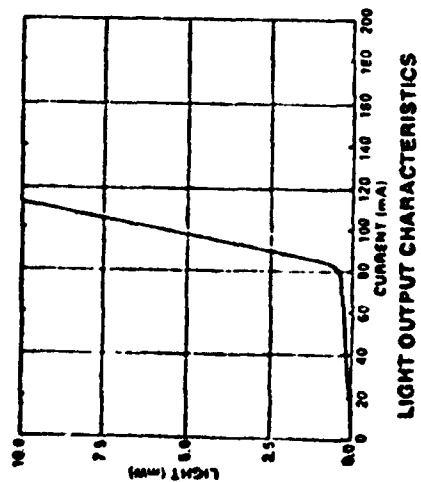


Figure 2.7 Heterostructure LED schematic.



- Bias Current - 100 mA
- Average Optical Power - 5 mW
- Modulation Index - .5
- Peak Optical Power - 7.5 mW
- Minimum Optical Power - 2.5 mW
- Bias Voltage - 1.75 Volts

Figure 2.8 Typical ILD characteristics.

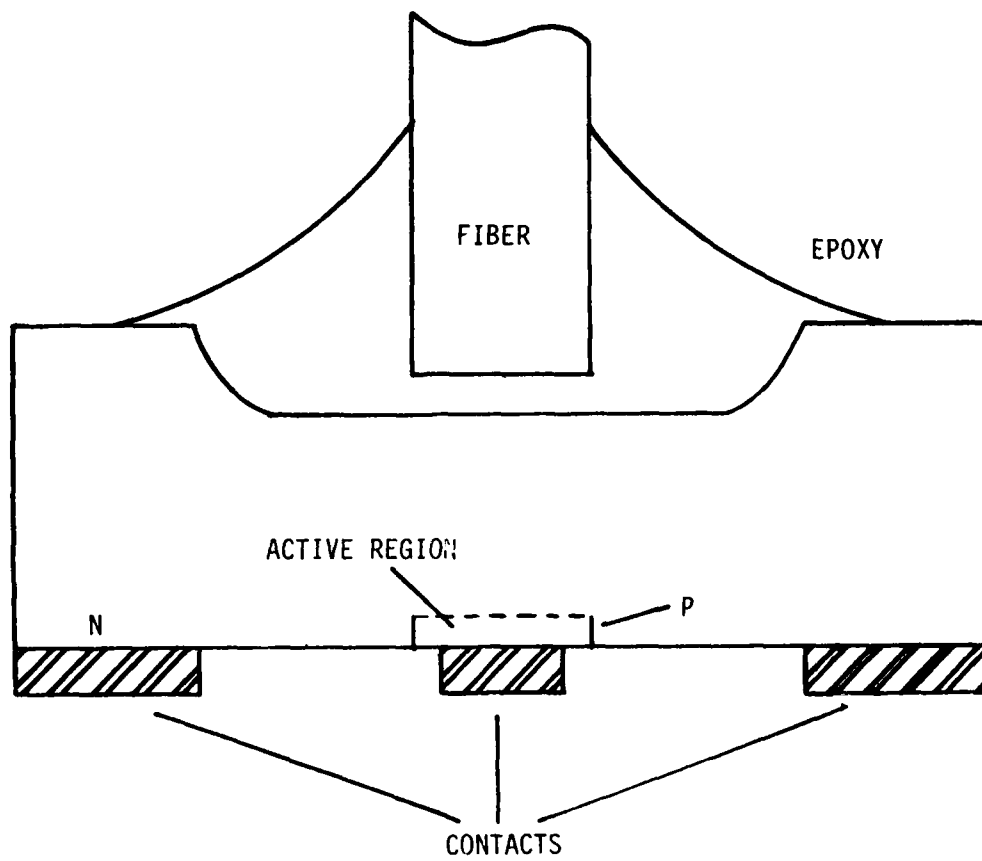


Figure 2.9 Burrus-type LED.

TABLE 1
COMPARISON OF THE PRESENT CHARACTERISTICS OF THE MAJOR CLASSES
OF LIGHT-EMITTING DIODES
(Reference 1)

<u>Characteristic</u>	<u>LED type</u>			
	<u>Planar</u>	<u>Dome</u>	<u>Edge</u>	<u>Burrus</u>
Active area (mm ²)	8-15	6-12	2-4	0.01-0.05
On-axis radiance at 100 mA (W/sr cm ²)	0.2-0.5	0.2-0.5	0.3-1.0	6-60
Total radiated power at 100 mA (mW)	1-3	2-4	1-3	0.5-10
Power coupled into single fiber (μW)	0.1-1.0	0.5-5	1-10	30-300
Half-power emission angle (degrees)	±5	±10	±15	±45
External quantum efficiency (%)	1-5	30-40	1-5	45-55

The advantages and disadvantages of these classes are compared in Table 2.

TABLE 2
COMPARISON OF THE ADVANTAGES AND DISADVANTAGES OF THE MAJOR
CLASSES OF LIGHT-EMITTING DIODES
(Reference 1)

<u>LED TYPE</u>	<u>ADVANTAGES</u>	<u>DISADVANTAGES</u>
Planar	potentially highest bandwidth and data transfer rate	largest emitting area lowest emission radiance
	easy fabrication and packaging	smallest coupled power into fiber
Dome	high radiated power	difficult fabrication
	well suited for coupling into bundles	requires parabolic reflector for improved radiance
	easy collection and focusing within small beam angle	
	small packed aperture diameter	
Edge	very large radiance	emission from side rather than top of device; hence, difficult packaging approach
	well suited for coupling into bundles	
	smallest packed aperture diameter of the low-radiance types	requires elliptical reflector for improved radiance
Burros	smallest emission area	unsuitable for fiber bundles
	largest half-power emission angle	double-heterojunction structure requires complex fabrication process
	high current density	
	no need for collimating optics or reflectors	
	allows mounting in stud package	

The best commercial LED's have an upper limit frequency response of approximately 100 MHz. This frequency response is inadequate for this project where at least a 1 GHz frequency responses is desired. In addition, LED's have a spectral spread which interacts with the graded index multimode fiber to produce unacceptable dispersions. For those reasons, LED's were not acceptable in the experimental phase shift device.

2.3 DETECTORS

The purpose of the optical detector is to output an electrical current which is proportional to the light intensity incident on the active region of the detector. The optical detector is a light-intensity to electrical-current transducer.

The technology bases for common optical detectors are silicon, germanium, and composite material (GaAs and GaAlAs). The silicon optical detector dominates in the 800 to 1100 nanometer spectral region because: (1) it is a sensitive detector of light in this region, and (2) the transistor industry created a mature technology based on silicon. Germanium and composite materials offer more sensitivity than silicon above 1100 nanometers. It is judged probable that composite material detectors will be the preferred technology in the 1100 to 1600 nanometer spectral region.

The following two subsections discuss the positive-intrinsic-negative (PIN) diode and the avalanche photodiode, both of which are commonly used in communications systems.

2.3.1 PIN DIODE

A schematic of a PIN (positive-intrinsic-negative) diode is shown in Figure 2.10. The step-by-step general description of the functions of these diodes are:

- (1) The diode is back biased by the external voltage.
- (2) The back bias creates a charge carrier depletion region in the 'I' region of the diode. The strength of the 'E' field across the depletion region is dependent on the width of the depletion region and the applied voltage.
- (3) On a statistical basis, the light photons at wavelength λ produce hole-electron pairs in the 'I' region provided that the band gap energy of the 'I' material is matched to the photon energy ($E_p = h c / \lambda$).
- (4) The 'E' field in the 'I' region sweeps the holes and electrons out of the 'I' region toward their opposite polarity electrodes.

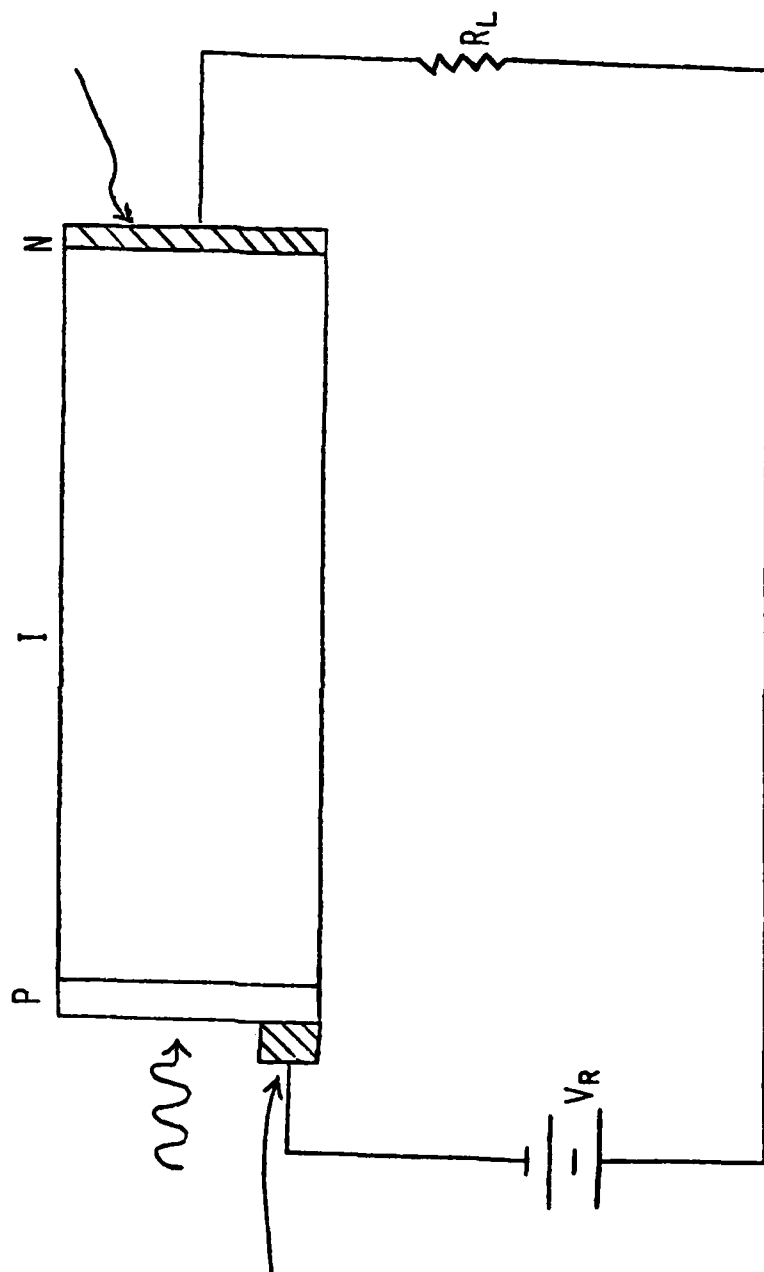


Figure 2.10 PIN photodiode schematic.

- (5) The positive and negative charge accumulations on the PIN electrodes induces an equalizing current through the external circuit.
- (b) The external current is a measure of the light intensity applied to the PIN.

The photodetector bandwidth should be approximately 2 GHz to support the system bandwidth goal of 1 GHz. Adapting material from Reference 4, the approximate rule is that the bandwidth of the photodetector is:

$$BW = (1/3) (1/\text{Rise Time}) = (1/3) (1/RT) \quad (3)$$

The required photodiode rise time is approximately 166 ps. The rise time of a photodetector is controlled by the width (W) of the depletion region (low carrier concentration region) where W is given by:

$$W = \frac{2\epsilon V_K^{1/2}}{q N_D} \quad (4)$$

- ϵ = dielectric constant
- q = charge of electron
- N_D = electron concentration in the N layer of the PIN structure
- V_K = applied reverse bias

The capacitance of the diode is estimated by the equation:

$$C = \epsilon A/W \quad (5)$$

A = cross-sectional area of the diode

The resistance of the diode is composed of the bulk resistance of the N layer and the spreading resistance of the P region. Commercially available photodiodes are highly doped and exhibit equivalent resistance of approximately 2 ohms. Therefore, the typical load resistance (R_L) of 50 ohms will dominate and the RC time constant will be:

$$T_{RC} = 2.2 R_L C \quad (6)$$

The other rise time controlling effect is the diffusion time of the electrons through the depletion region. This time constant is given by:

$$T_D = 0.79 W/V_s \quad (7)$$

V_s = electron saturation velocity

The frequency response is maximized when T_{RC} equals T_D or the total rise time is:

$$T^2 = T_D^2 + T_{RC}^2 = 2 T_D^2 = 2 T_{RC}^2$$

$$T = 1.414 T_{RC} = 1.414 T_D$$

$$T = 1.11 W/V_s \quad (8)$$

2.3.2 AVALANCHE PHOTODIODE (APD)

The mechanisms for current generation by light are the same in the APD and the PIN. The bias voltage of the APD is greater than the PIN bias voltage. Electron-hole pairs generated by the incident photons are accelerated by the APD's large electric field, and additional electron-hole pairs are formed by impact ionization. The direct and the impact ionization electron-hole pairs diffuse to the electrodes of the diode and induce the electric current in the external circuit. A gain is achieved in the APD by the impact ionization process.

Commercial APD's have: (1) bandwidths to 5 GHz, (2) sensitivities of 10 to 20 amperes of electrical current output per watt of optical energy input, and (3) a thermo-electric cooler to counter the APD's sensitivity to temperature. The APD's impact ionization voltage is adjusted to maintain full sensitivity without inducing current in the absence of light. Because of the full sensitivity adjustment, temperature changes and noise spikes could cause spontaneous electron excitation.

2.3.3 COMPARISON BETWEEN APD AND PIN PHOTODIODES

The APD is more sensitive than PIN photodiodes at wavelengths less than 1000 nm. The PIN photodiode is: (1) not as sensitive to temperature changes, (2) easier to package and implement, and (3) generally less expensive. The cheapest PIN photodiodes are \$10.00; highest performance APD's cost several thousand dollars. The bandwidth difference, however, is roughly equivalent to the price difference. These comparisons are for wavelengths less than 1000 nm. Performance differences for wavelengths from 1000 to 1600 nm will be discussed next.

2.3.4 LONGER WAVELENGTH PERFORMANCE AND FUTURE DEVELOPMENTS

Longer wavelength fiber optic systems are more attractive for communications systems (Reference 1) because: (1) fiber loss is less than 1 dB/km at 1200 to 1600 nm as opposed to 2 to 3 dB/km at 850 nm, (2) bandwidths of fibers are larger, and (3) emitters have longer lifetimes.

Silicon detectors bandgap energy limits them to wavelengths below 1100 nm. Germanium APD's have been used at the longer wavelengths, however, these APD's exhibit high shot noise. New compounds of indium, gallium, arsenic, and phosphorus are being used to develop better long wavelength detectors. PIN photodiodes are much easier to produce, and they perform almost as well as APD's at these wavelengths. Preamplifiers have been added to the PIN photodiodes to improve the responsivity. Antireflective coatings have been added and better coupling lenses have been developed to improve the amount of light available at the surface of the diode for conversion to electrical current.

2.3.5 APPLICATION TO CURRENT PROJECT

The most critical detector parameter for the current project is bandwidth. Because the fiber lengths associated with the phase shifter are short, dispersion of signals in the fiber and attenuation will be negligible and there is no advantage in going to the longer wavelengths. The shorter wavelength detector technology is much more developed, and it makes sense to choose the shorter wavelength (850 nm) APD's which have the required GHz bandwidths.

2.4 OPTICAL SWITCHES

A completely satisfactory optical switch for this project would exhibit: (1) Insertion Loss of 1 dB, (2) Switch speeds of 1 MHz, (3) Channel isolation of 40 dB, (4) No sensitivity to multiple modes, and (5) No sensitivity to polarization of the guided waves. No completely satisfactory optical switch was available at any point in this project life cycle. The descriptions of switches presented in this subsection are a result of the search for a suitable optical switch.

2.4.1 MECHANICAL AND ELECTROMECHANICAL SWITCHES

Mechanical switches have been realized in numerous forms. Some are commercially available. Though they often have low attenuation, they can be fragile, slow, and bulky.

2.4.1.1 Bell Labs Mechanical Fiber Optic Switch (Reference 5)

This switch uses an extension of the alignment principle employed in the loose tube splice. Fibers are moved into an inside corner of a tube with a square cross section. They are well aligned and couple light with low losses. Index matching fluid in the splice region further reduces loss. The switch is shown in Figure 2.11. A single fiber is free to move in the central region of a tube and is fixed at the end of the tube. Slight bending of the tube snaps the free end of the fiber into a corner of the tube, aligning it with the selected fixed fiber. By changing the direction of the bend, the input fiber moves to a different corner, providing positive switching with four switch output positions.

This switch is a promising design for practical low speed mechanical optical switches, and this switch can be made with either monomode or multimode fibers. It has four possible outputs for one input. The fibers are totally encapsulated, and no power is required to hold a given position. This switch has a lower insertion loss than any mechanical switch previously reported (< 0.5 dB for multimode fibers) and has excellent repeatability, durability, and crosstalk performance. It also requires inexpensive mechanical parts for its construction.

2.4.1.2 Nippon Electric Company (NEC) Mechanical Switch (Reference 6)

Two switches now commercially available for around 600-700 Dollars are the NEC fiber optic switches. They employ moving prisms instead of a moving fiber. Shown in

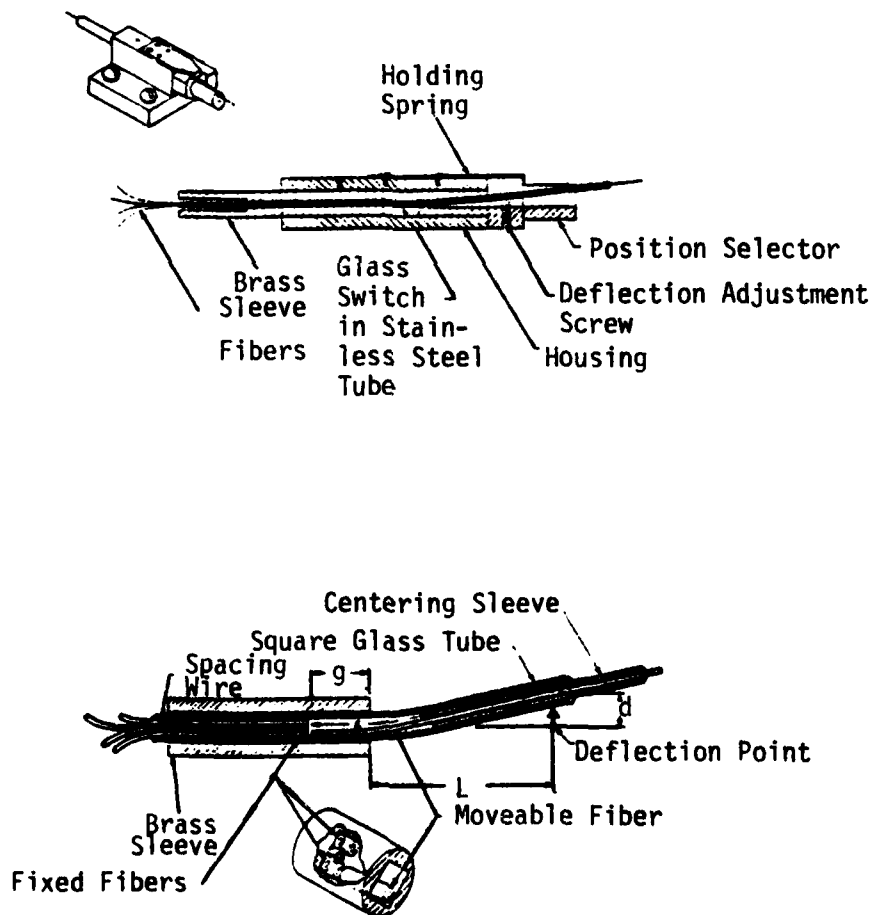
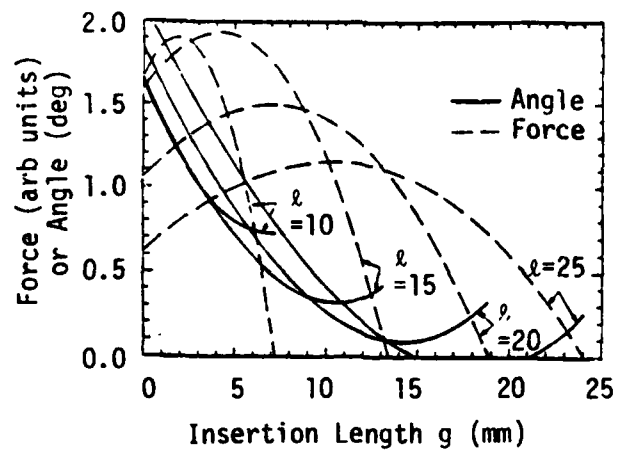


Figure 2.11 Bell Laboratories one to four switch.

Figure 2.12, are the 1x2 and 2x2 optical switches which employ moving glass prisms to divert light from one port to another. The performance of these switches is listed in Table 3 underneath their schematics. The advantage of this switch is that accurate displacement of the prism is not required.

The NEC 1x2 mechanical fiber optic switch was used in the phase shifter built by Georgia Institute of Technology. This device was switched hundreds of times with no increase in insertion loss. This switch is a feasible choice for devices with switching speeds above 4 milliseconds.

2.4.1.3 IBM Single-Pole Double-Throw Low Loss Fiber Optic Switch (Reference 7)

In this mechanical switch, the end of an optic fiber is moved between two predetermined positions by the mechanical movement of two wire conductors which cross each other and the fiber; the mechanical movement of the conductors being caused by current flowing through the conductors in the presence of four magnetic fields. The predetermined positions of the fiber are defined by fixed elements which limit the range of movement of the fiber. Output fibers lie at both predetermined positions. The fibers move to a seated position when current passes through wire conductors in a given direction while the loop is in a magnetic field. A simple reversal of current returns the switch to the original state.

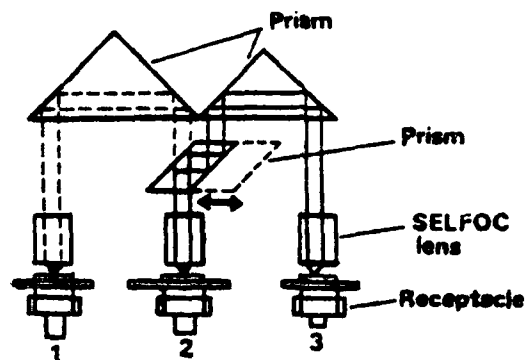
2.4.1.4 IBM Field-Assisted Fiber Optic Switch (Reference 8)

An alternate method used by IBM employs the coating of a multimode or single mode fiber with a metal such as chromium or titanium. The coated fiber is then deflected between two positions using electrostatic force. (Figure 2.13)

Other IBM mechanical F/O switches use the electrostatic holding force to move an optical fiber between two different positions defined by the alignment structure which also positions alternative output fibers. The electrostatic force is applied to the fiber, the fiber is pulled to an upper V-groove and aligned with the mating fiber. The fiber's natural elasticity will return it to the bottom position of the V-groove and align it with the corresponding fixed fiber.

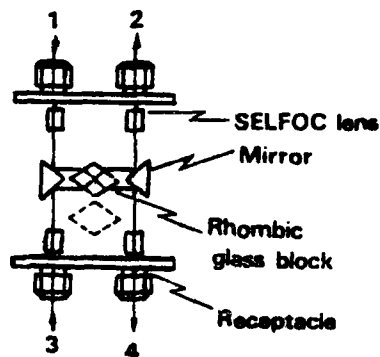
2.4.1.5 Mechanical One-To-Many Fiber Optic Switch (Reference 9)

This mechanical multimode fiber optic switch (Figure 2.14) uses a spherical mirror mounted on a galvanometer to switch multimode light from one fiber to many fibers



1 x 2 Optical Switch

Figure 2.12 NEC prism switch.



2 x 2 Optical Switch.

TABLE 3. NEC SWITCH CHARACTERISTICS

Type	1 x 2	2 x 2
Insertion Loss	1.5 dB	
Isolation	80 dB	
Reproducibility	0.02 dB	0.02 dB
Switching Speed	4mS	6mS
Life	10 ⁶ times	
Dimensions (mm)	22x30x55	33x22x37
Weight	100g	80g

Fiber Optic Switch

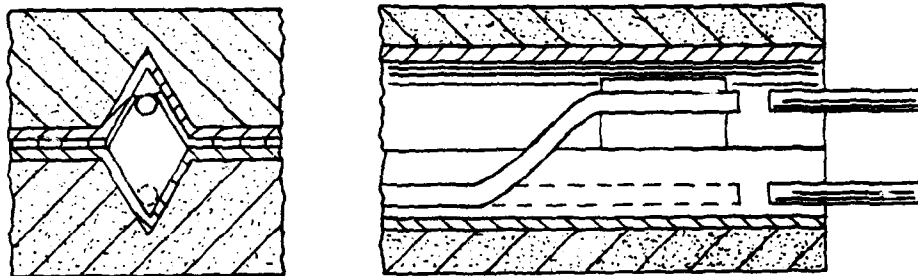


Figure 2.13. IBM field assisted switch.

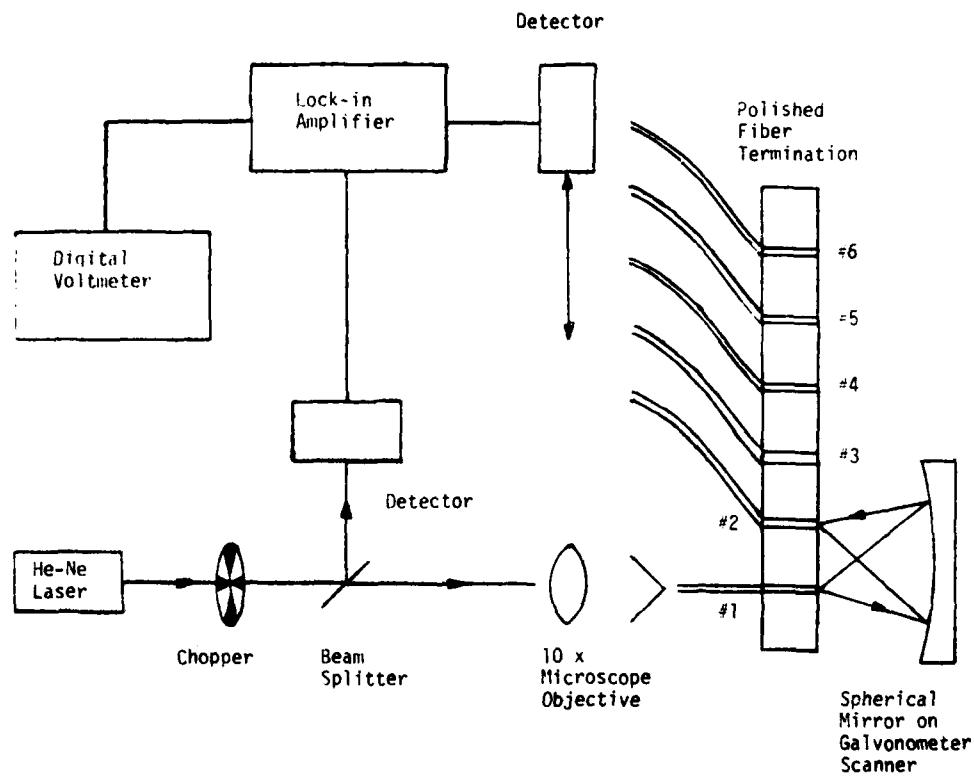


Figure 2.14. One-to-many switch.

located in a linear array in the imaging plane of the mirror. Characteristics of this switch include:

1. optical insertion loss less than 1.5 dB
2. optical isolation greater than 37 dB
3. switching rate of 300 Hz
4. potential for greater than one-to-ten fiber switchings
5. little degradation of device characteristics after 10^6 switchings

2.4.2 ELECTRO-OPTICAL SWITCHES

Electro-optical switching depends on changes in refractive index or changes in scattering caused by the application of an electric field to a material. The switches can be divided into those based on the pockel effect and those based upon optical scattering. The pockel effect is an index of refraction change that occurs with applied electrostatic field. This occurs in electrooptically active solid state materials. An optical scattering change can be induced in certain mixtures of liquids and long chain molecules. The orientation of the long chain molecules changes with the applied electrostatic field. This optical scattering is observed in liquid crystals.

Extensive research is being pursued for the development of electro-optical switches. The main research objectives are, gigahertz speed, efficient (> 99-percent) modulation depth, low voltage, and low insertion loss. Competing against the electro-optical switch are switches based on acousto-optic effects in the same ferroelectrics (LiNbO_3 , LiTaO_3) and semiconductors (GaAs , GaAsSb) that electro-optic switches are based upon.

Most electro-optic switches are single-mode switches. Development of single-mode switches dominate because these switches require two or three orders of magnitude less driving power. In addition, many switch mechanisms are only marginally functional for multimode fibers. This occurs because many devices depend on focusing of light and each mode focuses differently.

The basic configuration used for these single-mode switches is the electro-optic directional coupler (EDC). In the EDC device, two parallel guides are positioned very close (within a wavelength of light) to allow transfer of guided energy between them. Electric fields applied via electrodes placed in the vicinity of the guides vary the

coupling between the guides and, therefore, the energy transferred between the guides. EDC switches have been fabricated in LiNbO_3 using Ti indiffused waveguides, in GaAs optical stripline guides, and rib guides of MOS or Schottky barrier types. The GaAs directional coupler switch has provided up to 99.7% light crossover by using two pairs of differently polarized electrodes. GaAs rib guide switches have provided extinction ratios of 30 dB with capacitance values below 2 picofarad. Bandwidths up to 1 GHz have been achieved at the wavelengths of $1.15 \mu\text{m}$ with 8.2 dB insertion (power) loss using an LiNbO_3 EDC switch (Reference 10).

Switches with high extinction ratios (> 20 dB) and low operating voltages ($< 5\text{V}$) can be produced. The large insertion loss of the device must be reduced for practical communication switches. The dominant losses are light input/output coupling losses. This is especially true for single-mode devices where the coupling to and from the single mode fibers is lossy. Two methods for coupling guides to monomode fibers are: (1) evanescent coupling, and (2) end-fire coupling. Coupling efficiencies as high as 80% have been predicted and experimental values as high as 65% have been obtained.¹⁰ A practical way for fiber-to-indiffused guide alignment is the use of etched channels in Si substrates and inverting the LiNbO_3 substrate on the same Si substrate (called flip chip method). This approach was proposed for a four port data switching terminal module involving a high speed EDC switch in LiNbO_3 chip (Figure 2.15). An efficiency value of 47% was reported for fiber-to-guide coupling in this configuration. Coupling of LiNbO_3 single-mode devices to single mode fibers requires that the switches be independent of polarization because light out of a single-mode fiber is arbitrarily polarized. A polarization independent EDC switch has been demonstrated.

A 4x4 switching network (Figure 2.16) has been achieved by combining five switches on the same LiNbO_3 substrate, and crosstalk levels of 18 dB were reported.¹⁰ The first semiconductor switch matrix was realized using the GaAs rib-guide EDC configuration. The structure was a 2x4 network involving three EDC switches with 10 dB crosstalk levels and 15 V needed for switching. Although GaAs has lower electro-optic coefficients than LiNbO_3 , its use for switching networks is very attractive since it offers the possibility of monolithic integration of laser sources and switches.

2.4.2.1 Electro-Optic Switches as Coupled Wave Devices

Switched directional couplers, stepped $\Delta\beta$ couplers, and bistable $\Delta\beta$ couplers belong to the class of coupled wave devices. Coupled wave devices use guiding

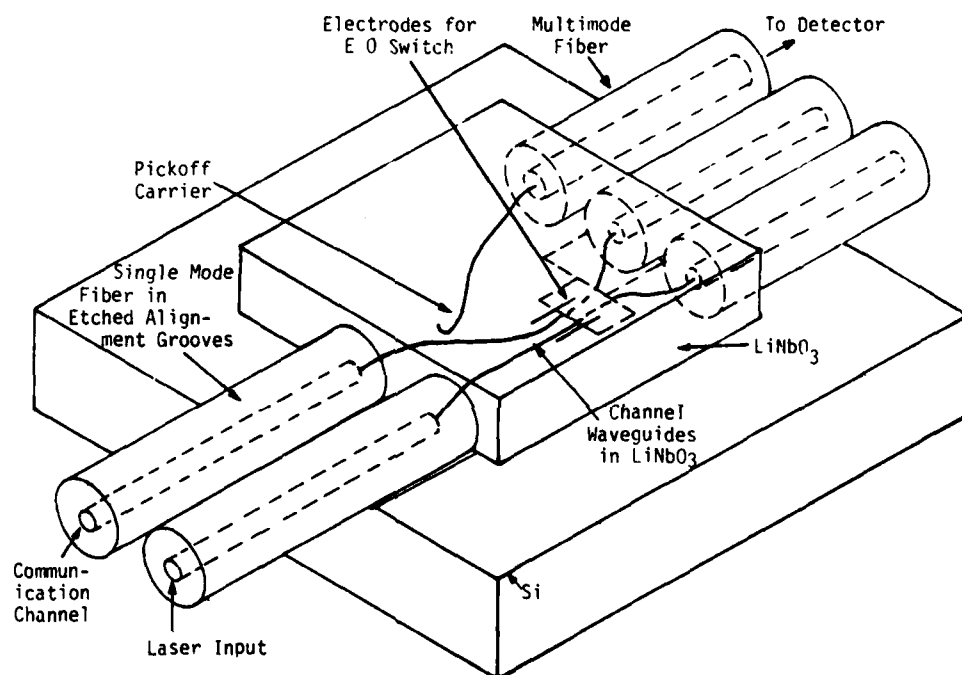


Figure 2.15. Four port EDC switch.

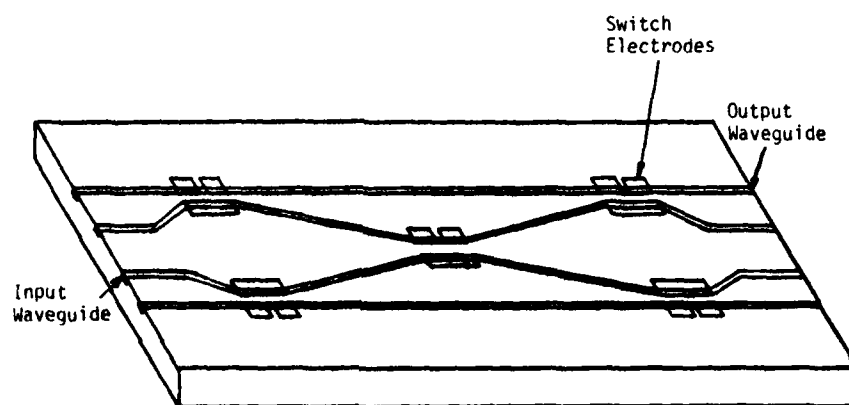


Figure 2.16. 4 x 4 switching network.

structures to support two decoupled modes that propagate freely and remain uncoupled as long as the structure is not disturbed. Assume two waves R and S (reference and signal). A perturbation in the original structure leads to a coupling of the two waves and to an energy exchange. An important requirement for a significant interaction between R and S is their synchronism or "phase matching." The simplest case requires equality of the propagation constants β_s and β_r of the two waves:

$$\beta_r = \beta_s \quad (9)$$

Two different types of coupled interactions are distinguished: codirectional interactions and contradirectional interactions. Codirectional interactions occur between two forward (or two backward) waves and contradirectional interactions occur between one forward and one backward wave.

The exchange of energy between two codirectional waves of complex amplitude R and S is described by the coupled wave equations:

$$R' - j\delta R = -jKS \quad (10)$$

$$S' - j\delta S = -jKR \quad (11)$$

prime indicates differentiation with respect to propagation distance z

K = coupling constant

δ = a normalized frequency which measures deviation from synchronism

At boundary conditions $R(0) = 1$ and $S(0) = 0$, the solutions to the coupled wave equations are:

$$S(z) = -jK \sin(z\sqrt{K^2 + \delta^2}) / \sqrt{K^2 + \delta^2} \quad (12)$$

$$R(z) = \cos(z\sqrt{K^2 + \delta^2}) + j\delta \sin(z\sqrt{K^2 + \delta^2}) / \sqrt{K^2 + \delta^2} \quad (13)$$

For the synchronized case ($\delta = 0$; phase matched waves), there is a sinusoidal exchange of energy between R and S.

$$S(z) = -j \sin(Kz) \quad R(z) = \cos(Kz) \quad (14)$$

2.4.2.2 Integrated Optics Directional Coupler

An integrated optics version of a directional coupler consists of two strip guides which are close and parallel over an interaction distance (L) (Figure 2.17). Synchronism for this device is determined by the difference between the propagation constants β_R and β_S of the two modes in the two strip guides.

$$2\delta = \beta_R - \beta_S = \Delta\beta_{RS} \quad (15)$$

The method used for energy transfer is called the $\Delta\beta$ technique, and δ is the normalized frequency which measures deviation from synchronism. The coupling constant (K) of a rectangular dielectric waveguide is an exponential function of the waveguide separation (C) and the decay constant (γ_y) in the film plane

$$K \propto \exp(-\gamma_y C) \quad (16)$$

Typical conversion lengths range from 1 mm to several millimeters. Full transfer of energy from one guide to another is achieved in an interaction length equal to d, where $d = \pi/2k$ for synchronized waves ($\delta = 0$). Experimental directional couplers have been prepared using a variety of structures and material systems, including ferroelectric crystals (LiNbO_3) and semiconductors (GaAs).

A switched directional coupler is simply a directional coupler controlled electrically to switch guided light from one waveguide to another. The control is through variation of the phase constants ($\Delta\beta$) of the dual waveguide structure.

In an electro-optic material, an applied electric field E induces a refractive index change n' of magnitude given by

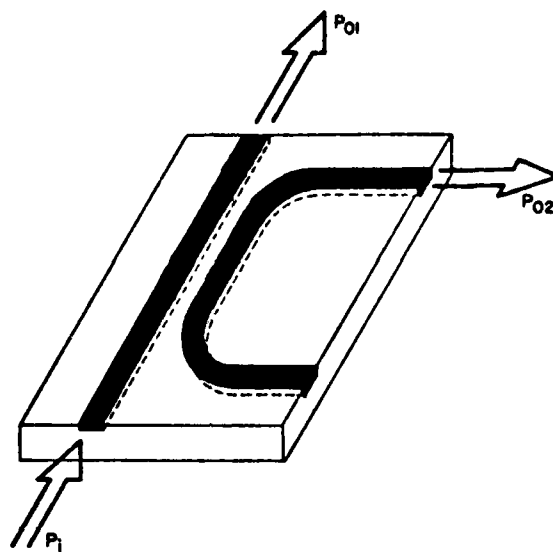


Figure 2.17 Integrated Optics Version of the Optical Directional Coupler

$$\Delta n' = -n^3 r' E/2 \quad (17)$$

n' = effective refractive index of material

r' = effective electro-optic coefficient

E = magnitude of electric field (by voltage)

When the field is applied to the two guides with opposite polarity an induced phase mismatch occurs,

$$2\delta = \Delta\beta \approx \frac{2\pi}{\lambda} \Delta n = \frac{2\pi}{\lambda} (n')^3 r' (E/2) \quad (18)$$

λ = free space wavelength

If the coupler is fabricated with an interaction length L (L = actual length of switch in which coupling occurs) which is equal to an odd multiple of the conversion length d , a complete transfer of light from one guiding structure to the other occurs if the guides are phase matched. An applied voltage will induce a phase mismatch $2\delta = \Delta\beta$ which spoils the interaction and leads to zero transfer of light. This spoiling of light transfer is the basis of the EDC fiber optic switch; light can be switched from one port to another.

2.4.2.3 Stepped - Delta Beta Coupler

It is difficult to fabricate the interaction length L and the conversion length d of switched directional couplers with the accuracy necessary for complete transfer of light. Electrical control cannot compensate for fabrication errors in the directional coupler switch. A configuration called the stepped delta beta coupler allows electrical adjustment for essentially complete light transfer. The electrodes are split into two sections, and voltages of opposite polarity are applied to the two sections, inducing mismatch of opposite sign. This switch can be analyzed by casting the coupled wave solutions for $S(z)$, $R(z)$ into matrix form and multiplying the appropriate matrices of the individual sections. The condition for the crossover state of this coupler is

$$\frac{k^2}{k^2 + \delta^2} \sin^2 \frac{L}{2} \sqrt{k^2 + \delta^2} = \frac{1}{2} \quad (19)$$

and the zero transfer state is obtained if

$$L/d = 2(2\gamma + 1) \quad (20)$$

where γ is an integer.

The stepped delta beta configuration has allowed the construction of optical switches with a crossover ratio of 400:1 (26 dB isolation) using Ti diffused strip guides in LiNbO_3 (Reference 11). This is quite an improvement over single delta beta configurations where the best isolation obtained for the two switch states was only 13 dB.¹¹

2.4.2.4 Bistable Delta Beta Coupler

The bistable delta beta coupler is an optical 4-port bistable switch which consists of an alternating delta beta coupler and an electrical feedback loop. In this loop, a portion of the zero transfer optical power is detected (by a silicon PIN photodiode, APD, or avalanche photomultiplier), and the voltage proportional to this power is applied to the control electrode of the delta beta coupler. This arrangement allows optically controlled switching between the crossover and the zero-transfer state of the coupler. An experimental device of this type was realized in Ti:LiNbO_3 ^{*} and had switching time of about 300 μs and optical switching energy of 3 picojoule (pj).¹¹

2.4.3 ELECTRO-OPTIC MULTIMODE SWITCHES

Single-mode devices have received special attention mainly because they require much less drive power per unit bandwidth than bulk devices. The disadvantage of single mode waveguide devices is that it is difficult to achieve efficient coupling to devices and components of different dimensions and geometries. The solution is to construct a device that can operate in several modes.

Several constructions are used for electro-optic multimode switches. The first, uses the concept of imaging in multimode waveguides. This device is capable of modulating or switching with relatively low drive voltage a laser beam with a few low order modes. It is also realizable in various sizes and geometries. Unfortunately, it can only be used at the light source since multimode fibers will break a single laser mode into

* Ti:LiNbO_3 is the symbol which represents Titanium indiffused Lithium Niobate.

hundreds of modes within a few feet. This switching effect has been obtained in several active waveguides of various widths and lengths with 8-20 volt drive and 13-20 dB extinction ratios (References 12 and 13). Megahertz speeds have also been observed.

The second type of electro-optical multimode switch uses the quadratic behavior of Snell's law for light incident at grazing angles onto boundaries containing small refractive-index discontinuities to cause electrically controllable amounts of refraction or reflection. This type, however, cannot switch all of the input light from one port to another and serves only as a 3 dB directional coupler switch.

The third approach involves the use of an electro-optic crystal in which one end of the crystal is polished into a cylindrical reflecting surface. The mirror is focused such that light entering one fiber will exit out of one of its output fibers. When voltage is applied to radial vane electrodes attached to the top of the crystal, a change in index of refraction occurs in the crystal and the focus of the mirror is spoiled such that most of the light couples into the second output fiber. The theoretical insertion loss of this device is 2 dB (Reference 14). Switching speeds in the megahertz have been observed.¹⁰

Another type of multimode switch is based on controlled reflection by a thin, uniform, liquid-crystal layer. Figure 2.18(a & b) illustrates the element structure of this switch. A light beam is incident obliquely at an angle ϕ upon a uniformly oriented liquid crystal (LC) sandwiched between polished pieces of high index glass that are coated with a transparent electrode material. Switching is accomplished by voltage control of the optical critical angle.

2.4.4 MAGNETO-OPTIC SWITCHING

The principle of switching using magneto-optic technology is a new but promising technique. The concept involves the efficient optical diffraction in parallel thin-film magnetic-strip domains of iron garnet. An external magnetic field influences the width and angular orientation of the domains and, hence, the optical diffraction and azimuth angles. This effect is called the Faraday effect, which is simply a rotation of the direction of polarization of linearly polarized light caused by an applied magnetic field. This switch should become commercially available sometime in 1982 (Reference 15). It is the fastest switch currently available on the market with switching speeds of 20 μ s and low insertion losses.

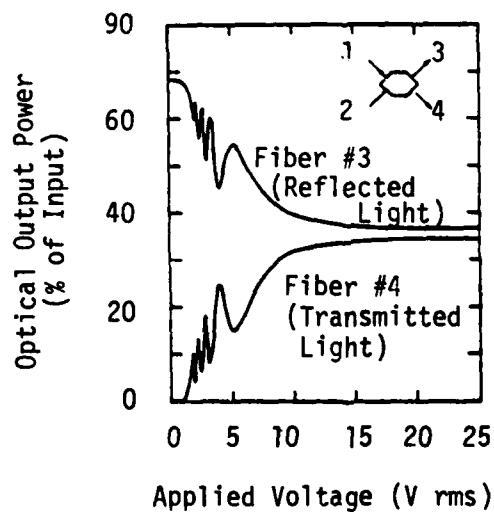
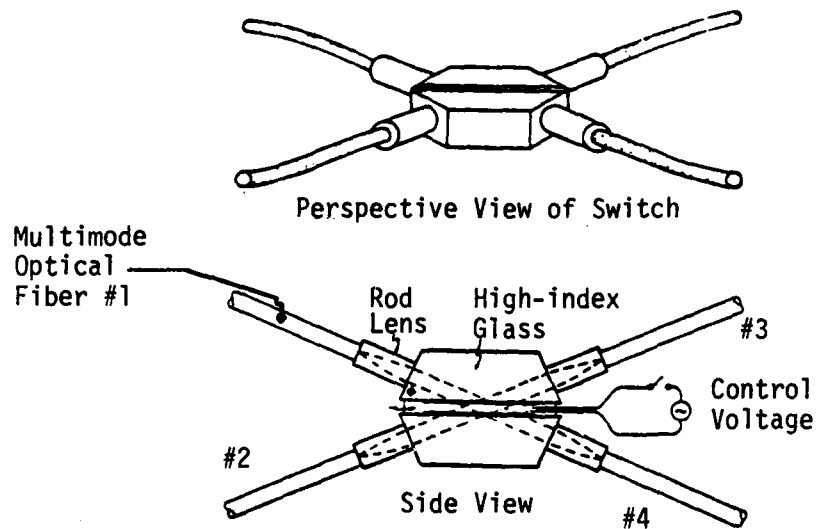


Figure 2.18 (a) Liquid crystal switch.

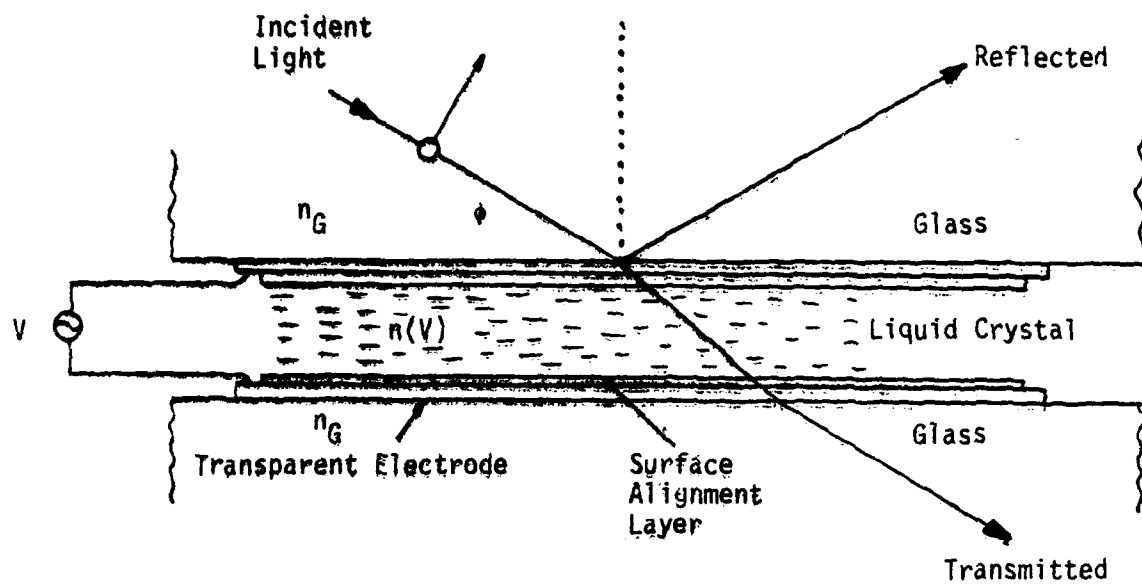


Figure 2.18(b) Liquid crystal switch.

2.4.5 ACOUSTO-OPTIC SWITCH

Acousto-optic interactions between guided optical waves and acoustic surface waves are being explored as a means of implementing compact, miniature light deflection devices. The device is sketched in Figure 2.19. The principle of operation is similar to the electro-optic Bragg deflector, except the index grating is induced via the acousto-optic effect rather than by a physical grating. The defining equation is

$$\Delta n = \frac{1}{2} n^3 p s$$

p = photo-elastic constant
 s = the acoustic strain amplitude

(21)

Typical operating characteristics for a Ti:LiNbO_3 deflector are: (1) 175 MHz acoustic frequency, (2) 35 MHz bandwidth, and (3) 50 watt drive power for a 70% deflection efficiency.

In the acousto-optic Bragg deflector, when light is incident near the Bragg angle on the induced grating, a portion of it is scattered and a coupled wave interaction between the scattered and incident light takes place. The coupling coefficient for this interaction is

$$K \approx (\pi/2) \cdot \Delta n$$
(22)

and synchronism occurs when Bragg conditions are met

$$\sin \theta_B = \lambda / (2 NA)$$
(23)

A = grating period
 N = effective film index
 θ_B = angle of incidence.

2.4.6 OPTICAL SWITCH SUMMARY

None of the commercially available optical switches were completely satisfactory for this project. This is evident in Table 4 where every multimode switch has at least one deficiency in speed, insertion loss, or power required.

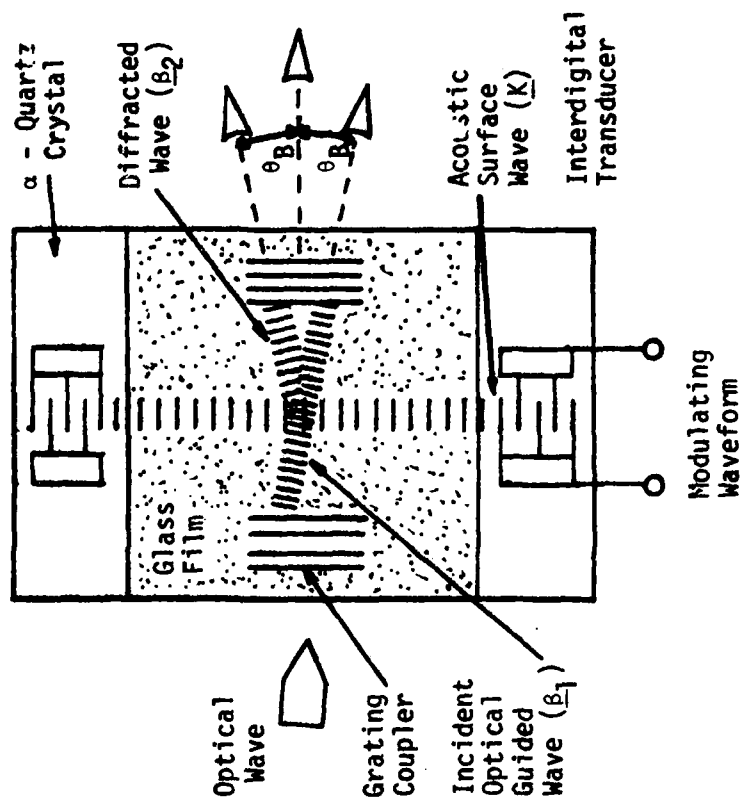


Figure 2.19 Acousto-optic switch.

TABLE 4
MULTIMODE FIBER OPTIC SWITCHING TECHNIQUES

Parameter	Electro-mechanical	Electro-optic [*] LiTaO ₃	Electro-optic [*] liquid crystal	Magneto-optic [*]	Acousto-optic [*] LiNbO ₃
Optical insertion loss	1 dB (approx.)	5.7 to 12 dB	1 dB (approx.)	4 dB minimum	< 4 dB
Switching speed	ms	ns	ms	μs	μs
Optical crosstalk	-40 dB	-30 to -12 dB	-48	-40 dB	-26 dB
Reliability	moving parts (but see text)	high	high	high	high
Control power requirements	2 to 4 V 0.1 to 0.2 A	400 to 500 V μA to mA	5 to 30 V 20 μA	2 to 4 V 0.1 to 1.0 A	2 - 10 V

* These four switch types are essentially experimental at the date of this report.

2.5 FIBER OPTIC COUPLERS

The purpose of fiber optic couplers is to split the light from one or more fibers, either evenly or unevenly, into one or more fibers. The applications of couplers include computer netting, data bases, wavelength division multiplexing, or any other application requiring the splitting of a light signal. There are two main types of commercial couplers: the tee and star couplers. Other types which will not be discussed are those using lenses, prisms, or reflective mirrors, and holographic couplers.

2.5.1 COUPLER PARAMETERS

Several parameters can be used to characterize couplers. The first is insertion loss (IL), which is a measure of the power loss from the input port to one of the output ports. Insertion loss is defined by

$$IL_{MN} = -10 \log \left(\frac{P_{MN}}{P_M} \right) \quad (24)$$

IL_{MN} = Insertion loss in dB from input M to output N

P_{MN} = Power output at N from input M

P_M = Power input at port M

The splitting loss (SL) is the loss due to the signal being split into N ports, assuming an evenly distributed coupler output. The splitting loss is defined by

$$SL = -10 \log \left(\frac{1}{N} \right) \quad (25)$$

SL = Splitting loss in dB

N = Number of output ports

The excess loss (EL) is the difference between the insertion loss and splitting loss. The excess loss is due to reflections, light absorption, and light radiation.

The uniformity factor (UF) specifies the degree of uniformity in the output ports. The uniformity factor is defined by

$$UF_M = \frac{P_{MN}(\max) - P_{MN}(\min)}{P_{MN}(\max)} \times 100\% \quad (26)$$

- UF_M = Uniformity factor (in percent) when input port M is used
 $P_{MN}(\max)$ = Maximum output signal from any port when input port M is used
 $P_{MN}(\min)$ = Minimum output signal from any port when input port M is used

The ideal coupler would have a uniformity factor of zero percent.

2.5.2 TEE COUPLER

Figure 2.20 is a diagram of a tee coupler used in a fiber optic bus system. In a system with N terminals, N tee couplers would be needed to allow communication between any two terminals. The most common method for making tee couplers is the fused biconical taper (FBT) method in which unjacketed fibers are twisted together, fused, and pulled to form a tapered region. The mode volume effect is used to split the light power. Higher order modes in the input fibers are forced into the cladding region of all the output fibers, and the mode energy couples back into the core region of the output fibers as the cross sectional area decreases. In this method, the lower order modes remain in the input fiber. However, this can be corrected by cutting the fibers in the tapered region, rotating them and fusing them back together. Unequal power distribution can be achieved by altering the length of fiber fused and the amount of tapering.

2.5.3 STAR COUPLER

Star couplers can either be transmissive or reflective. Reflective star couplers distribute light from any fiber selected as input to all fibers, including the fiber selected for input. Transmissive couplers are directional in that light input into any of the multiple input fibers is distributed to all the output fibers. The light in the fibers is distributed by either using a mixing rod or fusing the fibers together. Reflective couplers have the end of the mixing rod mirrored to reflect the energy. The mixing rod is a device whereby any light input into the input face will evenly illuminate the output face. This mixing rod can be a polished piece of glass which is covered with a low index of refraction material, thus becoming an optical waveguide. Figure 2.21 shows a transmissive star coupler using a mixing rod. Star couplers are usually designed so that the output power is evenly distributed among the fibers.

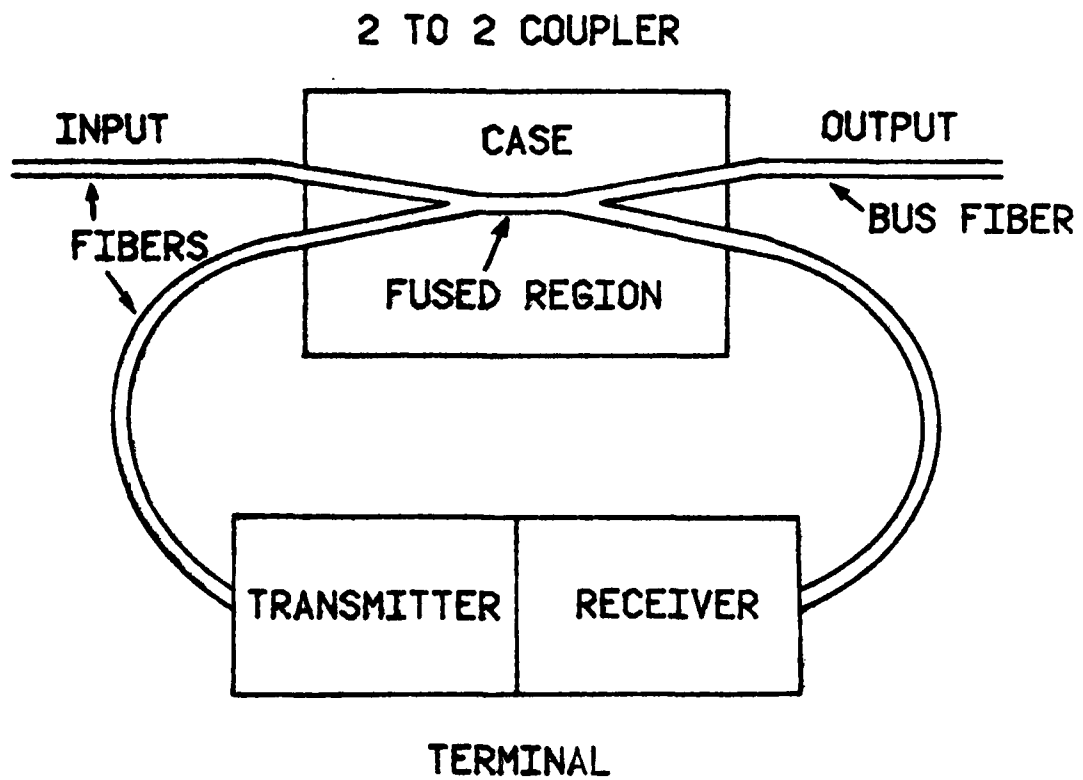


Figure 2.20 Tee coupler. Used in a fiber data bus system.

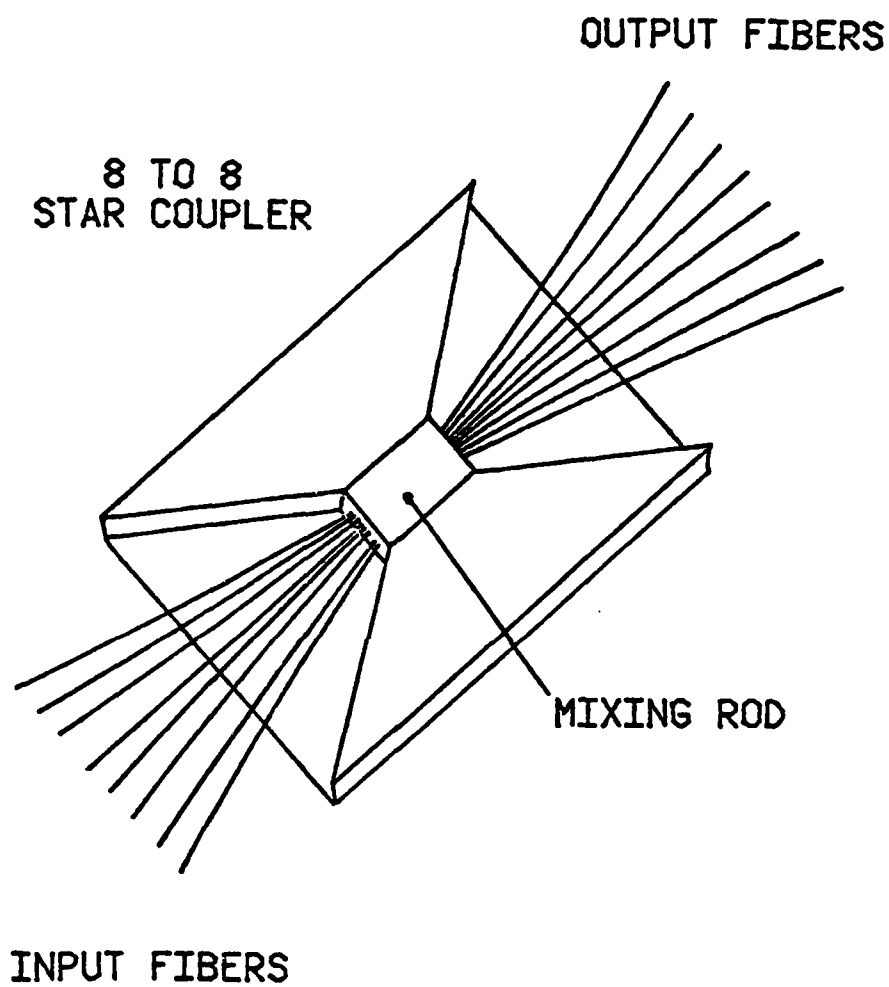


Figure 2.21 Star coupler. Using a mixing rod.

2.6 FIBER OPTIC INTERCONNECTIONS

The practical implementation of optical fiber as the medium of phase delay in phased array device will require the use of interconnection devices such as connectors or splices. A connector is a demountable device used to easily disconnect and reconnect fibers; and a splice is employed to permanently join optical fibers together. The losses introduced by splices and connectors will be an important consideration in the system design of a large scale phased array device. Fiber losses can be separated into two categories:

- (1) **Extrinsic Parameters** - A category related to the technique used to join the fibers and is caused by extrinsic (to the fiber) parameters such as transverse offset between the fiber cores, end separation, axial tilt, and fiber end quality.
- (2) **Intrinsic Parameters** - A category related to the properties of the fibers joined. These losses relate mostly to splices. Intrinsic parameters include variations in fiber diameter (both core and cladding), index profile, and ellipticity and concentricity of the fiber cores.

Figure 2.22 compares the relative influence on splice loss of the major extrinsic parameters of transverse offset, separation, and axial tilt. Splice loss is significantly more sensitive to transverse offset and axial tilt than it is to longitudinal offset. Fiber end quality has a minimal effect on splice loss if proper end preparation techniques are used in conjunction with an index-matching material such as glycerin. This index-matching material is used to reduce the Fresnel reflection loss which would be caused by the glass-air transition.

The mismatch of intrinsic multimode graded-index fiber parameters can also significantly effect the loss of a splice or connector. Figure 2.23¹ illustrates how splice loss is affected by core radius and Δ mismatch, and Figure 2.24¹ shows how it is affected by α profile. Alpha (α) is the parameter used to describe the fiber index of refraction profile ($\alpha = 2$ for parabolic profile) and Δ is equal to $(n_1 - n_2)/n_2$, where n_1 is the index of refraction at the core center and n_2 is cladding index of refraction.

2.6.1 SPLICING TECHNIQUES

Fusion splicing is the most widely used splicing method. Fusion splicing is accomplished by applying localized heating at the interface of two butted, prealigned

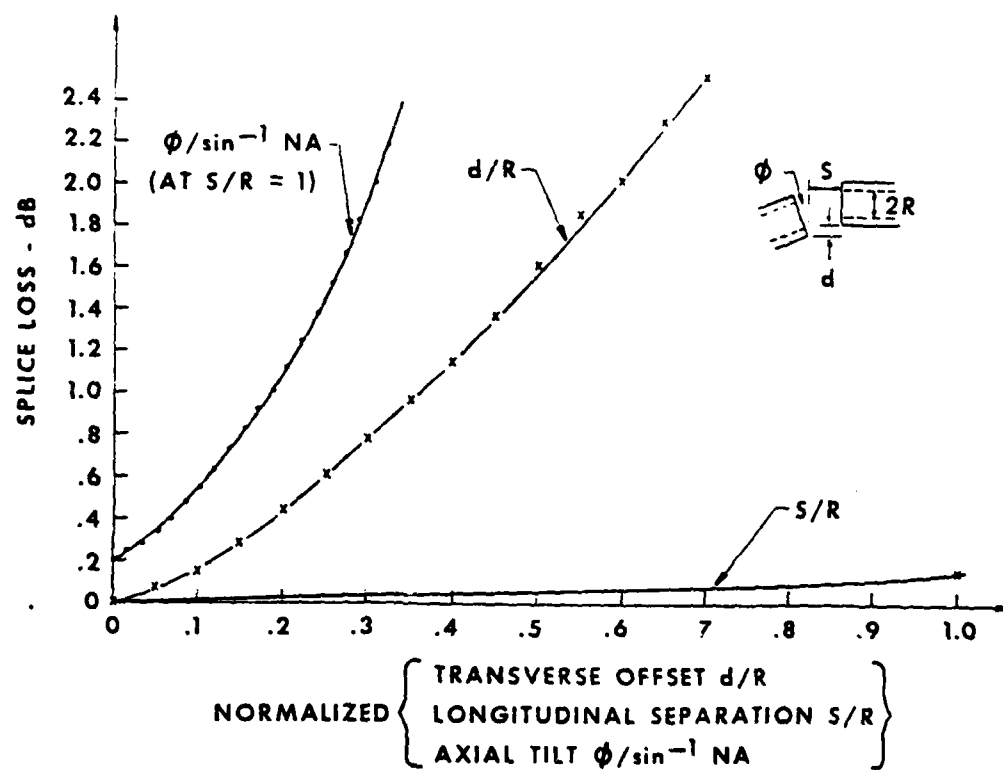


Figure 2.22. Splice loss due to extrinsic parameters.

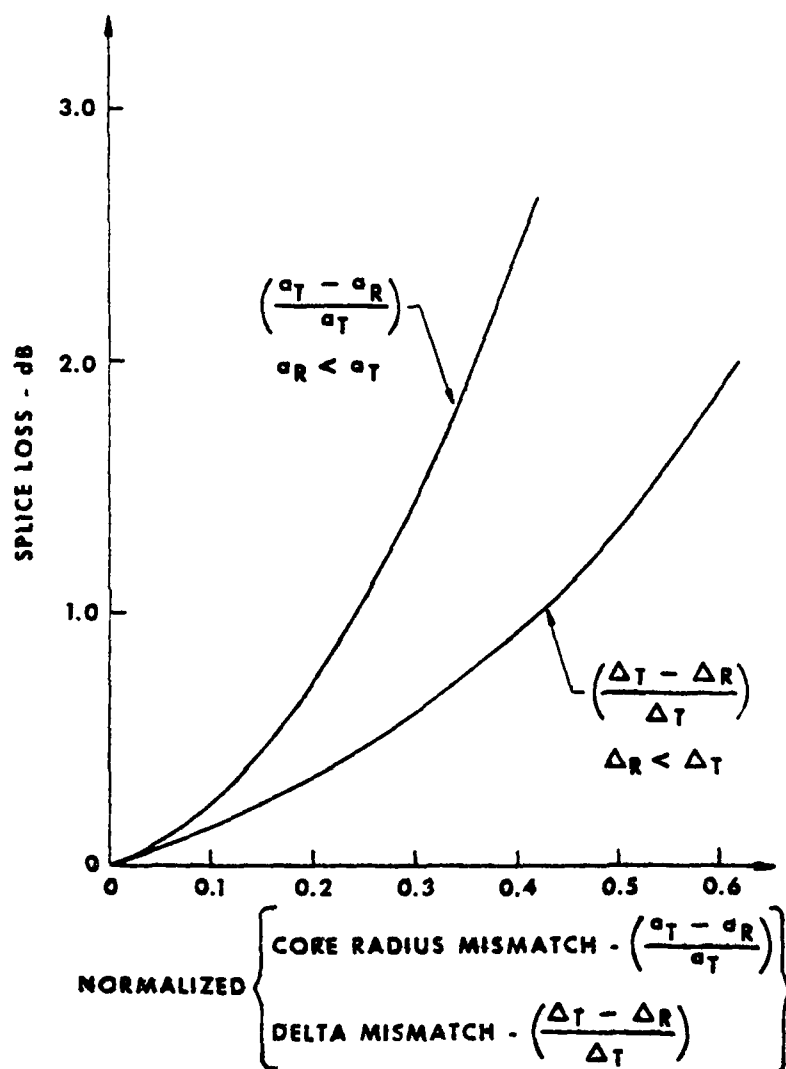


Figure 2.23 Splice loss due to intrinsic parameters.

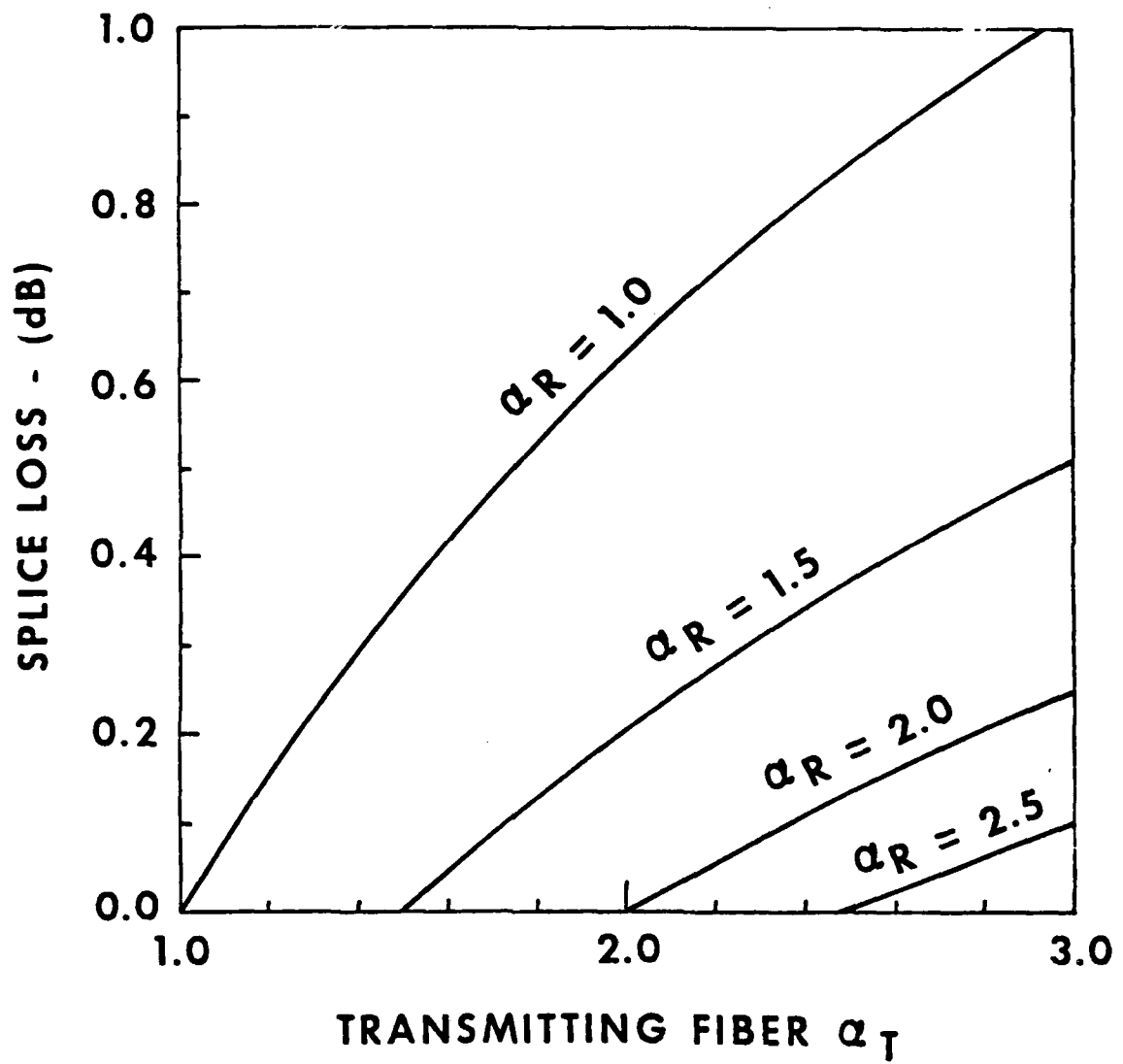


Figure 2.24 Splice loss due to α mismatch.

fiber ends and causing them to soften and fuse together. Figure 2.25 shows how fiber fusion can be achieved using an electric arc to produce the needed heat. An oxygen hydrogen torch may be used in place of an electric arc as the source of heat.

Fusion splicing can be used to join both single and multimode fibers. This is the most practical method for joining single mode fibers because of their extremely small core size (5-10 μm). The small core size makes other methods of connecting or splicing difficult due to errors introduced by mechanical alignment. Fiber splice losses of 0.1 dB for multimode fibers and 0.5 dB for single mode fibers are common using the fusion method.¹

The tensile strength of a fused fiber has been reported to be approximately 60% of the strength of the uncoated fiber before fusion. The decrease in strength is due to the combined effects of surface damage due to handling, surface defect growth during heating, and residual stresses induced as a result of changes in chemical composition.

The second class of permanent splices utilizes an alignment member and adhesive bonding to join individual fibers together. An example of this type of splice is shown in Figures 2.26. This technique of fabricating low loss laboratory type splices uses a loose fitting tube with a square cross section. Two fibers with prepared ends are inserted halfway into each end of a square cross section tube and the fibers are placed on a flat surface and bent in a curved pattern. This generates forces that rotate the tube so that a diagonal of the square cross section is in the same plane as the bent fibers. The fibers are therefore self-aligned in the same corner of the tube. The bent fibers are then pushed into the tube until they touch each other, and index matching epoxy is wicked into the tube to complete the splice. Graded index multimode fibers have been spliced together using loose tube splices with a splice loss of 0.07 dB.¹

2.6.2 FIBER OPTIC CONNECTORS

A wide variety of commercially available fiber connectors are used to interconnect both individual fibers and optical fiber cables. All of these connectors which are demountable are for multimode fiber only. Some of the types that were used in this project will be discussed.

The AMP, Inc., fiber optic connector for a single 125 micrometer outer diameter fiber was used in the phase delay network discussed earlier. Figure 2.27 shows the connector parts in the upper left and a cross section of a completed connector before polishing in the center left. The method of assembly is shown to the right. The ferrule

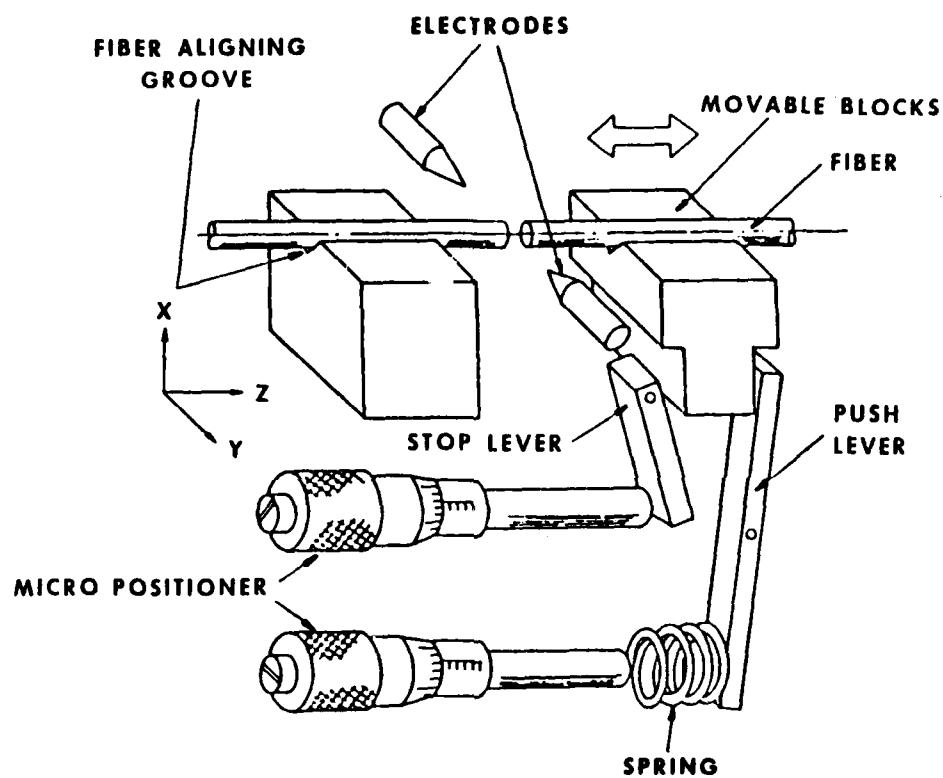


Figure 2.25. Fusion splicing apparatus.

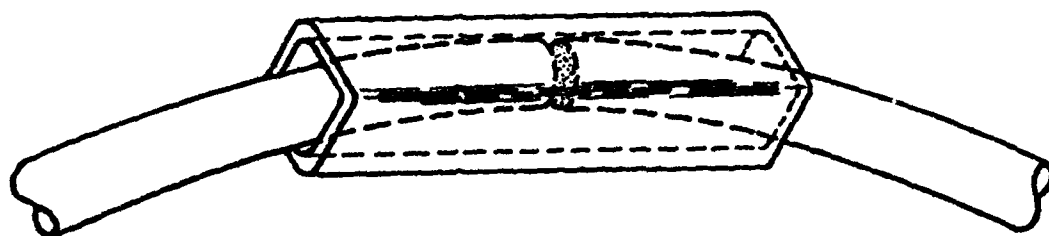
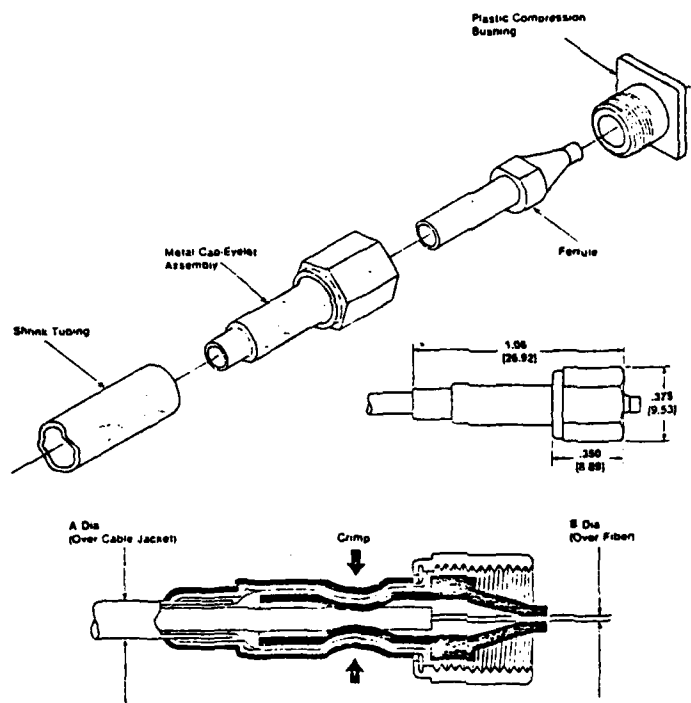
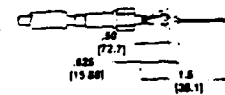


Figure 2.26 Loose tube splice.

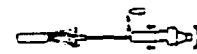


Dimensioning:
Unless otherwise specified, all
dimensions in inches and millimeters
Values in brackets are metric
equivalents

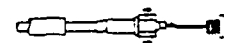
Typical Assembly



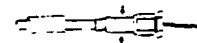
Step 1 — Cable preparation.



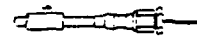
Step 2 — Apply epoxy, then
position Ferrule on cable.



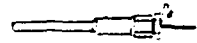
Step 3 — Position Metal Cap
Eyelot Over Ferrule and assemble
Compression Bushing.



Step 4 — Crimp assembly and
allow epoxy to cure.



Step 5 — Position Heat Shrink
Tubing over Eyelot and shrink in-
to place



Step 6 — Score fiber with
Cleaving Tool and break fiber.

Step 7 — Remove Compression
Bushing, assemble Metal
Polishing Bushing and polish as
required

Figure 2.27. AMP, Inc. connector.

shown in the diagram is a piece of plastic with a conical hole that tapers down to 132 μm in diameter, which is about 7 μm larger than the optical fiber. The fiber is epoxied into the ferrule and held in place. After the epoxy dries, the fiber, protruding out of the front face of the ferrule, is cleaved with a sapphire or hardened steel scribe. The end of the connector is then polished using different grits of lapping film (polishing paper); 30, 15, 3, and 0.3 μm grit film is used for polishing. After polishing, the fiber cable is ready to use.

Connections between fibers are accomplished by the use of a device called a splice bushing, as seen in Figure 2.28. The splice bushing is a threaded metal conical taper that butt joins the two connectors in an optical fiber system. Loss through these connectors was found to be 2 dB or less.

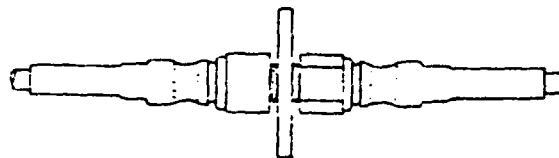
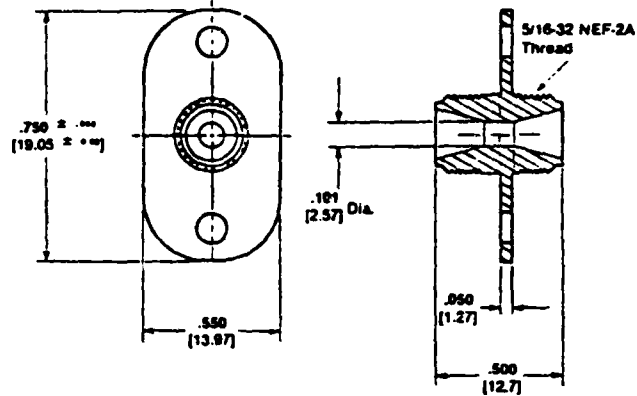
The other type of fiber optic connector used in the phase delay network was an NEC, Inc., connector. The assembly of the NEC connector is very similar to the AMP connector; the fiber is epoxied into a ferrule and polished when dry, but the construction and threading are different. The NEC ferrule is metal with a conical glass insert that is precision machined to a hole of 127 μm outer diameter. Unfortunately, this hole size of 127 μm occasionally did not accommodate the optical fiber. The outer diameter of optical fiber is often guaranteed within two percent of the 125 μm outer diameter. If the maximum variation of two percent occurred, one would have a fiber with an outer diameter of 127.5 μm , which is larger than the hole for the ferrule. This was observed in the laboratory when some fibers simply could not be inserted into the NEC ferrules. The NEC connector had less than 1 dB loss.

A connector used in the laboratory for temporary connections was the TRW Cinch Optalign[®] Fiber optic connector. The basic operation of this connector is shown in Figure 2.29. Four glass rods form the channel in which optical fibers meet. This is a dry connector; no epoxy is used. The fibers are held in place by clamps which hold the outer sheathing of the cable. It typically has 2-3 dB loss for each connection.

A promising connector uses a three-ball alignment configuration to center a fiber in a ferrule arrangement as shown in Figure 2.30. The fiber is located in a groove formed by two balls and held in place by a third ball. The two fiber ends are located with a microscope to ensure correct location and recessed with respect to the end plane of the three balls. The fibers are then permanently attached with an adhesive. The two sets of

[®]Registered Trademark of TRW

Metal — Die Cast Zinc, Zinc Plated
Part No. 227489-3



Typical Application

Figure 2.28 Splice bushing.

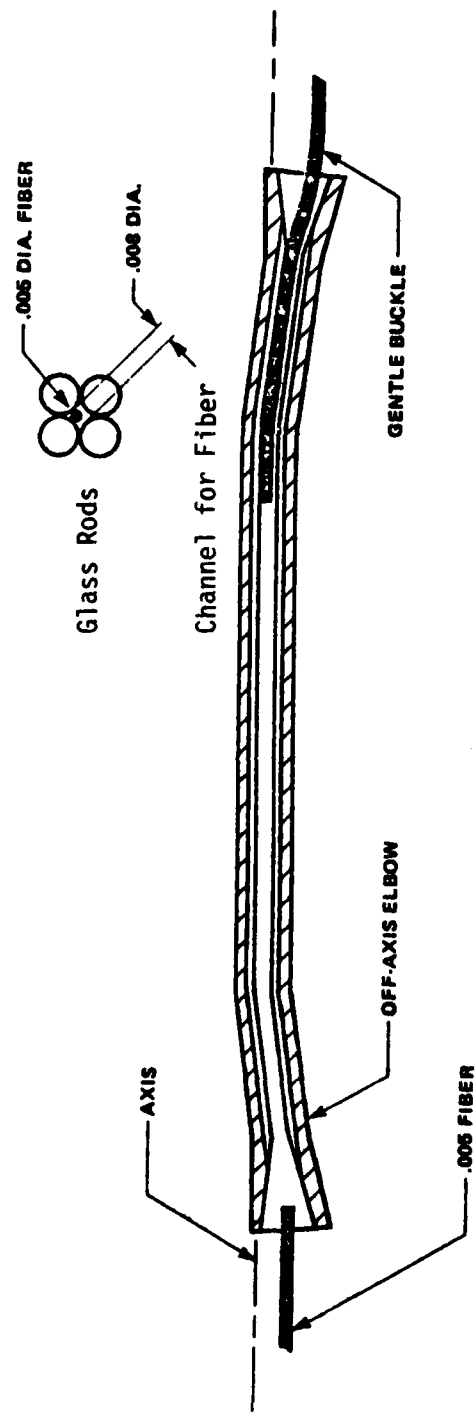


Figure 2.29 TRW cinch optical connector.

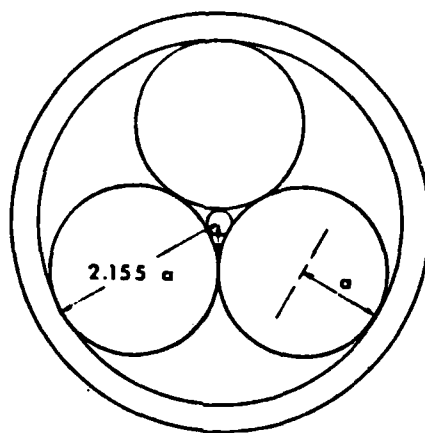


Figure 2.30 Fiber alignment by three balls.

three balls are pressed together at a relative rotation of 60° to obtain automatic alignment of the two fibers is brought about. The only high-precision components in this connector are the tungsten carbide balls that are inexpensive and easily manufactured with tolerances of ± 1 micrometer.

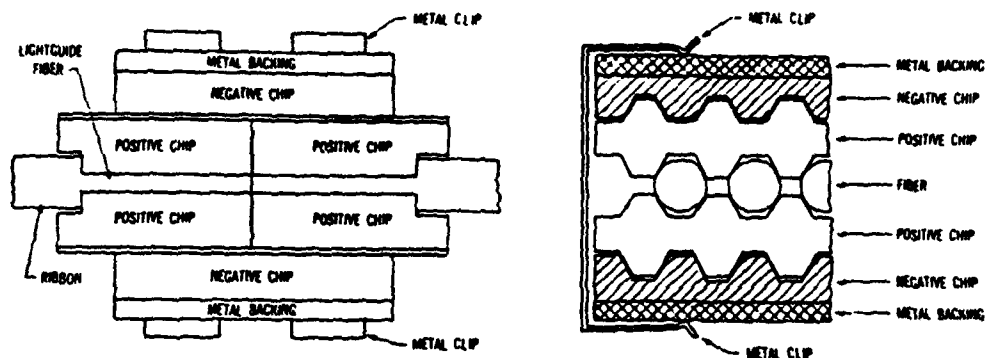
The final connector design that will be discussed is the etched silicon wafer for multifiber connections or array connections as shown in Figure 2.31. V-Grooves are etched into a pair of silicon wafers, and the V-grooves hold an array of fibers in precise alignment. An array half is formed by permanently affixing two positive preferentially etched silicon chips to the end of a fiber ribbon. The fiber ends are then simultaneously prepared for use by grinding and polishing the end of the array. The connector is held together with spring clips and index matching material is inserted to complete the connection. This array connector can then be disconnected and connected in the field. Its average insertion loss is 0.1 dB using identical 50/125 micrometer diameter graded index multimode fibers.

2.7 LABORATORY PRACTICES

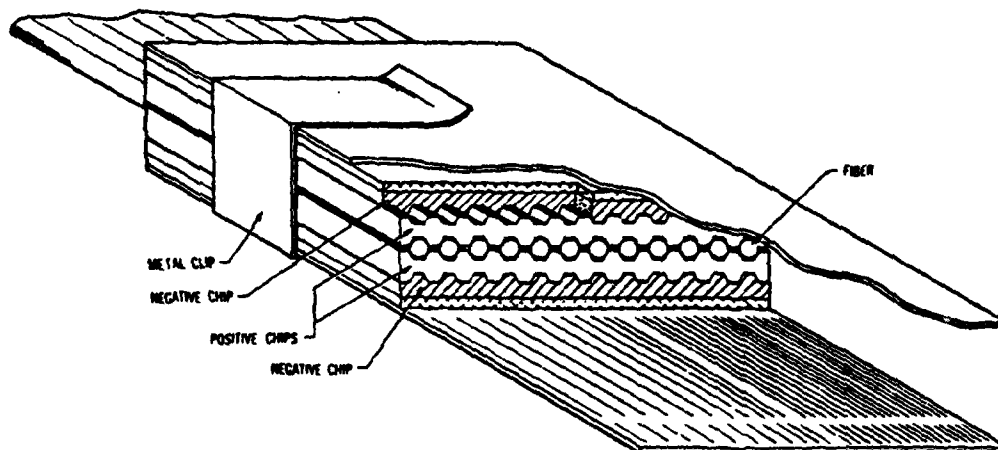
Experience was gained in the craft of making fiber optic connectors in breadboarding the fiber optic phased array system. Several types of connectors were tested, among these were AMP, NEC, TRW Cinch, Deutsch, and Amphenol. AMP and NEC connectors were used in the final system. The laser and receiver in the system use the AMP connector, and the NEC switch uses the NEC connectors. The Canstar coupler in the system was delivered with fiber pigtails, enabling it to be fitted with the appropriate connector. Figure 2.32 shows the connector types and locations used in the test system. Preparation of the AMP and NEC connectors are similar, therefore, only the AMP will be discussed in detail. The components of the AMP connector are shown in Figure 2.27.

2.7.1 CONNECTOR PREPARATION

The AMP connectors use a resilient mechanism to align the fiber in the center of the ferrule. This is done at the factory by compressing the ferrule in a circular drill fixture, then precisely drilling the hole for the fiber. This technique allows irregularities in the ferrule without affecting the centering of the fiber in the connector. Figure 2.33 shows the steps in assembling the connector parts. In preparation for installing the connector, the outer jacket of the fiber cable is removed using a pair of wire strippers. Heat shrink tubing and the metal retaining assembly are slid onto the cable. Next, the



**SIDE VIEW AND PARTIAL CROSS-SECTION
OF ARRAY CONNECTOR**



CROSS-SECTION OF ARRAY CONNECTOR

Figure 2.31 Diagram of array connector.

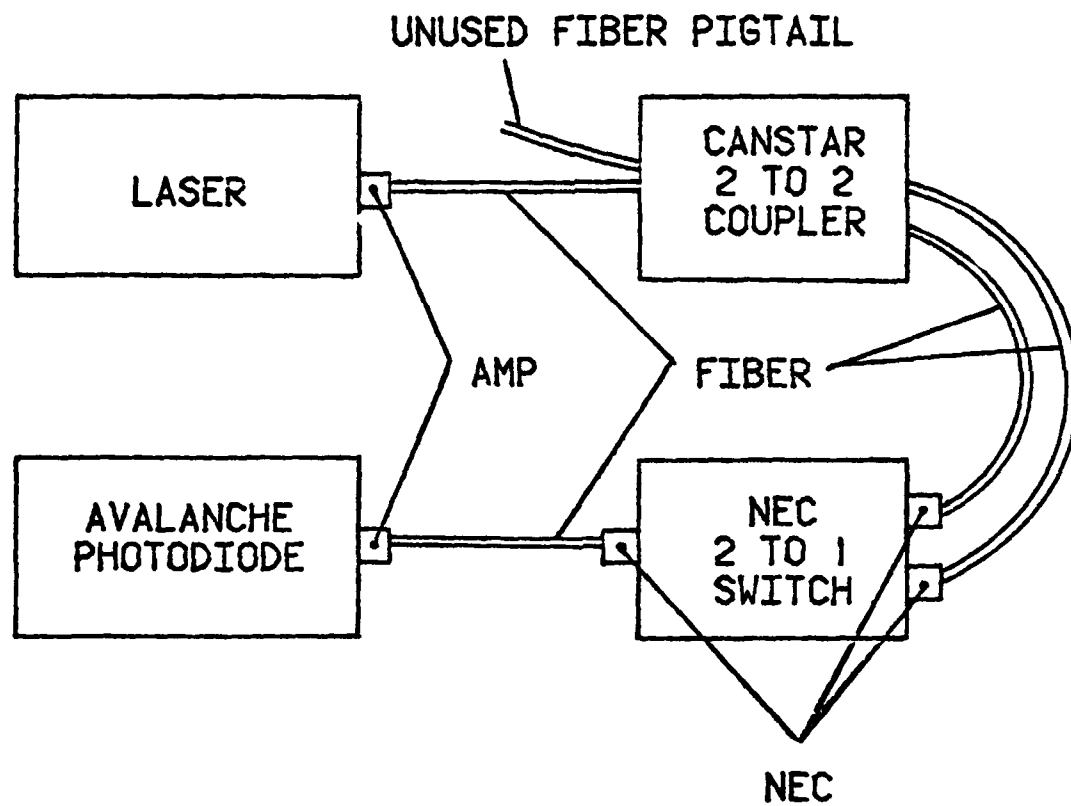


Figure 2.32 Location of AMP and NEC connectors.

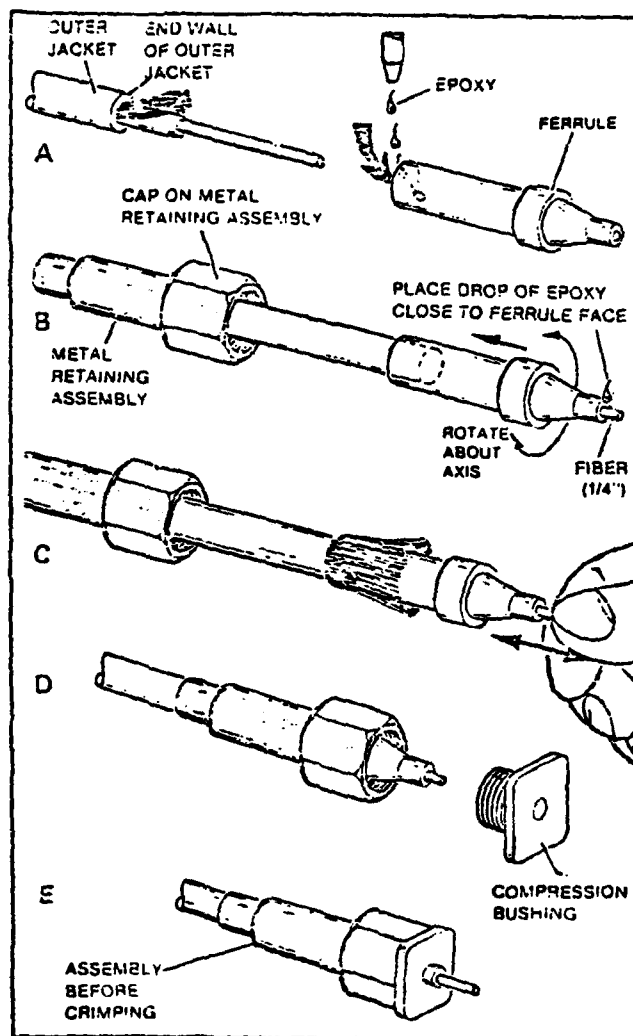


Figure 2.33 Fabrication of AMP connector.

fibrous strength members are trimmed and the Teflon[®] inner jacket is removed using the wire strippers. A quick clipping action with the strippers is needed to cut the Teflon jacket without stretching the Teflon jacket or breaking the fiber. An alternate technique to remove the Teflon jacket is to use a V groove block and a razor blade; this method was successful, but more tedious.

2.7.2 EPOXYING

Acetone was used to remove the protective plastic coating on the fiber and to clean the exposed glass fiber. Epoxy was then inserted into the ferrule until the ferrule was about half full. Epoxies with curing times varying from five minutes to 24 hours were tested. The longer curing times allowed more flexibility in finishing the connector fabrication, while the shortest curing times (five minutes) allowed for no mistakes. With the five minute epoxy, if epoxy was accidentally applied to the glass fiber before inserting it into the ferrule it would dry and inhibit the fiber from fitting into the ferrule. The 24 hour epoxy extended the time to fabricate a connector. The optimum choice was the one hour epoxy, which allowed adequate flexibility in the process and allowed fiber connector fabrication in a few hours. Once the epoxy has been inserted into the ferrule, the ferrule is slid onto the fiber with the fiber protruding from the end of the ferrule, and a drop of epoxy is placed on the fiber close to the ferrule face to ensure epoxy penetration at the ferrule face.

2.7.3 METAL RETAINING ASSEMBLY

The metal retaining assembly is slid over the ferrule and mated with the compression bushing. A crimping tool supplied with the connector kit is used to crimp the metal retaining assembly at two places, securing the assembly to the outer jacket of the fiber cable. The assembled connector is stored while the epoxy cures.

After the epoxy is cured, the heat shrink tubing is slid over the sleeve of the metal retaining assembly and is fitted using a heat gun. The fiber protruding from the end of the ferrule is scored with a scribing tool and broken off. The fiber must be scored just slightly away from the ferrule face to avoid the fiber breaking inside of the ferrule.

[®]Registered Trademark of E. I. DuPont

2.7.4 POLISHING

The end of the ferrule is carefully polished for maximum light transfer. A polishing table was designed and built for this purpose. Four different grades of polishing paper (30, 15, 3, 0.3 micrometer lapping film) are used in the polishing process. The four grades of paper are mounted on the polishing table with running water being supplied to remove the loose grit and glass particles from the lapping film. The compression bushing is removed and the rough polishing bushing is mounted onto the connector. The rough polishing bushing is used with the two rougher grades of polishing paper, while the fine polishing bushing is used with the two finer grades. "Figure-eight" stroke patterns are used in the polishing action. The ferrule is polished using progressively finer polishing paper until the face of the ferrule has been polished flush to the face of the polishing bushing. The polishing bushings are machined so that the optical fiber and its supporting ferrule are the correct length after polishing.

2.7.5 ANALYSIS OF CONNECTOR FABRICATION

Assembly of each type of connectors requires practice to achieve consistent results. All connector types required connection kits which usually included some type of specialized mounting, cutting, or crimping tool, as well as polishing paper if the device required polishing (TRW and Deutsch did not). A problem was discovered with the AMP ferrules purchased early in the project. The fiber could be threaded only once through the ferrule because of the material of the ferrule, dust, or some other foreign substance in the ferrule. Subsequent threading attempts were unsuccessful because of blockage. AMP ferrules purchased in the last few months of the contract period greatly reduced this problem. AMP product engineers stated that the material of the newer ferrules was superior to the older material, thus solving the blockage problem.

The NEC connectors employed metal ferrules which also required polishing. The NEC ferrules did not have the material blockage problems associated with the early AMP ferrules. The NEC ferrules tolerances are less than the tolerance of the fiber cladding. This was confirmed because in some cases the tolerance mismatch was sufficient to preclude threading the ferrule with the fiber.

Successful connectors were made with both the AMP and the NEC connector systems. The AMP system is preferred over the NEC system because of cost. The NEC system is expected to yield superior performance with matched optical fibers.

SECTION 3

LABORATORY SYSTEM DESCRIPTION

This report section discusses the fiber optics phasing device designed and constructed for this project. The section is subdivided into the two major areas of a system description centered around the system diagram and system analysis. The system description subsection reviews the individual components (optical fiber, ILD, APD, coupler, switch, and connectors) used in the constructed device. The system analysis subsection describes the results achieved. The subjects considered in the system analysis subsection are power transfer, frequency response, phase shift, signal-to-noise ratio, and dynamic range.

3.1 SYSTEM DESCRIPTION

The system block diagram is shown in Figure 3.1. The step-by-step description of this system is:

- (1) The RF oscillator amplitude modulates the ILD.
- (2) The ILD outputs approximately 3.0 milliwatts of RF modulated optical power. The optical power is primarily contained in a 10 nanometer wavelength region centered around a central wavelength of 850 nanometers.
- (3) Approximately 1.0 milliwatt of optical power is coupled from the ILD into the optical fiber.
- (4) The multimode optical fiber is connected to the optical directional coupler. The coupler splits the optical energy into two approximately equal amplitudes which are output to optical fiber delays one and two.
- (5) Both optical fiber delays are connected to the optical switch and, depending on the switch state, one of the delayed signals is presented to the APD.
- (6) The APD converts a portion of the received optical signal to an electrical signal and blocks the DC portion of this signal.
- (7) The RF signal is AC coupled to an electrical lead connected to the channel "B" input of the oscilloscope.
- (8) The reference RF signal is connected to channel "A" of the oscilloscope.
- (9) When the electrical signal is applied to the switch the switch changes state, lesser or greater delay is placed in the system, and there is an observable phase change between the oscilloscope channels.

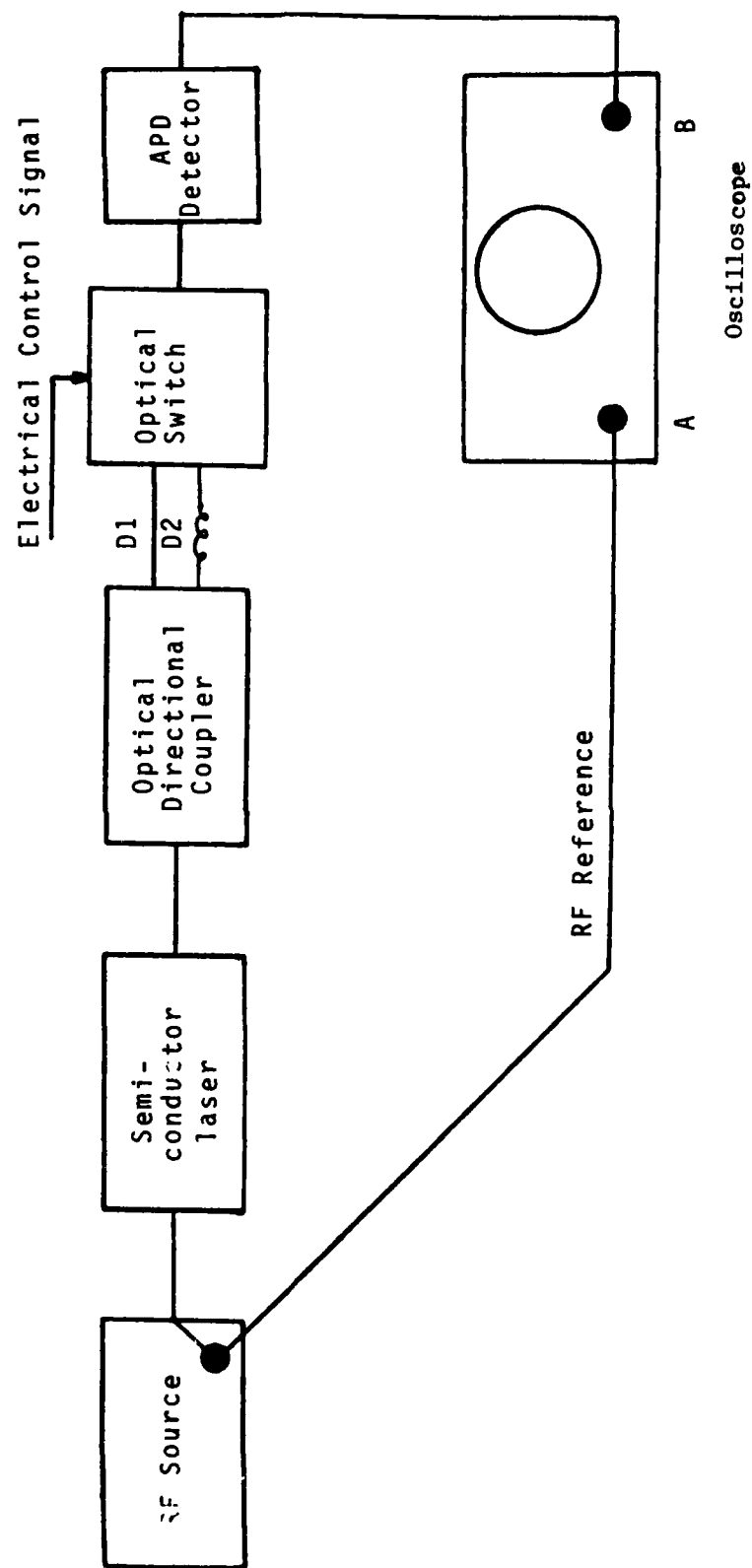


Figure 3.1 Fiber optic phase delay network.

The observed phase change is proportional to the path length change divided by the RF wavelength:

$$\Delta\phi = (\Delta PL / \lambda_{RF}) 360 \quad (1)$$

$\Delta\phi$ = phase change

ΔPL = path Length Change

λ_{RF} = RF Wavelength.

The system studied was a time delay phasing device. The experimental system was free from dependence of phase delay on frequency. It operated correctly from 10 kilohertz to 3.9 gigahertz. The limit at 3.9 Gigahertz was established partially by the semiconductor laser bandwidth and partially by the bandwidths of the observation oscilloscope. The important fact is that this technology holds the promise of a phase shifter that is truly a time delay device. The time delay phase shifter will allow broadband phase array antennas. This particular technology could be used to develop a single standard phasing device which could be applied from 10 kilohertz to 6 gigahertz.

3.1.1 ILD

The characteristics of the Injection Laser Diode (ILD) used in this project are shown in Table 5. This ILD was selected, primarily, because its bandwidth exceeded 1.0 gigahertz.

3.1.2 FIBER

The characteristics of the Galite[®] optical fiber used in this project are shown in Table 6.

TABLE 5. INJECTION LASER DIODE (ILD) CHARACTERISTICS

Manufacturer	B&H Electronics
Model Number	Oct-1000
Wavelength	850 nm
Bandwidth	DC to 1.5 GHz
Rise Time, Fall Time	210 ps
Optical Power Output	< 10 mW
Optical Power Coupled Into Fiber	< 3 mW
Emitter Size	0.5 x 2 μ m
Half Power Beam Angles Parallel Optical Plane Normal Optical Plane	10 degrees 50 degrees
Fiber Connector Type	Amp 'Optimate'
RF Input Connection	SMA, 50 ohms
Optical Bias Control	For linear operation, 15 ohms to 50 k ohms potentiometer between two 'optical bias' terminals. Terminals Open: laser below threshold, -0.8 V turns laser completely on. Terminals Shorted: laser fully on, +0.8 V turns laser off.
Optimum Linear Response (biased to center of transfer curve)	Approximately 7250 ohms
Maximum Input Voltage	+ 0.4 V (when laser is set at center bias point)
Power Supplies	+ 5 V @ 100 mA - 5 V @ 100 mA + 5 V @ 1.2 A (for cooler)
Case Size (inches) L x W x H	2.85 x 2.50 x 1.50

TABLE 6. GALITE® FIBER

Fiber Diameter	
(a) Buffer	230 micrometers
(b) Cladding	125 micrometers ($\pm 1\%$)
(c) Core	50 micrometers
Numerical Aperture	> 0.21
Maximum Attenuation @ 900 nm	< 10 dB/km
Tensile Strength	100,000 psi
Bandwidth (-3 dB)	810 MHz/km
Jacket Material	
(a) Primary Insulation	Hytrel®
(b) Overbraid	Kevlar®
(c) Cladding Coat	polyurethane
Core Index of refraction	1.47

®Registered Trademark of E. I. DuPont

3.1.3 AVALANCHE PHOTODIODE (APD)

The APD characteristics are shown in Table 7. The general characteristics of APD's were discussed in Section 2.

3.1.4 COUPLER

The coupler (Table 8) used has a power splitting ratio of 60/40 and an excess insertion loss of less than 1.0 dB. It is a 2x2 port device and the light transfer technique is biconical coupling of the fiber's higher order modes. As stated earlier, a fiber optic directional coupler was used for the division of light, input with one fiber, into two output fibers. The coupler used is commercially available and was purchased from Canstar Communications, Ontario, Canada.

This type of directional coupler consists of fused fibers. The coupler is constructed by twisting two fibers around each other and heating them under tension so that a tapering and fusing of the core cladding region of each fiber is produced. Light from the input fiber is injected into the cladding due to the decreasing angle of incidence at the cladding-core interface as the light propagates down the taper. Because the angle of incidence is small for the ray to be totally internally reflected, substantial light enters the cladding. Because the biconical fiber couples higher order modes first, only 40% of the total energy can be coupled into the other fiber. This is a 1.76 dB difference in splitting ratio. The loss through the coupler is typically well below 1 dB with a directivity of 40 dB. The coupler principles are illustrated in Figure 3.2.

3.1.5 OPTICAL SWITCH

This project used an NEC sliding prism switch to vary the delay length in the optical fiber path. The switch was completely acceptable for experimental purposes, but its slow switching speed is unacceptable for most phased array antenna controllers. It could be a useful device for systems that require low speed switching (i.e., RF filters, FFT arrays, sampling digitizer, etc.) The characteristics of this switch are shown in Table 9.

3.1.6 CONNECTORS

Experience was gained in fiber optic connector construction while breadboarding the fiber optic phased array device. Several types of connectors were constructed and tested; among these were AMP, NEC, TRW Cinch, Deutsch, and Amphenol. AMP and NEC connectors were used in the final system. The laser and receiver in the system use

TABLE 7. AVALANCHE PHOTODIODE (APD) CHARACTERISTICS

Manufacturer	B&H Electronics
Model Number	OC-3002LN
Bandwidth	DC to 4 GHz
Rise Time, Fall Time	80 ps
Quantum Efficiency	70% @ 0.85 micrometers
Noise Figure	4 dB
Detector Area Diameter	0.2 mm
Fiber Connector Type	Amp 'Optimate'
RF Output Connection	SMA, 50 ohms
Gain Adjustment	10 to 40 dB through an external potentiometer (15 ohms to 5000 ohms) connected to the two gain adjustment terminals.
Power Supplies	+ 18 V @ 100 mA - 18 V @ 100 mA - 150 V @ 10 mA + 5 @ 1.2 A (for cooler)
Case Size (inches) L X W x H	2.85 x 2.50 x 1.50

TABLE 8. COUPLER CHARACTERISTICS

Manufacturer	CANSTAR
Power Split	60/40
Excess Insertion Loss	< 1 dB
Type	Biconical Taper
Ports	2x2

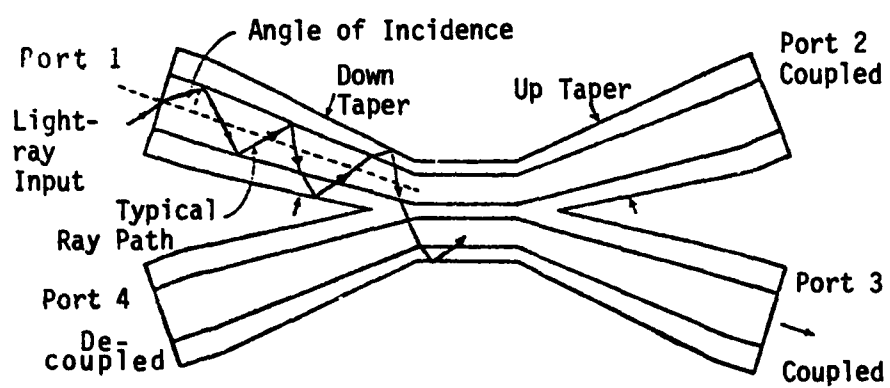


Figure 3.2 Biconical taper directional coupler.

TABLE 9. OPTICAL SWITCH

Manufacturer	NEC (Nippon Electric Co., Ltd.
Switch Device	Sliding Prisms
Switch Type	Bridging
Insertion Loss	< 1.8 dB
Crosstalk	< -60 dB
Switching Delay	< 10 ms
Drive power	12 V, 50 mA
Dimensions	26 X 17 X 53 mm
Weight	80 grams

the AMP connector, and the NEC switch uses the NEC connectors. The CANSTAR coupler in the system was delivered with fiber pigtails, enabling it to be fitted with the appropriate connector. Preparation of the AMP and NEC connectors are similar, therefore, only the AMP was discussed in detail. The components of the AMP connector are shown in Section 2.

3.2 SYSTEM ANALYSIS AND MEASUREMENTS

The approach taken in this analysis was to compute the signal-to-noise ratio (SNR) in a single fiber delay line with a CW signal because these calculations are a necessary step toward the analysis of a more complex fiber delay system. The computations include dispersion effects in a multimode fiber and the fact that the RF input signal is a pulse, rather than a CW signal. This section was divided into several parts. The first three discuss: (1) SNR calculations for a monomode fiber delay line with a CW signal, (2) SNR calculations for a multimode fiber delay line with a CW signal, and (3) calculations for a multimode fiber delay line with a pulsed signal.

The other parts deal with temperature stability, system losses, dynamic range, phase shift, and measured values of some of these quantities.

3.2.1 DERIVATION OF SIGNAL POWER FOR A MONOMODE FIBER DELAY LINE

Consider the fiber delay link consisting of an RF source, an ILD, an optical fiber, and a detector. The laser diode oscillates at a single optical frequency ω , and the light output is modulated by an RF radar pulse with carrier frequency Ω , RF bandwidth F_B , and pulse length τ . The optical fiber has a loss of α dB/km, and is L km long. The detector used is an avalanche photodiode (APD) followed by an amplifier. The output is delivered into a 50 ohm load. In this section, it is assumed that the signal's carrier frequency and RF bandwidth lie well within the bandwidth of the fiber, APD, and amplifier. Monomode fiber length-bandwidth products can be as high as hundreds of GHz-km, the laser's bandwidth is greater than 1 GHz, and the bandwidth of the APD is 4 GHz. The above assumptions are well justified if the carrier frequency and RF bandwidth are < 1 GHz. The modulated light output from the laser diode is assumed to be a CW sinusoidal signal at frequency Ω , with a modulation depth m .

The optical power fed into the fiber is then

$$P_{in}(t) = P(1 + m \cos \Omega t) + S(t) \quad (3.1)$$

where P is the average optical power and $S(t)$ is the spontaneous emission noise generated by the laser. The magnitude and spectral characteristic of this noise are quite complicated and have been investigated by several authors (References 1 and 2). Figure 3.3 illustrates the spectral properties of the laser noise at different mean photon levels in the laser mode. In Figure 3.4, the mean photon level in the laser mode was related to laser output power and plotted in relation to the normalized noise power (defined as laser noise power divided by laser output power). This plot can be used to determine absolute noise power for a specified laser operating power.

As observed from Figure 3.3, the noise power density shows a spike in the RF frequency range around 2-4 GHz; this spike can be orders of magnitude higher than those in the 0-1 GHz range. This noise spike is related to the relaxation oscillation of the laser diode. In addition to the unusually intense noise in this region, there are other undesirable effects such as high harmonic distortion. Therefore, the RF frequency should be below the frequency at which the noise spike appears in the laser diode response, and this analysis is similarly confined.

Propagation of the signal through a fiber of length L attenuates its power by a factor of $10^{-\alpha L/10}$, and hence the output optical power is

$$P_{out}(t) = 10^{-\alpha L/10} P_{in}(t) \quad (3.2)$$

The current generated by the APD is proportional to the incident optical power (lumping splicing and insertion losses into the attenuation term) and is given by

$$i(t) = \left((G\eta 2\pi)/(h\omega) \right) P_{out}(t) \quad (3.3)$$

where G and η are the avalanche gain and the internal quantum efficiency of the APD, respectively, h is Planck's constant, ω is the optical frequency, and e is the electronic charge. Using Equation (3.2) we have

$$\begin{aligned} i(t) = & \left((G\eta 2\pi)/(h\omega) \right) (1 + m \cos \Omega t) 10^{-\alpha L/10} \\ & + \left((G\eta 2\pi)/(h\omega) \right) S(t) 10^{-\alpha L/10} \end{aligned} \quad (3.4)$$

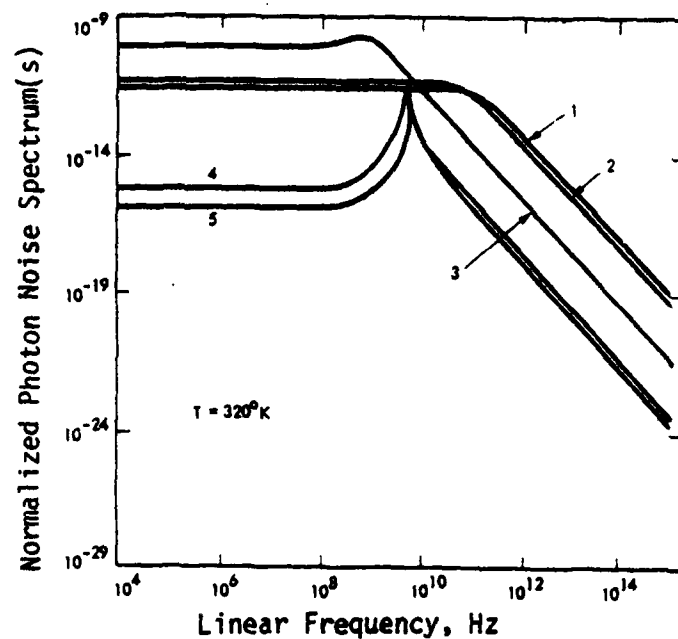


Figure 3.3 Relative laser noise spectrum for various mean photon levels in the laser mode, \bar{N}_p (from Reference 2).
 (1) $\bar{N}_p = 4.96$, (2) $\bar{N}_p = 1.97$, (3) $\bar{N}_p = 3.97 \times 10^2$,
 (4) $\bar{N}_p = 5.95 \times 10^4$, (5) $\bar{N}_p = 1.19 \times 10^5$

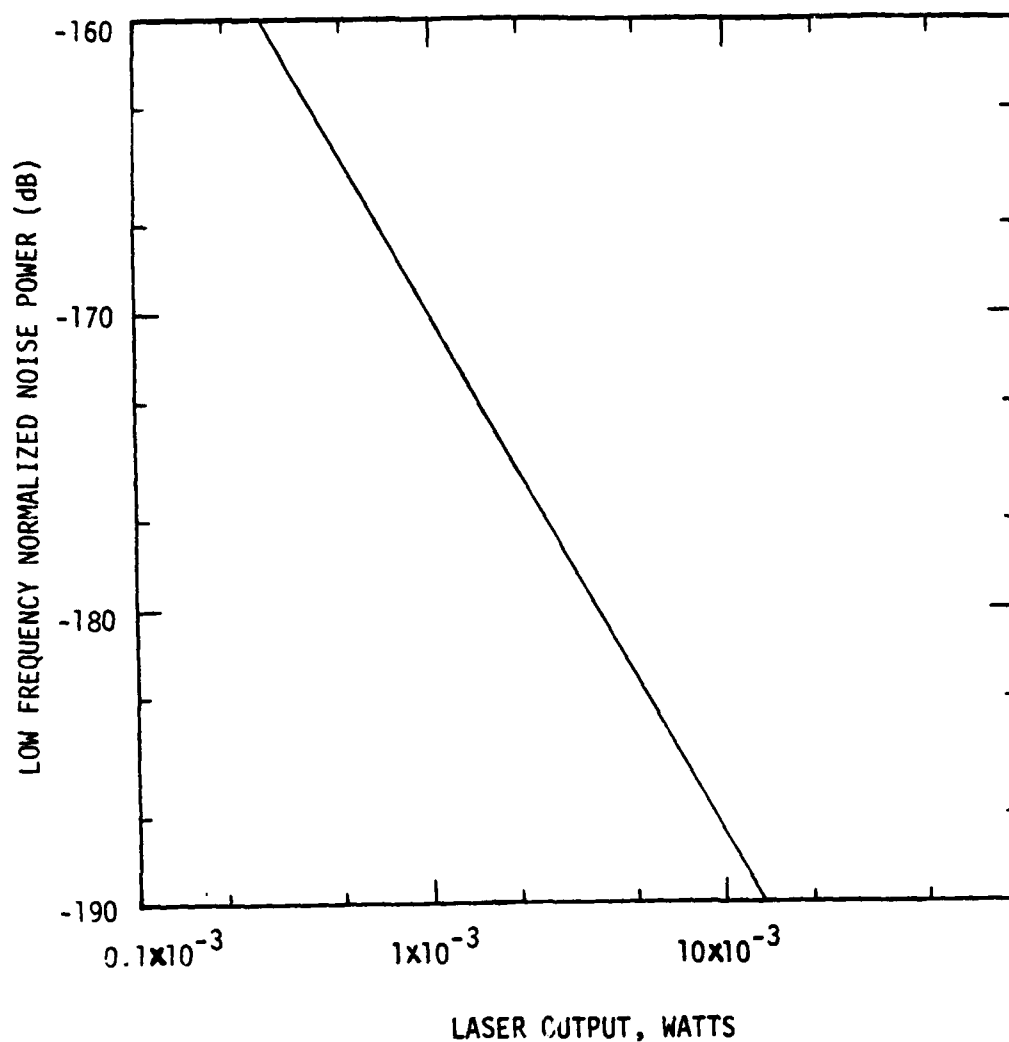


Figure 3.4 Low frequency (<1 GHz) normalized noise power versus laser output power. Normalized noise power is defined as absolute noise power per 1 Hz bandwidth divided by the average laser power.

The first term in Equation (3.4) represents the signal current. The second term is the laser noise current which will be considered separately.

This current is then passed through an amplifier which has bandwidth $\Delta\nu$ and current gain G_A . The power gain of the amplifier is G_A^2 . The signal current at the amplifier output port can be rewritten to include the amplifier current gain G_A

$$i_s(t) = \left((G_A G_{Pen} 2\pi) / (h\omega) \right) (m \cos \Omega t) 10^{-\alpha L/10} \quad (3.5)$$

where the DC signal term $\left((G_{Pen} 2\pi) / (h\omega) \right) 10^{-\alpha L/10}$ in Equation (3.4) disappears because the amplifier is assumed to be AC coupled to the APD. The average electrical signal power is given by

$$\langle P_s \rangle = \langle i_s^2(t) \rangle R$$

where R represents the 50Ω load and $\langle i_s^2(t) \rangle$ is defined by

$$\langle i_s^2(t) \rangle = \frac{1}{T} \int_{-T/2}^{+T/2} i_s^2(t) dt$$

or

$$\langle i_s^2(t) \rangle = 0.5 \left((G_A G_{Pen} 2\pi m) / (h\omega) \right)^2 10^{-\alpha L/5} \quad (3.6)$$

3.2.2 DERIVATION OF NOISE POWER

We will now consider four independent noise sources in the fiber link. These are: the dark current, laser noise, shot noise and thermal noise (Reference 3).

The shot noise current has a mean square value of

$$\overline{i_{N_{shot}}^2} = 2e \bar{I} \Delta\nu \quad (3.7)$$

where \bar{I} is the average amplified current given by

$$\bar{I} = \left((G_A G_{Pen} 2\pi) / (h\omega) \right) (P 10^{-\alpha L/10}) + G_A i_d \quad (3.8)$$

and i_d is the dark current of the APD.

Combining Equation (3.7) and (3.8) yields the shot noise current generated in the APD by the optical DC bias term

$$i_{N_{\text{SHOT}}}^2 = 2e \left((G_A 2\pi G_{\text{en}}) / (h\omega) \right) (P 10^{-\alpha L/10}) \Delta\nu \quad (3.9)$$

The shot noise current due to the dark current has a mean square value

$$\overline{i_{N_{\text{dark current}}}^2} = 2G_A e i_d \Delta\nu \quad (3.10)$$

Background light entering the APD in a closed fiber optic system was assumed to be negligible.

The thermal noise current has a mean square value given by

$$\overline{i_{N_{\text{thermal}}}^2} = G_A^2 (4 kT/R_L) \Delta\nu \quad (3.11)$$

where R_L is the load resistance (50Ω), k is the Boltzmann constant, and T is the temperature of the system (including the equivalent noise temperature of the amplifier).

The laser noise $S(t)$ is attenuated in passing through the fiber and generates a mean square noise current at the amplifier output equal to

$$\overline{i_{N_{\text{laser}}}^2} = \left((G_A G_{\text{en}} 2\pi) / (h\omega) \right)^2 \langle S^2 \rangle 10^{-\alpha L/5} \Delta\nu \quad (3.12)$$

which takes into account the amplifier power gain and bandwidth.

Thus, the total noise power is

$$\overline{i_N^2} = \overline{i_{N_{\text{shot}}}^2} + \overline{i_{N_{\text{thermal}}}^2} + \overline{i_{N_{\text{laser}}}^2} + \overline{i_{N_{\text{dark current}}}^2} =$$

$$2eG_A ((G\eta 2\pi)/h\omega) (P 10^{-\alpha L/10}) \Delta\nu \quad (3.13)$$

$$+ 2e G_A i_d \Delta\nu + G_A^2 (4KT/R_L) \Delta\nu + ((G_A G\eta 2\pi)/(h\omega))^2 \langle S \rangle^2 10^{-\alpha L/5} \Delta\nu$$

The signal-to-noise ratio is

$$S/N = \langle i_S^2 \rangle R / \overline{i_N^2} R = \langle i_S^2 \rangle / \overline{i_N^2}$$

or

$$S/N = (0.5) ((G_A G\eta 2\pi)/(h\omega))^2 10^{-\alpha L/5} / \overline{i_N^2} \quad (3.14)$$

where $\overline{i_N^2}$ is given by Equation (3.13). Equation (3.14) is the final form of the SNR for a monomode fiber delay link with a CW signal.

3.2.3 NUMERICAL ESTIMATIONS

In this section, the contributions of the four noise terms will be estimated.

Typical parameters for a silicon avalanche photodiode in the FOSF system are:

$$G = 100, \eta = 0.6, \text{ and } i_d = \text{dark current} = 16 \text{ nA}$$

Hence,

$$(G\eta 2\pi/h\omega) = 41.1 \text{ ampere/watt around the wavelength of GaAs laser diodes (850 nm).}$$

AD-A118 763

GEORGIA INST OF TECH ATLANTA ENGINEERING EXPERIMENT --ETC F/G 17/9
A FIBER OPTIC BEAM CONTROLLER FOR PHASED ARRAY RADARS.(U)

JUN 82 R B EFURD, E O RAUSCH, M A CORBIN

F19628-81-C-0026

UNCLASSIFIED

GIT/EES-A-2832

RADC-TR-82-173

NL

2-2

2-2

END

DATE

9-82

DTIC

The DC bias power coupled from the laser diode into the optical fiber is approximately 0.5 mW. Hence, the shot noise contribution is

$$2e[(G_A G_{en} 2\pi)/(h\omega)] P 10^{-\alpha L/10} = 6.6 \times 10^{-21} G_A 10^{-\alpha L/10} A^2/Hz$$

The dark current contribution is

$$2e i_d G_A = 5.1 \times 10^{-27} G_A A^2/Hz$$

Assuming an ambient temperature of 300 K and a noise figure of 6 dB, the thermal noise contribution is

$$G_A^2 (4KT/R_L) = 1.3 \times 10^{-21} G_A^2 A^2/Hz$$

The laser noise power is determined by specifying the average laser output power in Figure 3.4 and by multiplying that quantity by its corresponding normalized noise power (defined as the laser noise power divided by average laser output power). Given an average optical output of 1.5 mW from the laser diode, the laser noise power is approximately $\langle S^2 \rangle = 7.2 \times 10^{-21}$ watt/Hz. The optical noise power launched into the fiber is about 33% of $\langle S^2 \rangle$, or 2.4×10^{-21} watt/Hz. Hence, the electrical laser noise power at the amplifier output is

$$[(G_A G_{en} 2\pi)/(h\omega)]^2 \langle S^2 \rangle 10^{-\alpha L/5} =$$

$$4.1 \times 10^{-18} 10^{-\alpha L/5} G_A^2 A^2/Hz$$

The electrical signal power is

$$0.5 \left((G \eta 2\pi P_m) / (h\omega) \right)^2 10^{-\alpha L/5} G_A^2 =$$

$$2.1 \times 10^{-4} m^2 10^{-\alpha L/5} G_A^2 A^2$$

Thus, the signal-to-noise ratio is

$$S/N = \frac{A m^2 10^{-\alpha L/5} G_A}{(B 10^{-\alpha L/10} + C + G_A D + G_A E 10^{-\alpha L/5}) \Delta \nu} \quad (3.15)$$

where

$A = 2.1 \times 10^{-4}$	(signal)
$B = 6.6 \times 10^{-21}$	(shot noise)
$C = 5.1 \times 10^{-27}$	(dark current noise)
$D = 1.3 \times 10^{-21}$	(thermal noise)
$E = 4.1 \times 10^{-18}$	(laser noise)

Equation (3.15) is the principal result. The contribution of the various noises as a function of fiber length-attenuation product is shown in Figure 3.5. If the attenuation is 1 dB/km, then the x-axis will be scaled in km. Furthermore, for a fiber loss of 1 dB/km, laser noise dominates for $L < 15$ km, and the signal-to-noise ratio is approximately constant.

$$S/N = (A m^2) / (E \Delta \nu) = 5.1 \times 10^{13} m^2 / \Delta \nu \quad (3.16)$$

m , the modulation index, was chosen to be 1.

Beyond 15 km, the SNR is fiber length dependent, because the dominant noise in this region (i.e., thermal noise) is independent of αL , whereas the signal continues to decrease with αL .

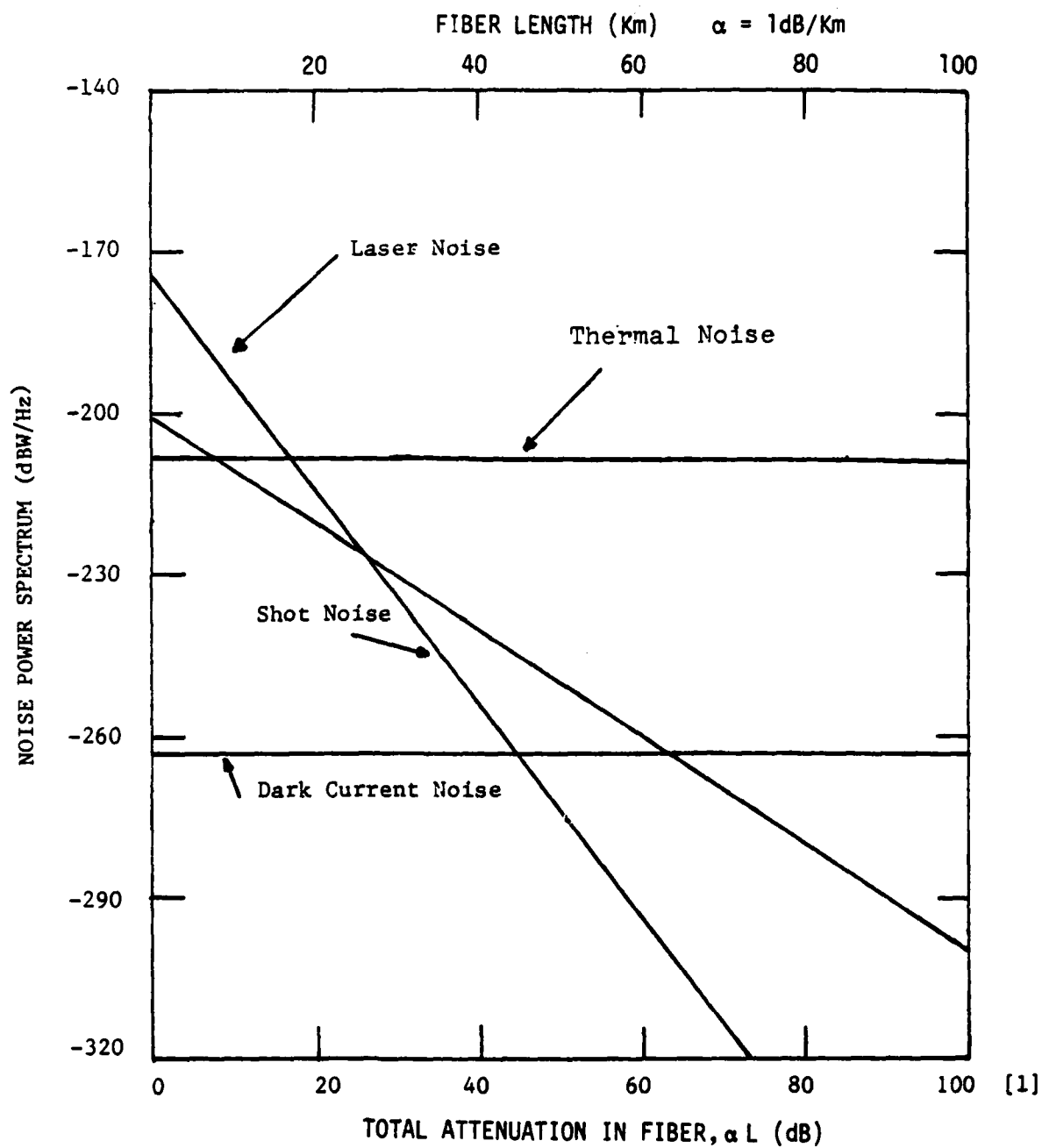


Figure 3.5 Noise power versus total attenuation in fiber. Amplifier gain, G_A , is 1. System bandwidth, $\Delta\nu$, is 1 Hz.

Hence, the SNR is given by

$$S/N = (A m^2 10^{-\alpha L/5}) / (D \Delta v)$$

or

$$S/N = (1.6 \times 10^{17} m^2 10^{-\alpha L/5}) / \Delta v$$

The SNR in dB for $L > 20$ km is linear with respect to αL as indicated in Figure 3.4.

3.2.4 DERIVATION OF SNR FOR A MULTIMODE FIBER DELAY LINE WITH A CW SIGNAL

In previous calculations, it was assumed that the carrier signal falls within the transmission bandwidth of the optical fiber. For single-mode fibers, the bandwidth-length product can be as high as 100 GHz-km (assuming a single mode laser source), while multimode fibers are commonly in the range of 1 GHz-km. For a 2 km delay line with a signal having a carrier frequency of 1 GHz, for example, the signal lies comfortably within the bandwidth of a single mode fiber, but not a multimode fiber. This effect will now be included and its consequences will be examined.

The bandwidth-limiting factor in multimode fibers is intermodal dispersion. Multimode fibers support a large number (several hundred) of transverse optical modes due to their relatively large size. These transverse modes, however, each carrying a sinusoidal modulation, travel down the fiber at different group velocities. Hence, the received signal is a sum of sinusoids of different phases. The result is a lowering of the modulation depth as compared with that at the input where each mode carries modulation with the same phase (Appendix A.)

The amount of intermodal dispersion in a multimode fiber is usually specified in time-spread/km. When an optical impulse is fed into the fiber, the output can be approximated by a gaussian pulse with half-width increasing linearly with fiber length. (See Reference 4.) Thus, the impulse response of the fiber is

$$g(t) = 1/(\gamma L \sqrt{\pi}) \exp(-t^2/(\gamma^2 L^2)) \quad (3.17)$$

where the intermodal dispersion constant (γ) is measured in ns/km and L is the total length of the fiber in km. The factor $(1/(\gamma L \sqrt{\pi}))$ is a normalization constant required for power conservation.

The response of the fiber due to an arbitrary input is given by the convolution integral

$$P_{out}(\tau) = \int_{-\infty}^{\infty} P_{in}(t-\tau)g(t)dt \quad (3.18)$$

For a purely sinusoidal input with modulation depth m ,

$$P_{in}(t) = P(1 + m \cos \Omega t)$$

and the output is

$$P_{out}(t) = P(1 + m \exp(-\gamma L \Omega/2)^2 \cos \Omega t) \quad (3.19)$$

where t was substituted for the variable τ . Hence the modulation depth is reduced to an effective value

$$m' = m \exp(-\gamma L \Omega/2)^2 \quad (3.20)$$

Details of the calculation are described in Appendix B. Since, according to Equation (3.15), the signal-to-noise ratio is proportional to m^2 , it follows that the SNR decreases as $\exp(-\gamma^2 L^2 \Omega^2/2)$. This effect was included in Figure 3.6 for two modulation frequencies. The effect is a sharp reduction in SNR once the modulation frequency falls outside the fiber bandwidth. As long as this is not the case, the difference between single mode and multimode fibers is minimal. For a 100 m multimode fiber, this requirement is satisfied if the modulation frequency is equal to or less than 1 GHz.

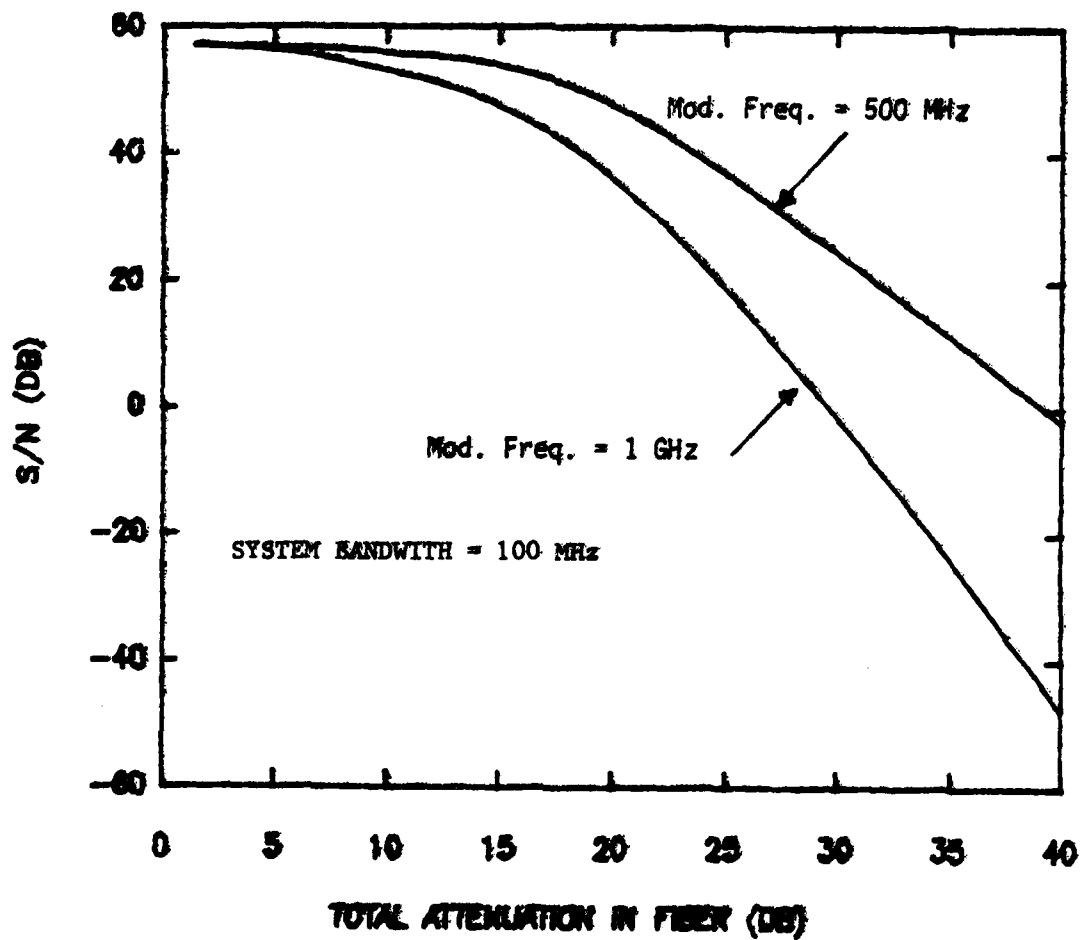


Figure 3.6 Signal-to-noise ratio versus total attenuation in multimode fiber

Good agreement was obtained between measured and calculated SNR values when a short optical transmission line (~ 1 m) was tested with a 10 MHz sinusoidal signal. The bandwidth of the system was 100 MHz. Figure 3.7 is a plot of measured SNR versus the logarithm of the AC input voltage, V_{in} . The relationship between SNR and V_{in} is

$$SNR = 20 \log (V_O/V_N)$$

where V_O is the peak to peak output signal and V_N is the rms noise voltage. If the system is linear, then V_O is directly proportional to V_{in} . Hence, a plot of SNR (in dB) versus $\log V_{in}$ should also be linear. This fact is indicated in Figure 3.7. For $V_{in} = 0.8$ V peak to peak, the laser output power was oscillating between 0 and 3 mW and the DC bias was set at 1.5 mW. These conditions correspond closely to the assumptions made in the analysis. Thus, the measured SNR at $V_{in} = 0.8$ V should be similar to the analytical SNR at $\alpha L = 0$ in Figure 3.5. The actual values are

Calculated SNR = 57 dB

Measured SNR = 54 dB

3.2.5 POWER CALCULATIONS OF A PULSED SIGNAL IN A MULTIMODE FIBER DELAY LINE

This section describes the interaction of a pulsed optical signal with the response function of a multimode fiber as a function of fiber length and pulse width of the input signal. Details of the calculations are given in Appendix C.

In previous sections, the RF input signal was assumed to be a continuous sinusoidal signal of frequency Ω with a fixed modulation index m , i.e.,

$$P_{in}(t) = P(1 + m \cos \Omega t)$$

In this section, the RF signal is not continuous, but assumes a pulse shape with a Gaussian envelope. The optical signal power launched into the multimode fiber is given by

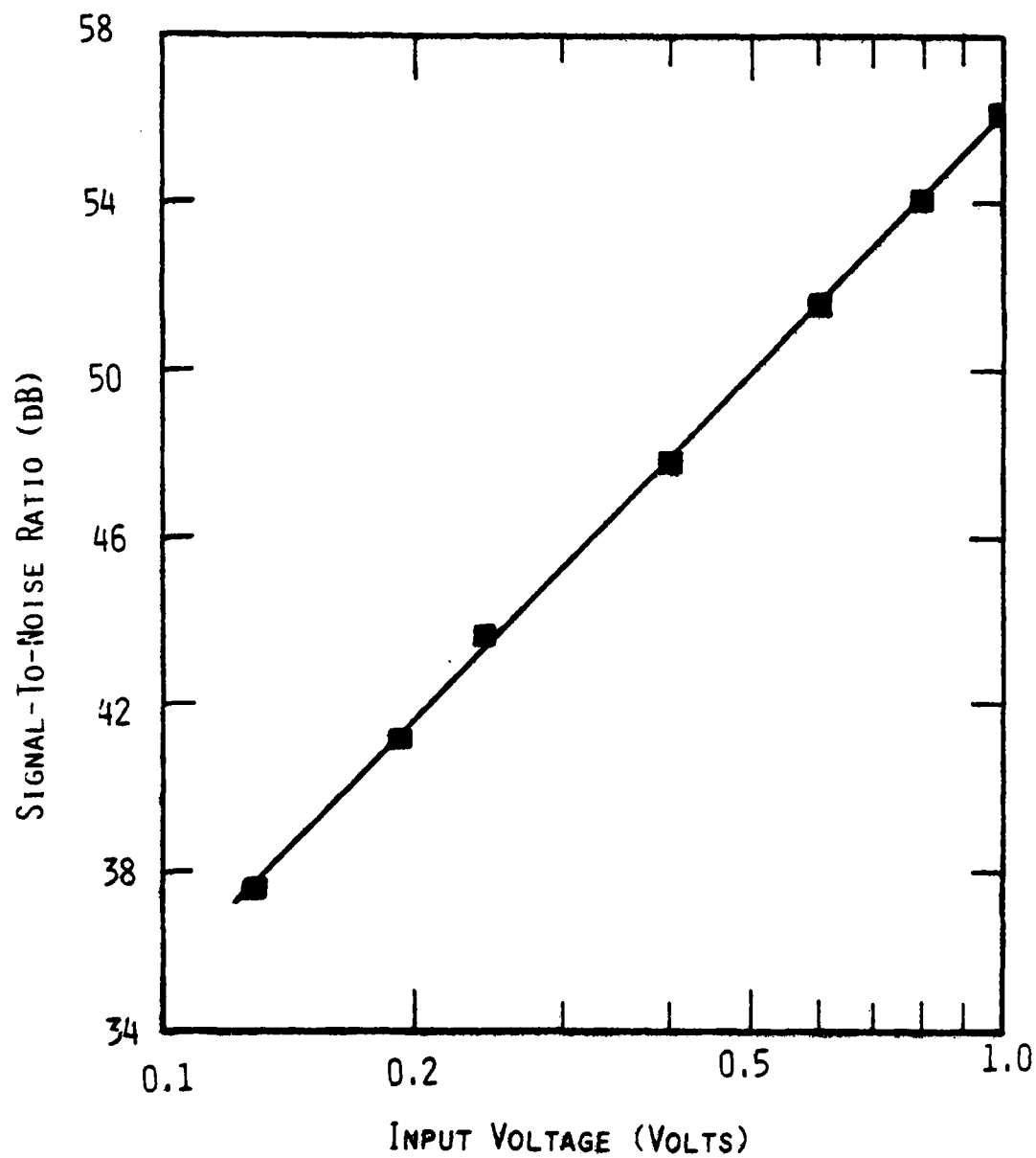


Figure 3.7 Measured signal-to-noise ratio in a short (~1m) optical transmission line versus input voltage.

$$P_{in}(t) = P(1 + m e^{-\alpha t^2} \cos \Omega t) \quad (3.21)$$

where α is related to the standard deviation of the input pulse. The output power is given by the convolution of $P_{in}(t)$ with the impulse response function of the fiber (Equation (3.18)). Hence P_{out} can be written as

$$P_{out}(t) = P/(\gamma L \sqrt{\pi}) \int_{-\infty}^{\infty} 1 + m \exp(-\alpha(t-\tau)^2) \cos \Omega(t-\tau) \exp(-\tau^2/(\gamma^2 L^2)) d\tau \quad (3.22)$$

The solution to the integral is

$$P_{out}(t) = P(1 + m' e^{-\alpha' t^2} \cos \Omega' t) \quad (3.23)$$

where

$$m' = m \exp((- \Omega^2 \gamma^2 L^2)/(4 \gamma^2 L^2 \alpha + 4)) \sqrt{\alpha \gamma^2 L^2 + 1}$$

$$\Omega' = \Omega/(\alpha \gamma^2 L^2 + 1)$$

and

$$\alpha' = \alpha/(\alpha \gamma^2 L^2 + 1)$$

Note that if $\alpha \gamma^2 L^2 \ll 1$, Equation (3.23) reduces to Equation (3.21). The convolution can change the modulation frequency Ω . This phenomenon is explained by invoking the Fourier representation of the convolution integral, i.e., Equation (3.18) can be written as

$$P_{out}(t) = F^{-1}(F(P_{in}) F(g))$$

where $F(P_{in})$ and $F(g)$ are the Fourier transforms of $P_{in}(t)$ and $g(t)$, respectively, and F^{-1} denotes the inverse Fourier transform. For example, if the input signal $P_{in}(t)$ has a wide pulse width, then the Fourier transform of P_{in} will be narrow in extent. Furthermore, if the fiber dispersion (i.e., γL) is small, then the Fourier transform of $g(t)$ will be essentially constant over the extent of $F(P_{in})$. In this case, $F(P_{in})$ will be essentially unchanged by $F(g)$. If the converse is true, i.e., if $P_{in}(t)$ is a narrow pulse and γL is large, then $F(P_{in})$ will be changed significantly by $F(g)$ which means there exists a large interaction between the fiber response function and the input pulse $P_{in}(t)$.

We will now address the magnitude of the term $\alpha\gamma^2 L^2$. $\gamma = 0.2 \times 10^{-9}$ s/km, $L < 100$ m, and α is related to the standard deviation of the pulse according to Equation (3.24).

$$\alpha = 1/2\sigma^2 \quad (3.24)$$

Assuming a 10 nanosecond pulse width, i.e., $3\sigma = 10^{-8}$ s, then $\sigma = 0.3 \times 10^{-8}$ s and $\alpha = 5.6 \times 10^{16}$ s⁻²

Hence,

$$\alpha\gamma^2 L^2 = 2.2 \times 10^{-5}$$

The change in frequency is now calculated as

$$\Delta\Omega = \Omega - \Omega' = \Omega - \Omega/(\epsilon + 1) = \epsilon\Omega$$

where

$$\epsilon = \alpha\gamma^2 L^2$$

If Ω is assumed to be 500 MHz, then $\Delta\Omega$ is 11 kHz.

The inevitable conclusion is that in a multimode fiber link the change in frequency is negligible if

$$\alpha \gamma^2 L^2 \ll 1 \quad (3.25)$$

If α is defined as in Equation (3.24), the inequality in Equation (3.25) reduces to

$$\sigma^2 \gg \gamma^2 L^2 / 2 \quad (3.26)$$

which states that the variance of the input signal must be much greater than the total change in variance for the frequency change to be negligible.

In the expansion of the Gaussian wave packet within the fiber delay the expansion parameter α' is given by

$$\alpha' = \alpha / (\alpha \gamma^2 L^2 + 1) = 1/2 \sigma'^2$$

Solving for the new variance yields

$$\sigma'^2 = \alpha \frac{\alpha \gamma^2 L^2 + 1}{2\alpha}$$

The change in variance between the input and output pulse is given by

$$\sigma_D^2 = \sigma'^2 - \sigma_0^2 \quad (3.27)$$

where

$$\sigma_0^2 = \frac{1}{2\alpha}$$

Hence,

$$\sigma_D^2 = ((\alpha \gamma^2 L^2 + 1) / (2\alpha)) - 1/2\alpha$$

or

$$\sigma_D^2 = \frac{\gamma^2 L^2}{2}$$

This result clearly demonstrates that changes in the variance of the input pulse width σ_D^2 are proportional to fiber length L and the dispersion constant γ in a multimode FO transmission line.

The inequality in Equations (3.26) can now be rewritten as

$$\sigma^2 \gg \sigma_D^2$$

In words, the variance of the pulse σ^2 must be much greater than the changes in variance. To obtain an estimate of the wave packet expansion, we must first express the pulse amplitude at the -3 dB point in terms of σ since γ was also measured at that point, i.e., we must solve Equation (3.28) for t

$$0.5 = \exp(-t_{0.5}^2 / 2\sigma^2) \quad (3.28)$$

or

$$t_{0.5} = 1.18 \sigma$$

Thus, variance expansion at the -3 dB point is given by

$$E_{-3dB} = (1.18)^2 \sigma_D^2 = (1.18)^2 \gamma^2 L^2 / 2 = 0.7 \gamma^2 L^2$$

Let $L = 20$ m, and $\gamma = 0.2$ ns/km. Then,

$$E_{-3dB} = 0.01 \text{ ps.}$$

3.2.6 TEMPERATURE STABILITY

Temperature variations affect the output intensity of injection lasers and the sensitivity of the photodiodes. For example, APDs exhibit wavelength shifts of 0.4 nm/°C to 0.5 nm/°C at the peak of the response curve (Reference 5), and lasers show a shift toward higher threshold currents with increasing temperature accompanied by a change in the slope of the transfer curve (Reference 6). Both effects have been eliminated with temperature compensating circuitry for the laser and the APD used in this project.

Temperature changes also affect the propagation time of an optical signal in a fiber. The change in propagation delay $\delta\tau/\delta T$ for a fiber is given (Reference 7) by:

$$\frac{\delta\tau}{\delta T} = \frac{1}{c} \left(\frac{\delta n}{\delta T} L + n \frac{\delta L}{\delta T} \right) \quad (3.29)$$

$\delta L/\delta T$ is the change in fiber length with temperature which can be expressed as $\delta L/\delta T = \alpha L$, where $\alpha = 8 \times 10^{-7}/^\circ\text{C}$ is the linear thermal expansion coefficient for the combined silica fiber core and cladding and $\delta n/\delta T$ is the index of refraction at the center of the fiber core. $\delta L/\delta T$ can be replaced with αL in Equation (3.29) and L can be factored out. The terms that remain within the brackets are $\delta n/\delta T$ and αn . For multimode silica fibers, $\delta n/\delta T$ was measured (Reference 8) to be $1 \times 10^{-5}/^\circ\text{C}$ over a temperature range of -40°C to $+70^\circ\text{C}$ which is much greater than $n\alpha$ ($n\alpha = 1.2 \times 10^{-6}$). Therefore, propagation delay changes in multimode silica fibers are primarily due to refractive index variations with temperature.

Of importance here is the maximum allowable temperature variation in the fiber delay network, assuming the difference in delay changes, $\Delta\tau$, between any two fiber delay lines routed to different transmission elements, is specified to be $< \pm 0.01$ ns. Let $\delta\tau$ be the delay change for the largest delay which has an effective fiber length L_1 . Let $\delta\tau_2$ be the delay change for the smallest delay with a corresponding effective fiber length L_2 . Then $\Delta\tau$ is given by

$$\Delta\tau = \delta\tau_1 - \delta\tau_2 = \left(\frac{L_1 - L_2}{c} \right) \left(\frac{\delta n}{\delta T} \right) \delta T \quad (3.30)$$

where $L_1 - L_2$ is taken to be the difference (19.8 m) between the longest 20 m and the shortest (0.2 m) multimode fiber and $\delta N/\delta T$ is $10^{-5}/^{\circ}\text{C}$. Substituting these parameters into Equation 3.30 and solving for δT yields a maximum allowable temperature change of about $\pm 15^{\circ}\text{C}$.

3.2.7 MAXIMUM SNR

The maximum SNR of the multimode fiber delay line is defined as the ratio of maximum to minimum detectable output power. The minimum detectable power for short fibers is obtained when the signal power is equal to the average laser noise power. Thus, the calculated maximum SNR, is

$$\text{SNR}_C = \langle i_S^2 \rangle / \langle N_{\text{LASER}}^2 \rangle \quad (3.31)$$

where $\langle i_S^2 \rangle$ is the maximum signal power. This calculated value is the maximum SNR at $\alpha L < 15$ dB which is 57 dB for a 100 MHz system bandwidth.

The measured maximum SNR can be derived from Figure 3.8 which shows the system's gain linearity. The two curves (A&B) differ because they were taken with different gain amplifiers in the circuit. The B curve amplifier was limited to 500 MHz bandwidth while the A curve amplifier exceeded one gigahertz in bandwidth. V_O is the output voltage and V_i is the input voltage. The range extends from a minimum observable V_O of 0.0053 to a maximum V_O of 4.0 volts. The measured value is

$$\text{SNR}_m = 20 \log (V_{O \text{ MAX}}/V_{O \text{ MIN}})$$

$$\text{SNR}_M = 57 \text{ dB}$$

which is in good agreement with the calculated value.

3.2.8 ANALYSIS SUMMARY

3.2.8.1 Induced Delay/Induced Pulse Spreading

A multimode fiber transmits several hundred modes which are slightly displaced in time at the fiber exit plane. If the original pulse launched into the fiber is Gaussian,

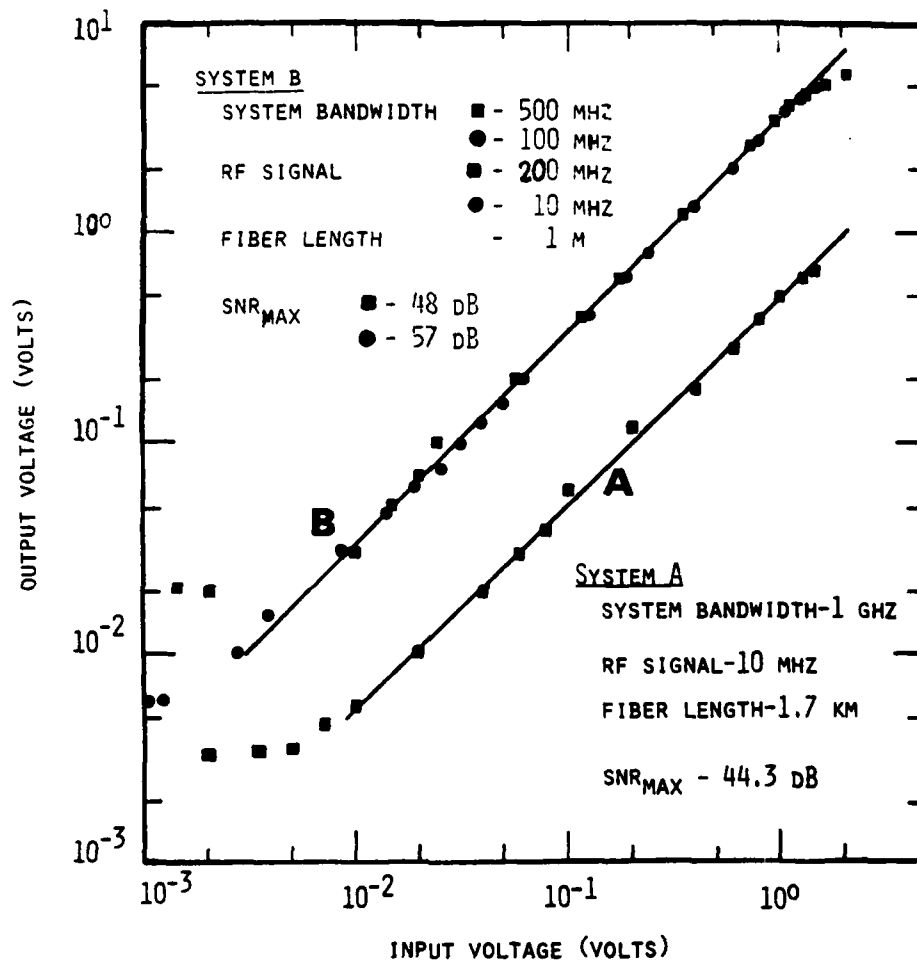


Figure 3.8. AC output voltage from fiber optic transmission line versus input voltage.

these multiple delayed pulses will overlap and produce a slightly broadened Gaussian pulse. The net result is an induced pulse spreading with a concurrent, but much lesser, effect on the RF carrier. The pertinent inequality is:

$$\sigma^2 \gg \sigma_D^2$$

where σ^2 is the variance of the input Gaussian pulse and σ_D^2 is the induced spread in variance defined by

$$\sigma_D^2 = \gamma^2 L^2 / 2 \quad (3.32)$$

γ is the fiber dispersion in nanoseconds per kilometer and L is the fiber length in kilometers. The above equation and inequality assert the following: (1) The variance of the induced pulse spreading is proportional to the square of the total dispersion in the system defined by $\gamma^2 L^2$, and (2) the variance of the input pulse must be much greater than the induced spread in variance for the delay fiber to function as a coherent device.

3.2.8.2 S/N Ratio

The system has a maximum theoretical S/N ratio of approximately 57 dB for a bandwidth of 100 MHz. The measured S/N ratio was 57 dB for the same conditions.

3.2.9 PHASE SHIFT

This section will quantify the delay caused by precisely cut fibers. The time delay (D) caused by a fiber of length L is given by:

$$D = \frac{L}{V} = \frac{L}{c/n} = \frac{Ln}{c} \quad (3.33)$$

D	=	time delay caused by fiber
L	=	length of fiber
V	=	velocity of light propagation in fiber
c	=	velocity of light in free space
n	=	index of refraction of optical fiber.

The difference in the lengths of the two test fibers was measured to be 4.20 centimeters. This is the total difference in the light path because the remaining path lengths are common to both switch states. The index of refraction of the optical fiber was from 1.47 at the core to 1.45 at the cladding, and it varied as a parabolic curve. Since the individual group velocities of the modes within the fiber depend on the various group indexes of the modes, the index of refraction at the very center of the core of the graded index fiber is used. Using these values, along with the speed of light ($c = 2.98 \times 10^8$ meters/second), the time delay caused by the difference in fiber lengths is:

$$D = \frac{(0.042 \text{ meters}) (1.47)}{(2.98 \times 10^8 \text{ meters/second})} = 0.2072 \text{ nanoseconds} \quad (3.34)$$

If the laser is RF modulated with frequency F , then the period of one cycle is the inverse of the frequency, and the phase difference caused by a time delay is given by:

$$\phi = \frac{D}{T} (360^\circ) = DF(360^\circ) \quad (3.35)$$

$$\begin{aligned} \phi &= (0.2072 \times 10^{-9} \text{ seconds}) F(360^\circ) \\ &= (7.459 \times 10^{-8} \text{ degrees}) (F) \\ &= 74.59 \text{ degrees per 1 GHz} \end{aligned}$$

The difference in length of the test fibers corresponds to a delay of 74.59 degrees phase difference per GHz of RF frequency. The phase difference is linearly proportional to frequency. The calculated phase difference from 2 GHz to 4 GHz is plotted (solid line) in Figure 3.9.

3.2 9.1 Measured Phase Shift

The phase difference due to the switchable fiber length difference was measured using both Hewlett Packard (HP) 8410 network analyzer system and a Tektronix sampling scope. The HP 8410 enabled measurements to be made from 2 GHz to 4 GHz, however, a lower frequency (0.1 GHz to 2 GHz) sweeper was unavailable. The measured phase difference as a function of frequency is shown in Figure 3.9. The measured values show excellent agreement with the calculated values and also show the linearity of the fiber

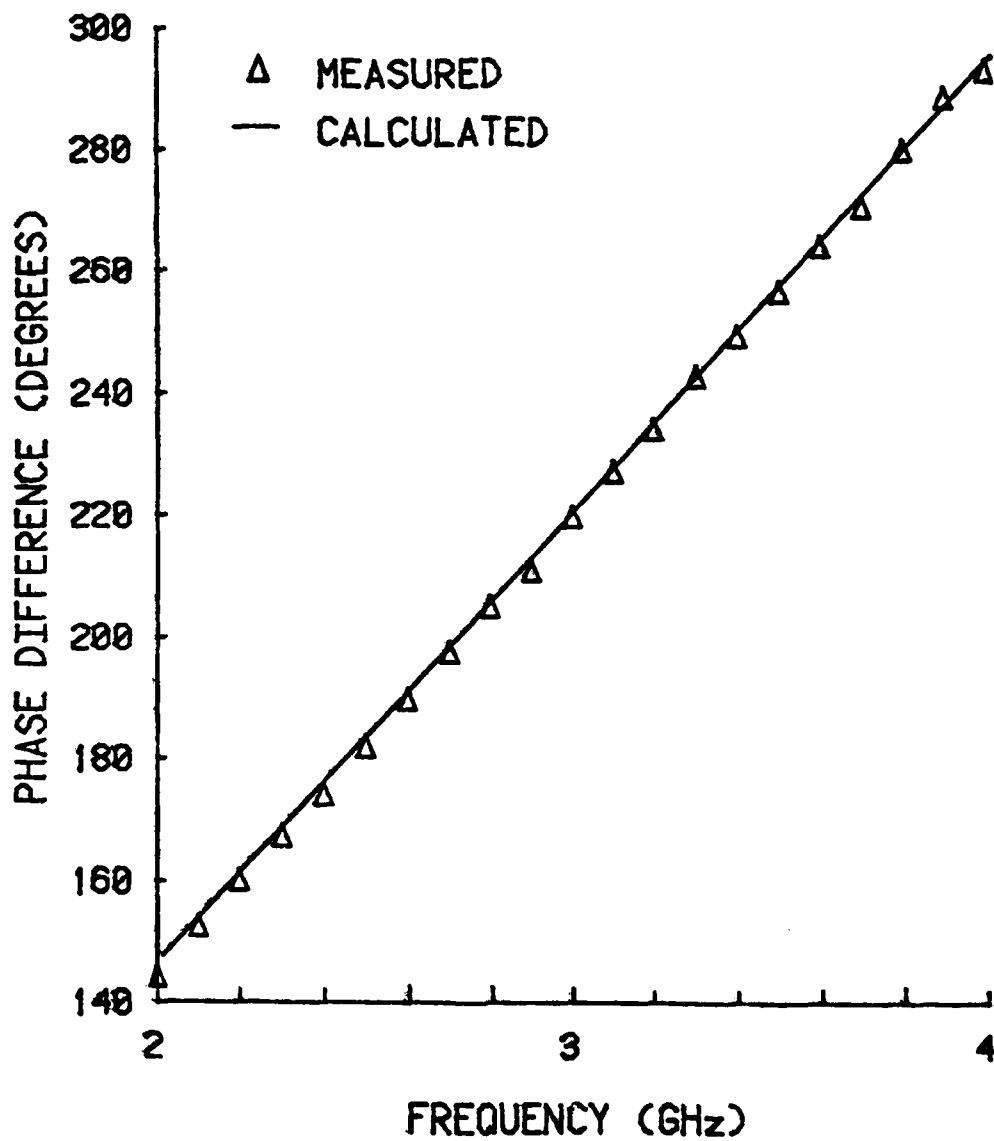


Figure 3.9 Measured and calculated phase difference of optical fiber pair in test system.

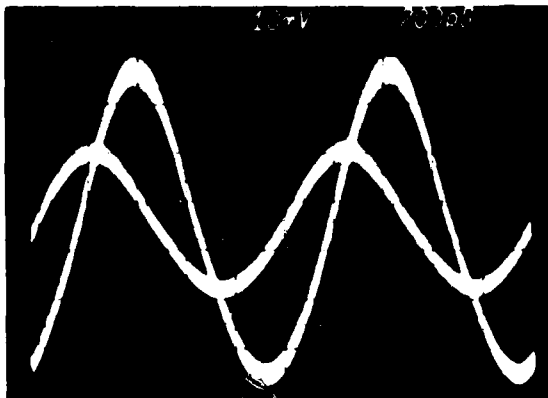
optic delay system. The error of the measured phase difference using the HP 8410 is approximately two degrees.

A Tektronix Sampling Oscilloscope, consisting of a 7613 mainframe and S-2 sampling head, was also used to measure the phase difference. The S-2 has a bandwidth of DC to 4 GHz. The phase difference measurement error using the oscilloscope was much greater than that for the 8410 network analyzer, therefore, only the measured values using the network analyzer are plotted. Figure 3.10 shows oscilloscope display at 1, 2, 3, and 4 GHz. In each picture, the RF signal through both of the fiber paths were superimposed by double exposing the film. The RF signal generator was used to trigger the oscilloscope so that the phase difference displayed is the true phase difference. In each of the four pictures, the smaller and larger signals correspond to the shorter and longer length fibers, respectively.

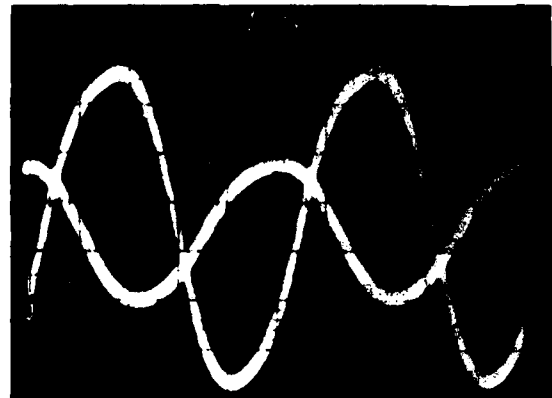
The difference in the amplitude of the two signals was caused by excess loss in the connector for the shorter fiber. As the frequency increases, one can see that the phase difference increases, i.e, the larger sine wave slides further past the smaller sine wave. From both the network analyzer and oscilloscope measurements, excellent agreement was found with the calculated values.

3.10 FREQUENCY RESPONSE

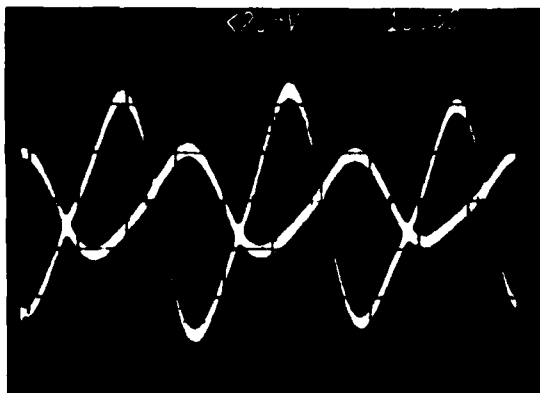
The frequency response of the laser-receiver system is shown in Figure 3.11. The data plotted was taken at the factory with a fiber connecting the laser to the receiver, and, thus, losses due to the coupler and switches are not incorporated. The S_{21} parameter plotted is the gain when the APD is terminated in a matched 50 ohm load. The laser and receiver limit the frequency response of the fiber optic phasing system, since the lengths of fibers used have negligible pulse dispersion and the coupler and switch are extremely broadband devices. The two data sets plotted in Figure 3.11 are similar in shape, and both show fairly uniform response out to 3 GHz. The advertised guaranteed bandwidths for the laser and receiver are 1.5 GHz and 4.5 GHz, respectively. The measured response shows that the actual response of the laser is much greater than the advertised bandwidth. The magnitude of the gain of the entire fiber optic phased system would be much less (-5 to -15 dB) than the plotted values. The variance in the gain is due to connector, coupler, and switch losses and the bias point of the laser.



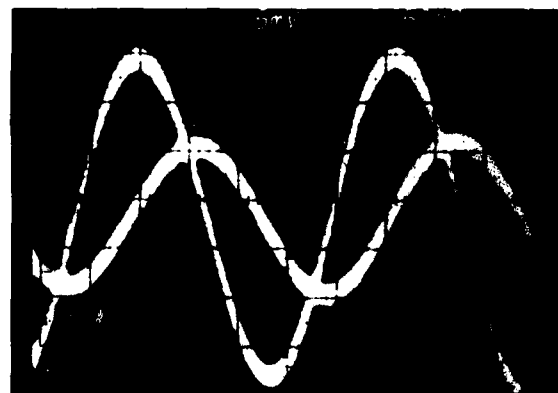
1 GHz Signals Showing Phase Delay



2 GHz Signals Showing Phase Delay



3 GHz Signals Showing Phase Delay



4 GHz Signals Showing Phase Delay

Figure 3.10 Oscilloscope Display at 1,2,3 and 4 GHz

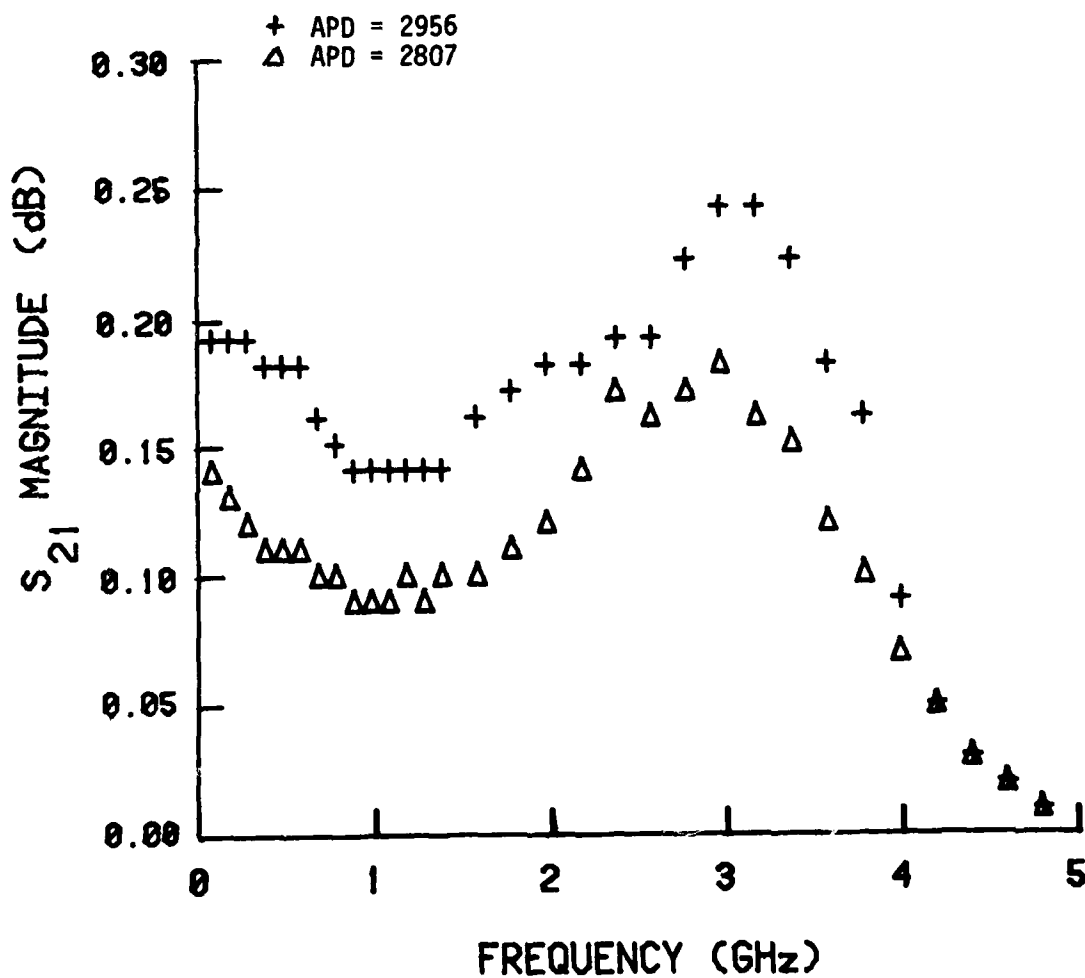


Figure 3.11. Laser-receiver system gain vs. frequency. Both curves found experimentally using laser #2807.

SECTION 4

CONCLUSIONS

The conclusions drawn from the general experience gained in executing this project and the information extracted directly from the experiment are contained in this report section. The conclusions drawn consider: (1) The meaning of the experimental results, (2) The projection of these results into future hardware, and (3) The impact of this future hardware on radar system designs. It is necessary to combine the experimental results with some model of future technology before coherent conclusions can be drawn.

4.1 CONCLUSIONS DRAWN FROM EXPERIMENTAL RESULTS

The conclusions drawn from experimental results are:

- (1) A discrete component experimental time delay phased array radar can be built with commercially available technology.
- (2) A practical time delay phased array radar cannot be built with commercially available technology.
- (3) The principal technology problem is the lack of a commercial multimode optical switch with suitable characteristics.

4.2 CONCLUSIONS DRAWN FROM EXPERIMENTAL RESULTS AND AN INTUITIVE MODEL OF NEAR TERM TECHNOLOGY CHANGES

The experimental results are combined with other data and the conclusions drawn are:

- (1) The combination of the time delay precision (10 ps) and the time delay magnitudes (1 μ s) achievable in an optical waveguide has no direct competition from other technologies.
- (2) The monomode optical switch problem has been solved in the laboratory and fast commercial switches will, in time, become available.
- (3) The time delay antenna will become technologically practical.
- (4) There is insufficient information available to determine if the time delay phased array antenna will become economically practical.

4.3 IMPACT ON RADAR SYSTEM DESIGN

The impact of the low loss, wide bandwidth, and electrically passive fiber optic components on radar system design is difficult to fully predict. The several obvious conclusions are:

- (1) The antenna/transmitter can be remote from the remainder of the radar
- (2) The subsystems of the radar could be organized around a fiber optics communications bus. This would require the subsystem designs to be tightly coupled to the bus design, but would isolate subsystem designs. Computer architecture design technology could be adapted to radar system architecture.
- (3) A successful fiber optics time delay phasing device will increase the economic vitality of the distributed amplifier/sub-antenna/receiver approach to phased array radar system design.
- (4) Spatial and temporal processing of radar signals in optical fiber network will occur at gigahertz data processing rates which is orders of magnitude faster than current or near-term projections for digital processors.

SECTION 5

RECOMMENDATIONS

The recommendations of this section are keyed to a value judgement by RADC. This value judgement is implicit in these two questions:

- (1) Does a time delay phased array antenna have value if its beam switching speed is limited to a few hundred beams per second?
- (2) Are a large number of beams per second (i.e., 0.1×10^6 to 1.0×10^6 per second) so fundamental to the utility of the time delay array antenna that the optical switch problem should be resolved before other work is performed?

5.1 YES TO QUESTION ONE AND NO TO QUESTION TWO

If the answers to these questions are YES-ONE and NO-TWO, then it is recommended that a time phased device be constructed from four-position mechanical optical switches and passive couplers. This device will need 1024 states.

The recommended device is illustrated in Figure 5.1. The sequential steps in the operation of the time delay unit are: (1) The modulated light is injected into the single port of the optical switch, (2) The switch connects the light through one of four possible delay paths, and (3) The light is recombined by a 4 to 1 directional coupler. Five time delay units are connected as shown in this figure. The achievable delay for this five unit system is 12 wavelengths with a resolution of 5.625 degrees. The number of distinct states are four to the fifth power, or 1024. In an array antenna which uses this approach, each state corresponds to a beam position.

The selected switch is the Bell Laboratories developed mechanical switch described in Section 2 of this report. These switches are known to switch in a few milliseconds, to exhibit losses less than 0.5 dB, and to be reliable. Because they are a 1-to-4 device they reduce the number of stages relative to a 1-to-2 device.

5.2 NO TO QUESTION ONE AND YES TO QUESTION TWO

If the answer to these two questions is a NO-ONE and YES-TWO, then it is recommended that an electro-optical or magneto-optic multimode switch development be started. As back-up to the multimode switch development, an investigation of single mode switches, fibers, couplers, and connectors for the time delay device is also recommended.

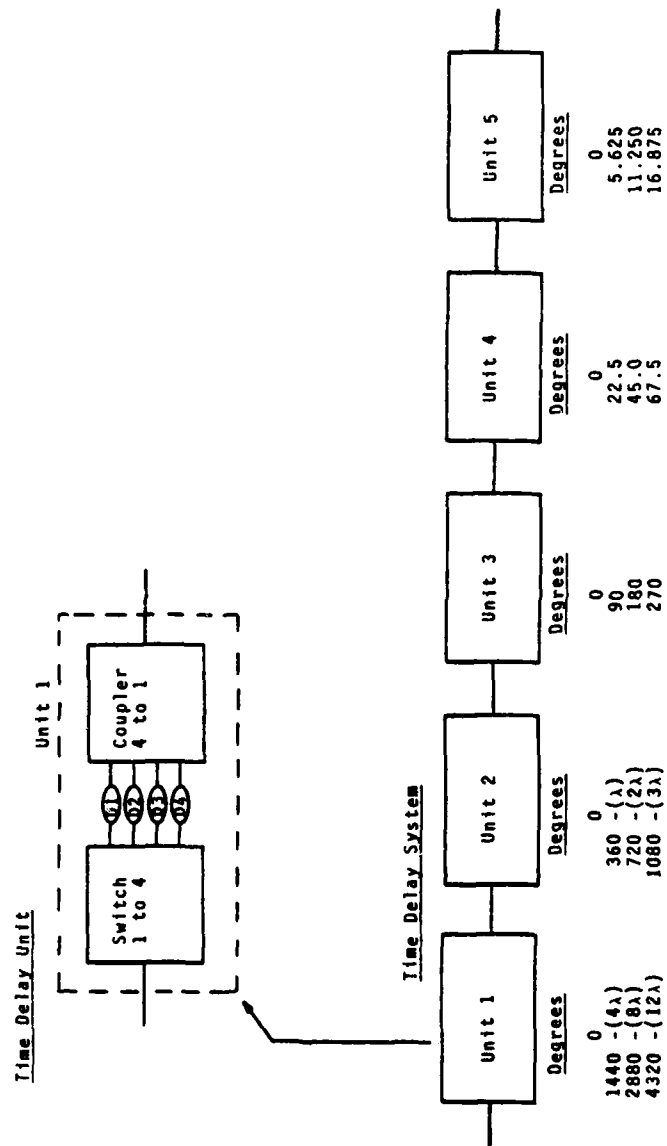


Figure 5.1 Four position optical switch time delay phasing system.

The execution of the effort associated with multimode switches would entail:

- (1) Gathering of detail fabrication techniques from the developing laboratory.
- (2) Transfer of these fabrication techniques to Georgia Institute of Technology's micro-fabrication center.
- (3) Fabrication of example switches.
- (4) Test and evaluation of these multimode optical switches.

The execution of the parallel activity for the monomode electro-optical switch would entail:

- (1) Gathering of detail fabrication techniques from the developing laboratory.
- (2) Transfer of these fabrication techniques to Georgia Institute of Technology's micro-fabrication center.
- (3) Fabrication of example switches.
- (4) Test and evaluation of these monomode switches.
- (5) Test and evaluation of the coupling to these monomode switches.
- (6) Test and evaluation of the monomode fiber delays, light source, detectors, couplers, and connectors.

The monomode case entails both the fabrication of switch samples and a full test of other monomode components of a fiber optics phasing device.

Beyond these immediate developmental research recommendations lies the possibility of the fully integrated electro-optical time delay device. In this hypothetical device, the input RF amplifiers, oscillators, optical sources, optical fiber, optical switches, optical couplers, optical detector, and output RF amplifier are integrated on a single GaAs chip. This chip is inserted between the RF source and the power amplifier associated with each element of a distributed array antenna. The presently unknown economics of this custom chip could be greatly improved by its ability to serve on antennas with center frequencies from a few tens of megahertz to several gigahertz.

REFERENCES

1. Cherin, A., Fiber Optics Communications, unpublished material, Bell Laboratories, Norcross, Ga., 1980
2. Yariv, A., Introduction to Optical Electronics, Second Edition, Holt, Rinehart and Winston, 1971
3. Wolf, F., Handbook of Fiber Optics, Garland STPM Press, N. Y., 1979
4. Godfrey, L.A., Designing for the Faster Response Ever, Optical Spectra, October, 1979
5. Miller, et al, "Electronics Letters," "A High Performance Optical Fiber Switch," Vol. 16, No. 20, Sept., 1980
6. Ohashi, Y., "Japanese Developments in Fiber Optic Systems, Part 2," IFOC, March and May 1980
7. Comerford, IBM Tech. Dis. Bull., Vol. 21, No. 6, Nov., 1978
8. Brady, et al, IBM Tech. Dis. Bull., Vol. 22, No. 7, Dec., 1979
9. Spillman, Applied Optics, Vol. 18, No. 12, June 1979
10. Botez and Herskowitz, Proc. of IEEE, Vol. 68, No. 6, p. 711, June 1980
11. Kogelnik, Herwig, Fibers and Integrated Optics, "Coupled Wave Devices," p. 281-298, 1979
12. Campbell and Li, J. Appl. Phys. 50 (10), p. 6149, Oct., 1979
13. Campbell and Li, Appl. Phys. Lett. 33(3), p. 710, Oct., 1978
14. McMahon, D. It., Laser Focus, "Multimode Optical Switching," March, 1979
15. Laser Focus, February, 1982, p. 55
16. D. E. McCumber, Phys. Rev., 141, 306 (1966)
17. D. J. Morgan and M. J. Adams, Phys. Stat. Sol. (a) 11, 243 (1972)
18. A. Yariv, Introduction to Optical Electronics, Holt, Rinehart and Winston, 280 (1971)
19. S. D. Personik, Bell System Technical Journal, 50, 843 (1971)
20. G. R. Elion and H. A. Elion, Fiber Optics in Communications Systems, Marcel Dekker Press (1978)

21. S. T. Eng and Bergman, *Applied Optics*, 19, 3335 (1980)
22. L. G. Cohen and J. W. Fleming, *Bell Systems Technical Journal*, 58, No. 4, 945 (1979)
23. I. H. Malitson, *J. Opt. Soc. Amer.*, 55, No. 10, 1205 (1965)

APPENDIX A

THE SUM OF TWO SINUSOIDS

Given two sinusoidal waves y_1 and y_2 with identical frequencies, but displaced in phase,

$$y_1 = A \sin \omega t$$

$$y_2 = A \sin (\omega t - \phi)$$

the resultant sum is

$$y = y_1 + y_2 = A(\sin \omega t + \sin (\omega t - \phi)) \quad (\text{A.1})$$

Using the trigonometric identity

$$\sin a + \sin b = 2 \cos \left(\frac{a-b}{2} \right) \sin \left(\frac{a+b}{2} \right) \quad (\text{A.2})$$

Equation (A.1) can be rewritten as

$$w = 2A \cos (\phi/2) \sin(\omega t - \phi/2) \quad (\text{A.3})$$

or

$$y = A_R \sin (\omega t - \phi_R) \quad (\text{A.4})$$

where the resultant amplitude A_R and phase ϕ_R are given by

$$A_R = 2A \cos (\phi/2) \text{ and } \phi_R = \phi/2$$

If ϕ is the phase difference between two transverse modes propagating through a fiber then, at the output of the fiber, ϕ is in general non-zero. Hence, the resultant amplitude A_R is less than $2A$ (i.e., the sum of the amplitudes of the two sinusoids).

APPENDIX B

DERIVATION OF THE OUTPUT POWER OF A CW SIGNAL PROPAGATING THROUGH A MULTIMODE FIBER

Given the input power of the signal

$$P_{in}(t) = P (1 + m \cos \Omega t) \quad (B.1)$$

and the response function of the fiber

$$g(t) = (1/(\gamma L \sqrt{\pi})) \exp (-t^2/(\gamma^2 L^2)) \quad (B.2)$$

$P_{out}(t)$ is then given by the convolution of $g(t)$ with $P_{in}(t)$.

$$P_{out}(\tau) = \int_{-\infty}^{\infty} P_{in}(t-\tau) g(t) dt$$

or

$$P_{out}(t) = \int_{-\infty}^{\infty} P(1 + m \cos \Omega(t-\tau)) \frac{1}{(\gamma L \sqrt{\pi})} \exp (-t^2/(\gamma^2 L^2)) dt \quad (B.3)$$

$$P_{out}(t) = P/(\gamma L \sqrt{\pi}) \int_{-\infty}^{\infty} (1 + m \cos \Omega (t-\tau)) \exp \left(-t^2/(\gamma^2 L^2) \right) dt$$

$$P_{out}(t) = (P/\gamma L \sqrt{\pi}) \int_{-\infty}^{\infty} \exp \left(-t^2/(\gamma^2 L^2) \right) dt$$

$$+ (Pm/(\gamma L \sqrt{\pi})) \int_{-\infty}^{\infty} \cos \Omega (t-\tau) \exp \left(-t^2/(\gamma^2 L^2) \right) dt$$

The solution of the first integral is

$$(P/(\gamma L \sqrt{\pi})) (\gamma L \sqrt{\pi}) = P \quad (B.4)$$

The solution to the second integral is

$$(Pm/(\gamma L \sqrt{\pi})) \int_{-\infty}^{\infty} \cos \Omega (t-\tau) \exp \left(-t^2/(\gamma^2 L^2) \right) dt$$

$$= (Pm/(\gamma L \sqrt{\pi})) \int_{-\infty}^{\infty} (\cos \Omega t \cos \Omega \tau + \sin \Omega t \sin \Omega \tau) \exp \left(-t^2/(\gamma^2 L^2) \right) dt$$

but

$$\int_{-\infty}^{\infty} \sin \Omega t \sin \Omega \tau \exp \left(-t^2/(\gamma^2 L^2) \right) dt = 0$$

since $\int_{-\infty}^{\infty}$ even function \cdot odd function = 0

Hence we need to solve only

$$(P_m \cos \Omega \tau) / (\gamma L \sqrt{\pi}) \int_{-\infty}^{\infty} \cos \Omega t \exp \left(-t^2 / (\gamma^2 L^2) \right) dt$$

which yields

$$(P_m \cos \Omega \tau) / (\gamma L \sqrt{\pi}) (\gamma L \sqrt{\pi}) \exp(-\Omega^2 \gamma^2 L^2 / 4) \quad (B.5)$$

By combining solutions to the two integrals in Equations (B.4) and (B.5), the output power can be written as

$$P_{out}(t) = P (1 + m \exp(-\Omega^2 \gamma^2 L^2 / 4) \cos \Omega t)$$

APPENDIX C

THE CONVOLUTION OF A GAUSSIAN PULSE WITH A GAUSSIAN RESPONSE FUNCTION

The objective in Appendix C is to convolve the input pulse $P_{in}(t)$

$$P_{in}(t) = P (1 + m \exp(-\alpha t^2) \cos \Omega t) \quad (C.1)$$

with the response function of the fiber $g(t)$.

$$g(t) = (i/\gamma L \sqrt{\pi}) \exp(-t^2/(\gamma^2 L^2)) \quad (C.2)$$

The convolution of the two functions is

$$P_{out}(\tau) = \int_{-\infty}^{\infty} P_{in}(t-\tau) g(t) dt \quad (C.3)$$

or

$$P_{out}(\tau) = P / (\gamma L \sqrt{\pi}) \int_{-\infty}^{\infty} (1 + m \exp(-\alpha(t-\tau)^2) \cos \Omega(t-\tau)) \exp(-t^2/(\gamma^2 L^2)) dt \quad (C.4)$$

The integral can be separated

$$P_{out}(\tau) = P / (\gamma L \sqrt{\pi}) \int_{-\infty}^{\infty} \exp \{-t^2 / (\gamma^2 L^2)\} dt \quad (C.5)$$

$$+ P / (\gamma L \sqrt{\pi}) \int_{-\infty}^{\infty} m \exp(-\alpha(t-\tau)^2) \exp \{-t^2 / (\gamma^2 L^2)\} \cos \Omega(t-\tau) dt$$

The solution of the first integral is

$$(P / (\gamma L \sqrt{\pi}) \int_{-\infty}^{\infty} \exp \{-t^2 / (\gamma^2 L^2)\} dt = (P / (\gamma L \sqrt{\pi})) (2\gamma L \sqrt{\pi} / 2) \quad (C.6)$$

$$= P$$

Thus

$$P_{out} = P \left(1 + \frac{1}{(\gamma L \sqrt{\pi})} \right) \int_{-\infty}^{\infty} m \exp(-\alpha(t-\tau)^2) \exp \{-t^2 / (\gamma^2 L^2)\} \cos \Omega(t-\tau) dt \quad (C.7)$$

The integral in Equation (C.7) can be solved by first combining the exponential terms given by

$$E = -\alpha(t-\tau)^2 - t^2 / (\gamma^2 L^2) = -\alpha(t^2 - 2t\tau + \tau^2) - t^2 / (\gamma^2 L^2)$$

$$E = -(\alpha t^2 - 2\alpha t\tau + \alpha\tau^2 + t^2 / (\gamma^2 L^2))$$

$$E = -t^2 (\alpha + 1 / (\gamma^2 L^2)) - 2\alpha t\tau + \alpha\tau^2$$

Setting $A = \alpha + 1/(\gamma^2 L^2)$ and completing the square yields

$$E = -A (t^2 - 2\alpha t\tau/A + \alpha^2 \tau^2/A^2 + \alpha \tau^2/A - \alpha^2 \tau^2/A^2)$$

$$E = -A ((t - \alpha \tau/A)^2 + \alpha \tau^2/A - \alpha^2 \tau^2/A^2)$$

or

$$E = -A(t - \alpha \tau/A)^2 - \alpha \tau^2 + \alpha^2 \tau^2/A$$

Let $C = -\alpha \tau^2 + \alpha^2 \tau^2/A$, then

$$E = -A(t - \alpha \tau/A)^2 + C$$

$P_{out}(\tau)$ can now be rewritten as

$$P_{out}(\tau) = P + P(m \exp(C)/(\gamma L \sqrt{\pi})) \int_{-\infty}^{\infty} \exp(-A(t - \alpha \tau/A)^2)$$

$$\cos \Omega(t - \tau) dt \quad (C.8)$$

Set $X = t - \alpha\tau/A$, then $dX = dt$ and $t - \tau = X + \alpha\tau/A - \tau$. The integral becomes

$$\begin{aligned}
 & \int_{-\infty}^{\infty} \exp(-A(t-\alpha\tau/A)^2) \cos \Omega(t-\tau) dt \\
 &= \int_{-\infty}^{\infty} \exp(-AX^2) \cos \Omega(X + \alpha\tau/A - \tau) dX \\
 &= \int_{-\infty}^{\infty} \exp(-AX^2) (\cos \Omega X \cos \Omega \tau/(A(\alpha-A)) - \sin \Omega X \sin \Omega \tau/[A(\alpha-A)]) dX \\
 &= \int_{-\infty}^{\infty} (\exp(-AX^2) \cos \Omega X \cos \Omega \tau/[A(\alpha-A)]) dX - \int_{-\infty}^{\infty} (\exp(-AX^2) \sin \Omega X \\
 &\quad \sin \Omega \tau/[A(\alpha-A)]) dX
 \end{aligned}$$

The integral with the sine functions is zero because $\int_{-\infty}^{\infty}$ even function \cdot odd function $dx = 0$. Thus, we need only to evaluate the integral with the cosine functions.

$$\begin{aligned}
 & \int_{-\infty}^{\infty} \exp(-AX^2) \cos \Omega X \cos \Omega \tau/(A(\alpha-A)) dX \\
 &= \cos \Omega(\alpha-A) \tau/A \int_{-\infty}^{\infty} \exp(-AX^2) \cos \Omega X dX \\
 &= (\sqrt{\pi}/\sqrt{A}) \cos \Omega(\tau/A)(\alpha-A) \exp(-\Omega^2/4A) \tag{C.9}
 \end{aligned}$$

The convolution function of Equation (C.8) can now be written as

$$P_{out}(t) = P + ((P_m)/(\gamma L) \exp(C)) (1/\sqrt{A}) \cos \Omega(t/a)(\alpha - A) \exp(-\Omega^2/4A) \quad (C.10)$$

Evaluating C , $\Omega^2/4A$ and $t/(A(\alpha - A))$ yields

$$C = -\alpha t^2 / (\alpha \gamma^2 L^2 + 1)$$

$$\Omega^2/4A = (\Omega^2 \gamma^2 L^2) / (4\alpha \gamma^2 L^2 + 4)$$

and

$$t/A (\alpha - A) = -t / (\alpha \gamma^2 L^2 + 1)$$

where

$$A = \alpha + 1/(\gamma^2 L^2)$$

and the variable τ was replaced by t .

Substituting these expressions into Equation (C.10) yields the final expression of $P_{out}(t)$.

$$P_{out}(t) = P (1 + \frac{m}{\sqrt{\alpha\gamma^2 L^2 + 1}} \exp((- \Omega^2 \gamma^2 L^2) / (4\alpha\gamma^2 L^2 + 4)) \exp(-\alpha t^2) / (\alpha\gamma^2 L^2 + 1)) \cos \Omega (1/(\alpha\gamma^2 L^2 + 1)) t) \quad (C.11)$$

where α and γ are constants. Equation (C.11) can be simplified by writing

$$m' = \frac{m}{\sqrt{\alpha\gamma^2 L^2 + 1}} \exp(-\Omega^2 \gamma^2 L^2) / (4\alpha\gamma^2 L^2 + 4)$$

$$\Omega' = \Omega / (\alpha\gamma^2 L^2 + 1)$$

$$\alpha' = \alpha / (\alpha\gamma^2 L^2 + 1)$$

Hence $P_{out}(t)$ becomes

$$P_{out}(t) = P (1 + m' \exp(-\alpha' t^2) \cos \Omega' t) \quad (C.12)$$

<u>No. of Convolutions</u>	<u>Ω'</u>	<u>α'</u>
1	$\Omega/(\alpha\gamma^2 L^2 + 1)$	$\alpha/(\alpha\gamma^2 L^2 + 1)$
2	$\Omega/(2\alpha\gamma^2 L^2 + 1)$	$\alpha/(2\alpha\gamma^2 L^2 + 1)$
3	$\Omega/(3\alpha\gamma^2 L^2 + 1)$	$\alpha/(3\alpha\gamma^2 L^2 + 1)$
N	$\Omega/(N \alpha\gamma^2 L^2 + 1)$	$\alpha/(N \alpha\gamma^2 L^2 + 1)$

MISSION of Rome Air Development Center

RADC plans and executes research, development, test and selected acquisition programs in support of Command, Control, Communications and Intelligence (C3I) activities. Technical and engineering support within scope of technical competence is provided to C3I Program Offices (POs) and other key elements. The principal technical mission areas are: communications, electromagnetic warfare and control, surveillance of ground and aerospace objects, intelligence data collection and handling, information system technology, ionospheric propagation, solid state devices, microwave physics and electronic reliability, maintenance and compatibility.

